Precipitation extremes around the world

Unraveling historical extremes and future changes

Gründemann, Gaby J.

DOI
10.4233/uuid:efee1e53-d081-4fcb-9a3c-39650de2a13e

Publication date
2023

Document Version
Final published version

Citation (APA)
Gründemann, G. J. (2023). *Precipitation extremes around the world: Unraveling historical extremes and future changes*. [Dissertation (TU Delft), Delft University of Technology]. https://doi.org/10.4233/uuid:efee1e53-d081-4fcb-9a3c-39650de2a13e

Important note
To cite this publication, please use the final published version (if applicable).
Please check the document version above.

PRECIPITATION EXTREMES AROUND THE WORLD

UNRAVELING HISTORICAL EXTREMES AND FUTURE CHANGES

Gaby Gründemann

PRECIPITATION EXTREMES AROUND THE WORLD

UNRAVELING HISTORICAL EXTREMES AND FUTURE CHANGES

PRECIPITATION EXTREMES AROUND THE WORLD

UNRAVELING HISTORICAL EXTREMES AND FUTURE CHANGES

Dissertation

for the purpose of obtaining the degree of doctor
at Delft University of Technology
by the authority of the Rector Magnificus prof. dr. ir. T. H. J. J. van der Hagen,
chair of the Board for Doctorates
to be defended publicly on
Wednesday 6 December 2023 at 12:30

by

Gaby Joanne GRÜNDEMANN

Master of Science in Water Science & Engineering,
UNESCO-IHE, Delft, the Netherlands,
born in Amsterdam, the Netherlands.

This dissertation has been approved by the promotors.

Composition of the doctoral committee:

Rector Magnificus	chairperson
Prof. dr. ir. N. C. van de Giesen	Delft University of Technology, promotor
Dr. ir. R. J. van der Ent	Delft University of Technology, copromotor
Independent members:	
Prof. dr. M. Marani	University of Padova, Italy
Prof. dr. ir. I. Popescu	IHE Delft Institute for Water Education
Dr. ir. A. E. J. ten Veldhuis	Delft University of Technology
Prof. dr. ir. R. Uijlenhoet	Delft University of Technology
Prof. dr. A. P. Siebesma	Delft University of Technology

Keywords: extreme precipitation, extreme value distribution, climate change, seasonality
Printed by: Ipskamp Printing
Front & Back: Natacha Ratto

ISBN 978-94-6473-310-5

An electronic version of this dissertation is available at
http://repository.tudelft.nl/.

CONTENTS

1

INTRODUCTION

1

1.1 MOTIVATION

Water is essential for all life on Earth. From satisfying our basic needs for drinking water and fueling agricultural production to supporting ecosystems, water is an indispensable resource. Precipitation, predominantly in the form of rain and snowfall, serves as nature's way of replenishing our freshwater resources. However, when precipitation occurs in excessive amounts, it can transform from a life-sustaining source to a life-threatening phenomenon. Extreme precipitation events act as the driver of numerous adverse impacts, including flooding, soil erosion, land slides, and debris flows (e.g., Berghuijs et al., 2019; Marc et al., 2018; Nikolopoulos et al., 2015; Steger et al., 2023; Tramblay et al., 2021; Wasko et al., 2020a). The consequences of such events can be catastrophic, resulting in loss of life, infrastructure damage, ecological disruption, and severe disruption of socioeconomic activities.

Informed knowledge of the characteristics and patterns of historical precipitation extremes is crucial for understanding their behavior and predicting future occurrences. This understanding enables us to improve hydrological predictions and develop effective strategies to mitigate the risks associated with extreme precipitation events. The changes in intensity, seasonality, and timing of precipitation extremes have far-reaching consequences, making it essential to comprehend historical trends and projected future changes. By integrating historical observations, statistical methods, and climate model projections, we can gain a comprehensive understanding of precipitation extremes. This knowledge forms the foundation for informed decision-making, guiding infrastructure planning, disaster risk reduction, water resources management, and promoting sustainable development.

1.2 STATISTICAL METHODS IN HYDROLOGY

Per definition, extreme events are a rare occurrence, resulting in limited occurrences in our available data records. Yet, through the use of statistical methods, such as extreme value distributions, we can extrapolate the data beyond the period of record. However, we need to apply statistical methods to long data records to get acceptable uncertainty ranges.

The foundation of extreme value theory in hydrology can be attributed to the pioneering work of Emil Gumbel during the 1940s and 1950s (Gumbel, 1941, 1958). Gumbel's contributions revolutionized hydrology by providing a statistical framework that describes and quantifies the frequency of extreme events using return periods. The introduction of the Gumbel distribution laid the foundation for subsequent advancements in extreme value theory and became a cornerstone in the field of hydrology.

Building upon Gumbel's foundation, the Generalized Extreme Value (GEV) distribution emerged as a more flexible statistical model for analyzing extreme events in hydrology. Although initially introduced by Maurice Fréchet (1927), GEV gained recognition in hydrology through the contributions of Gumbel, as well as statisticians like Hosking and Wallis (e.g., Hosking, 1985; Hosking et al., 1985; Hosking and Wallis, 1993). Similar to the Gumbel distribution, GEV is fitted to block maxima, such as annual maxima, but incorporates an additional parameter. This flexibility enables GEV to account for different types of tail behavior exhibited by extremes, including exponential, light and heavy

tails. This flexibility makes the GEV distribution applicable to a wide range of hydrological variables, such as rainfall, streamflow, and flood magnitudes (e.g., Courty et al., 2019; Ding et al., 2016; Mascaro, 2018; Morrison and Smith, 2002).

Since these pioneering works, many other extreme value distributions and methods have been proposed and applied to estimate precipitation extremes. Examples include the Gamma distribution (e.g., Buishand, 1978; Swift and Schreuder, 1981), the Generalized Gamma distribution (e.g., Papalexiou and Koutsoyiannis, 2016; Stacy, 1962), the Generalized Pareto distribution for peaks over threshold (e.g., Hosking and Wallis, 1987; Langousis et al., 2016; Serinaldi and Kilsby, 2014), the Lognormal distribution (Biondini, 1976; Swift and Schreuder, 1981), the Metastatistical Extreme Value distribution (Marani and Ignaccolo, 2015; Zorzetto et al., 2016), and the Weibull distribution (e.g., Swift and Schreuder, 1981; Wilson and Toumi, 2005). These studies generally rely on the use the annual maxima, peaks over thresholds, or non-zero daily precipitation to fit the distribution. This thesis also relies on several classical as well as more recently emerged extreme value techniques.

1.3 EVOLUTION OF PRECIPITATION DATA

For decades, rain gauges have been used to collect local precipitation data. For some locations, such as the one in Padova, Italy, records date back as far as 1713 and are still active to this day (Camuffo et al., 2020; Marani and Zanetti, 2015). However, such long records spanning three centuries are exceptional. In most areas, the number of active gauges has been declining in the recent years (Mishra et al., 2009). Moreover, the spatial distribution of gauges is highly heterogeneous. Many stations are located in Europe and the US, yet there are many areas globally without any local precipitation records (Kidd et al., 2017). Although recent initiatives, such as the Trans-African Hydro-Meteorological Observatory (TAHMO, van de Giesen et al., 2014), have increased global coverage, the available records in these regions are limited to a few years at most.

Nowadays, gauging stations are just one of the many sources of precipitation data. The launch of new satellite missions and advancements in computational power have paved the way for other valuable sources of observation-based precipitation data. Examples include satellite-derived precipitation datasets, such as CMORPH (Joyce et al., 2004), IMERG (Huffman et al., 2015), PERSIANN (Hong et al., 2004; Hsu et al., 1997), and TMPA Huffman et al. (2007), reanalysis like ERA5 (Hersbach et al., 2018, 2020) and MERRA2 (Gelaro et al., 2017), or compilation products like the MSWEP dataset (Beck et al., 2019b). Although these datasets have their limitations, such as uncertainties and errors in the (remote-sensing) measurements, model bias, and lack of homogeneity due to a change in the available observational data (Beck et al., 2017, 2020; Bosilovich et al., 2008; Cao et al., 2018; Kang and Ahn, 2015; Levizzani et al., 2011; Prakash et al., 2018; Sun et al., 2018), they offer high spatio-temporal precipitation estimates and therefore provide valuable insights into precipitation patterns and changes on the global domain.

In addition to these evolving sources of observation-based precipitation estimates, climate models play a crucial role in understanding historical and projected changes in precipitation patterns. Climate models simulate the Earth's climate system by incorporating various physical processes, such as atmospheric dynamics, oceanic interactions,

and land surface interactions. By running simulations under different emission scenarios, climate models provide projections of how precipitation extremes may evolve in the future, considering the increased moisture-holding capacity of the atmosphere due to global warming (Allen and Ingram, 2002). However, it is important to acknowledge the inherent uncertainties associated with climate model output. These uncertainties arise from factors such as model parameterizations, internal climate variability, the inability to explicitly resolve convective processes and uncertainties in future greenhouse gas emissions and efforts to mitigate them (Loriaux et al., 2013; Westra et al., 2014).

1.4 THIS THESIS

The objective of this doctoral research is to unravel the characteristics and changes of extreme precipitation in the recent past and future. To achieve this objective, this thesis uses a range of statistical methods and tools tailored to the analysis of large precipitation datasets. The advancements in global datasets, increased computational power and novel statistical approaches enable us to perform comprehensive analyses on the global domain. The chapters in this thesis contribute to the overall research objective as follows:

- Chapter 2 examines historical return levels of extreme precipitation for various durations ranging from three hours up to ten days. We estimate these return levels using different extreme value distributions and introduce a "heaviness amplification factor" to compare the tail behavior of the distributions.
- Chapter 3 focuses on characterizing the seasonality and timing of extreme daily precipitation occurrences and explores historical changes thereof.
- Chapter 4 addresses the projected difference in changes in common to rare precipitation extremes under global warming. By using 25 global climate models with four possible future scenarios, we aim to provide robust results that capture the changes of precipitation extremes in the future.

The concluding chapter 5 synthesizes the main findings, discusses their implications, and offers an outlook for future research opportunities in this field.

2

HISTORICAL PRECIPITATION EXTREMES

This chapter is based on:

Gründemann, G. J., Zorzetto, E., Beck, H. E., Schleiss, M. A., van de Giesen, N. C., Marani, M., van der Ent, R. J. *Extreme precipitation return levels for multiple durations on a global scale,* Journal of Hydrology, **621**, p. 129558, 2023.

SUMMARY

Quantifying the magnitude and frequency of extreme precipitation events is key in translating climate observations to planning and engineering design. Past efforts have mostly focused on the estimation of daily extremes using gauge observations. Recent development of high-resolution global precipitation products, now allow estimation of global extremes. This research aims to quantitatively characterize the spatiotemporal behavior of precipitation extremes, by calculating extreme precipitation return levels for multiple durations on the global domain using the Multi-Source Weighted-Ensemble Precipitation (MSWEP) dataset. Both classical and novel extreme value distributions are used to provide insight into the spatial patterns of precipitation extremes. Our results show that the traditional Generalized Extreme Value (GEV) distribution and Peak-Over-Threshold (POT) methods, which only use the largest events to estimate precipitation extremes, are not spatially coherent. The recently developed Metastatistical Extreme Value (MEV) distribution, that includes all precipitation events, leads to smoother spatial patterns of local extremes. For durations of 5 and 10 days, however, there are less events per year to fit the distribution (37 and 22 on average, respectively), leading to larger inter-annual variability and possible overestimation of the extremes. While the GEV and POT methods predict a consistent shift from heavy to thin tails with increasing duration, the MEV method predicts a relatively constant heaviness of the tail for any precipitation duration, opening up an important research question on what is the 'correct' tail behavior of extreme precipitation for different durations. The generated extreme precipitation return levels and corresponding parameters are provided as the Global Precipitation EXtremes (GPEX) dataset. These data can be useful for studying the underlying physical processes causing the spatiotemporal variations of the heaviness of extreme precipitation distributions.

2.1 INTRODUCTION

Extreme precipitation events are a major contributor to natural disasters (CRED, 2019). Accurate estimates of the severity of intense precipitation events are needed for an enhanced disaster risk understanding, such as that of floods and landslides. The urgency of this is indicated as the first priority of the Sendai Framework for Disaster Risk Reduction (UNSIDR, 2015). The accurate quantification of extremes is also necessary for infrastructure planning and design. Some countries already provide spatiotemporal estimates of extreme precipitation based on extreme value distributions (EVDs), for example, for Australia (Ball et al., 2019), the Netherlands (Beersma et al., 2018), and the US (e.g., Perica et al., 2015, 2018). However, many countries and regions do not have sufficient local data available (van de Giesen et al., 2014; Gründemann et al., 2018; Kidd et al., 2017), such that spatially-distributed extreme precipitation estimates are not possible.

Several previous studies have developed global-scale datasets of extreme precipitation. Courty et al. (2019) calculated intensity-duration-frequency curves at the global domain and their scaling with different event durations using reanalysis data and the Generalized Extreme Value (GEV) distribution with fixed tail parameter. Dunn et al. (2020) produced the HadEX3 dataset, which contains 29 generic precipitation and temperature indices, although these indices are not based on EVDs. Furthermore, this dataset has a coarse 1.25° latitudinal × 1.875° longitudinal resolution, with data-gaps due to insufficient available gauge data. Other global studies mostly focused on examining which type of distribution is most suitable to capture the tail behavior of extreme precipitation (Cavanaugh and Gershunov, 2015; Cavanaugh et al., 2015; Papalexiou et al., 2013). In addition, the spatial patterns of the parameter that controls the tail decay have been studied for the GEV distribution (Papalexiou and Koutsoyiannis, 2013; Ragulina and Reitan, 2017), and the Generalized Pareto (GP) distribution (Serinaldi and Kilsby, 2014). However, several issues remain to be addressed in order to obtain global-domain extreme precipitation return levels: 1) the choice of the dataset, 2) the focus on daily extremes without considering sub-daily extremes, 3) the choice of the time blocks over which block-maxima are determined, and 4) the exploration of possible alternatives to the classical EVDs, especially with respect to the tail behavior.

1. Several (quasi-)global gridded precipitation datasets have been developed in recent years, each with strengths, weaknesses, and uncertainties. See Beck et al. (2019a), Rajulapati et al. (2020), and Sun et al. (2018) for recent overviews of available datasets. Most of these datasets are based on gauge, reanalysis, or satellite sensor data. Notable examples of gauge-based datasets include GPCC-FDR (Becker et al., 2013; Schneider et al., 2011) and REGEN (Contractor et al., 2020). However, gauges are extremely unevenly distributed across the globe (Kidd et al., 2017; Schneider et al., 2014), and the number of active gauges has been declining in recent decades (Mishra and Coulibaly, 2009). Satellite-based products such as CMORPH (Joyce et al., 2004), GSMaP (Ushio et al., 2009), IMERG (Huffman et al., 2015), and PERSIANN (Hong et al., 2004) have a relatively high spatio-temporal resolution. However, they do not cover regions outside of 60°N/S, and are only available from 2000 onwards, which significantly hinders their use for extreme value analyses. Precipitation products with a true global coverage and long records

are reanalyses, such as ERA-5 (Hersbach et al., 2020), JRA-55 (Kobayashi et al., 2015), and MERRA-2 (Gelaro et al., 2017). However, reanalysis products tend to exhibit strong local and systematic biases in the magnitude and frequency of precipitation (Decker et al., 2012; Liu et al., 2018; Ménégoz et al., 2013).

2. Global-scale analyses of precipitation extremes are generally based on daily precipitation records (Cavanaugh et al., 2015; Koutsoyiannis, 2004a,b; Nerantzaki and Papalexiou, 2019; Papalexiou and Koutsoyiannis, 2013; Papalexiou et al., 2013; Ragulina and Reitan, 2017; Serinaldi and Kilsby, 2014). In practice, however, multiple durations are needed for the design of infrastructure (e.g., Nissen and Ulbrich, 2017) or urban drainage networks (e.g., Mailhot and Duchesne, 2009). It is known that precipitation extremes of different durations scale differently with temperature (Schleiss, 2018; Wasko et al., 2015), but little is known about the variation of EVD location, scale and tail parameters for different temporal resolutions. Studies that did derive extreme precipitation statistics for durations ranging from minutes to a few days have mostly focused on small regions (McGraw et al., 2019; Nissen and Ulbrich, 2017; Overeem et al., 2008).

3. Studies estimating return levels of extreme precipitation by using annual maxima typically use calendar years to delineate the annual periods from which maxima values are extracted (e.g., Marani and Zanetti, 2015; De Paola et al., 2018; Papalexiou and Koutsoyiannis, 2013; Ragulina and Reitan, 2017; Villarini et al., 2011). When the variable of interest is river discharge instead of precipitation, however, hydrological years are typically used instead of calendar years (Ward et al., 2016). For discharge values this is important, since peak discharge and flooding could occur during the transition from 31 December to 1 January and one event would be included in two calendar years. Although not often considered, this could also happen for precipitation, especially for longer duration extremes. The annual maxima method could pick multiple values from a single rainy season that may, for example, be highly influenced by the El Niño-/Southern Oscillation, which is known to impact precipitation extremes (Allan and Soden, 2008; Rasmusson and Arkin, 1993).

4. The Generalized Extreme Value (GEV) distribution, the most widely used EVD, is typically fitted through one of two approaches: a) using annual maximum precipitation series and maximum likelihood (Coles, 2001) or L-moment (Hosking, 1990) estimation approaches, or b) using a Peak-Over-Threshold (POT) method to fit a Generalized Pareto Distribution to excesses above the threshold and a Poisson process to the sequence of threshold exceedances (Coles, 2001). In contrast to GEV and POT, the recently developed Metastatistical Extreme Value (MEV) distribution is fitted using all events with recorded precipitation instead of only the most severe. The inclusion of more events reduces the uncertainty due to sampling effects, which is important when dealing with short time series (Hu et al., 2020; Marani and Ignaccolo, 2015; Marra et al., 2018, 2019a; Miniussi and Marani, 2020; Zorzetto et al., 2016; Zorzetto and Marani, 2019). Additionally, GEV parameter estimation depends heavily on a few large values, which makes it very sensitive to the possible presence of outliers, a relatively common occurrence in remote

sensing estimates of precipitation amounts (Zorzetto and Marani, 2020). The GEV tail behavior is controlled by its shape parameter, which is very sensitive to sampling effects and the choice of the method used for estimation. To overcome these problems, some studies have suggested to use one universal value of the shape parameter that is applicable to the whole world Koutsoyiannis (2004a,b), or a shape parameter value within a narrow range between exponential and heavy-tail behavior (Papalexiou and Koutsoyiannis, 2013), or one shape parameter per region, that is similar within climate types and elevation ranges (Ragulina and Reitan, 2017).

In this study we aim to overcome these issues partly by 1) using a precipitation dataset that merges gauge, reanalysis, and satellite data, 2) estimating extremes for several event durations, 3) using hydrological years in our analyses, and 4) comparing results from three different extreme value methods (GEV, POT and MEV). Specifically, we are interested in quantitatively characterizing the behavior of extreme precipitation and the spatiotemporal variation of extreme value distributional tails at the global domain.

2.2 MATERIAL AND METHODS

2.2.1 DATA

The global precipitation product used in this study is the Multi-Source Weighted-Ensemble Precipitation (MSWEP-V2.2) dataset. MSWEP is particularly suited for our purpose due to its global coverage, long temporal span, high spatial and temporal resolution. We used data from 1 January 1979 to 31 October 2017 at a 0.1° latitude × 0.1° longitude resolution at 3-hourly time steps. We selected all land-cells between 90°N and 58°S for our analysis. MSWEP precipitation estimates are derived by merging five different satellite- and reanalysis-based global precipitation datasets. The dataset is one of the few precipitation products with daily (as opposed to monthly) gauge corrections, applied using a scheme that accounts for gauge reporting times (Beck et al., 2019b). MSWEP has shown robust performance compared to other widely used precipitation datasets (e.g., Alijanian et al., 2017; Bai and Liu, 2018; Beck et al., 2017, 2019a; Casson et al., 2018; Hu et al., 2020; Sahlu et al., 2017; Satgé et al., 2019; Zhang et al., 2019), thus underlying its potential for improving the characterization of extreme precipitation worldwide. We refer to Beck et al. (2019b) for a comprehensive description of the dataset.

QUALITY CONTROL

The integration of erroneous gauge observations into MSWEP-V2.2 can occasionally result in implausible precipitation values. Therefore, we implemented a three-step quality control procedure on the 3-hourly data prior to the analysis. We first discarded negative values, which are physically impossible. The second step was to discard outliers, which we defined as values deviating from the mean by more than 30 standard deviations. The number of 3-hourly blocks containing outliers per grid cell are included in Supporting Information Section 2.1 Fig. S2.1 (Gründemann, 2023). We also discarded data surrounding the outliers for the same time step using a 11 × 11 grid-cell window, as erroneous gauge observations may have influenced surrounding cells in the production of the MSWEP dataset. The 11 × 11 grid-cell window was chosen based on the procedure used in MSWEP to merge gauges and other rainfall products (Beck et al., 2019b). In the

third step, we removed all years with > 30 discarded days or < 5 'wet' 3-hourly periods, identified using a threshold of 0.2 mm $3h^{-1}$ following Wasko et al. (2015). Finally, we only included in the analysis data from grid cells with at least 30 years of data remaining, as a minimum record length of 30 years is customary and recommended for analyzing extremes (Arguez and Vose, 2011; Kendon et al., 2018; Westra et al., 2013).

DURATIONS AND IDENTIFICATION OF INDEPENDENT EVENTS

The durations we selected for our analysis are 3, 6, 12 and 24 hours, and 2, 3, 5 and 10 days. In order to create statistically-independent precipitation events for multiple durations, we first calculated the running parameter, which is the minimum distance between two independent events (Fukutome et al., 2015). To separate 3-hourly events and ensure independence for each precipitation event at each grid-cell, we followed the declustering method to limit the autocorrelation of the samples of Marra et al. (2018). In order to do so, we calculated the temporal autocorrelation of the time series for each grid-cell, for time lags up to 10 days. 10 days was deemed sufficient to allow the autocorrelation to drop to very low values and remove the correlation between two events. The long-lag noise for each time lag is the 75th quantile of the autocorrelation as in Marra et al. (2018). The resulting running parameter equals the first time lag at which the temporal autocorrelation is comparable to the long-lag noise. The running parameter is calculated for each grid-cell. For the 3-hourly duration, we removed the blocks containing non-zero rainfall within a correlation window and only kept the highest value. For longer durations, independent events satisfy two conditions: (1) events are separated at least by the running parameter (the length of the independence that was determined by declustering); and (2) 3-hourly blocks are only included once. To ensure this, 3-hourly blocks are summed together using moving windows to create intensities for longer durations. Then, one of two cases arises: (a) the running parameter is smaller than the duration: then the event is already independent (condition 1). We simply take the highest intensity in a moving window, and remove all overlapping ones to satisfy condition 2; (b) the running parameter is greater than the duration: we only take the highest value in the window of the running parameter (condition 1), and remove all overlapping blocks (condition 2).

HYDROLOGICAL YEAR

A common challenge in global-scale assessments is the delineation of the hydrological year, given the regional variability in the climatological precipitation seasonality. We therefore developed an uniform way to define the hydrological year. To avoid splitting one rainy season over two different years, we computed the median of the monthly precipitation for each grid-cell, and defined the start of the hydrological year to be the first day of the driest month. Supporting Information Section 2.2 Fig. S2.2a shows the starting month of the hydrological year as determined by this method. These data are also available in the GPEX dataset (Gründemann et al., 2020). As MSWEP-V2.2 spans the interval from 1 January 1979 to 31 October 2017, we discarded the data prior to the start of the first hydrological year, thus keeping 38 complete years. Only where the hydrological year starts in December there are just 37 complete years, which occurs in 5.8 % of the grid cells.

We also investigated whether there is a significant difference between the use of calendar and hydrological years for the estimated daily extremes for GEV and MEV. The POT method is based on the values over a high threshold, irrespective of when they occurred. Therefore, there is by definition no difference in calculating the extremes using hydrological or calendar years for the POT method. To determine the difference for GEV and MEV, we first calculated the daily return levels for normal calendar years, using the MSWEP data from 1979 to 2016. Then, we calculated the return levels for the same distributions and the same years, by removing the months before the start of the hydrological year from the year 1979 and adding them to the year 2016. We did this in order to use the exact same data and ensure that the differences in the return level estimates are solely due to a different starting month.

2.2.2 EXTREME VALUE DISTRIBUTIONS

Three different extreme value distributions were fitted to the MSWEP data to calculate extreme precipitation return levels, and to provide an indication of dependence of the spread in return levels as a function of the distribution used. These three extreme value distributions are the GEV, POT and MEV. Annual (hydrological year) maxima were used to estimate the three parameters of the GEV using the L-moments approach, because of its robust performance for small samples (Hosking, 1990). The GEV cumulative distribution function (CDF) is given by:

$$G(z) = \begin{cases} \exp\left\{-\left[1+\xi\left(\frac{z-\mu}{\sigma}\right)\right]^{-\frac{1}{\xi}}\right\}, \xi \neq 0 \\ \exp\left\{-\exp\left[-\left(\frac{z-\mu}{\sigma}\right)\right]\right\}, \xi = 0 \end{cases} \tag{2.1}$$

with location parameter $\mu \in (-\infty, \infty)$, scale parameter $\sigma > 0$, and shape parameter $\xi \in (-\infty, \infty)$. The annual extremes estimated by GEV are translated into those of the parent distribution, following Koutsoyiannis (2004a, equation 3).

As a second EV model we used a Peaks Over Threshold approach, describing precipitation accumulations exceeding a high threshold using a GP distribution, while modelling the frequency of threshold exceedances using a Poisson point process (Coles, 2001; Davison and Smith, 1990). This framework also yields GEV as the resulting extreme value distribution, which is then used to determine the quantile corresponding to a given return period. The GP CDF is given by:

$$H(y) = \begin{cases} 1-\left(1+\frac{\xi y}{\beta}\right)^{-\frac{1}{\xi}}, \xi \neq 0 \\ 1-\exp\left(-\frac{y}{\beta}\right), \xi = 0 \end{cases} \tag{2.2}$$

where $y > 0$ are precipitation excesses over the threshold, with $\beta > 0$ and $\xi \in (-\infty, \infty)$ the GP scale and shape parameters respectively. A relevant aspect in applying the POT model is a suitable choice of the threshold used to define precipitation exceedances. Our global-scale application requires studying the distribution of precipitation extremes across markedly different climatic regions, thus excluding the adoption of a constant threshold value. We studied the effect of the threshold choice using multiple selection methods on a global sample of grid cells (see Supporting Information Section 2.3 and

and Fig. S2.4). Our results showed that the choice of the method had a limited effect on the estimated return levels (Fig. S2.4a). We therefore chose to perform our global analysis by selecting for each cell a threshold value such that it is exceeded on average 3 times each hydrological year. Because of this choice, the sample size available for fitting the GP distribution remains constant across different precipitation durations. The method used to fit the parameters of the GP distributions was the Probability Weighted Moments (PWM; e.g., see Hosking and Wallis, 1987).

The third model we used is the MEV distribution (Hosseini et al., 2020; Hu et al., 2020; Marani and Ignaccolo, 2015; Miniussi et al., 2020a,b; Zorzetto et al., 2016). In the MEV framework, all 'ordinary' precipitation events, i.e. all events above a small threshold, are used to infer the EV distribution. The threshold we applied is 0.2 mm $3h^{-1}$, coinciding with the earlier defined 'wet event'. Weibull parameters were estimated for each hydrological year separately, based on all wet events using the PWM method (Greenwood et al., 1979) as done in Zorzetto et al. (2016). The MEV-Weibull CDF is given by:

$$\zeta_m(x) = \frac{1}{M}\sum_{j=1}^{M}\left\{1-\exp\left[-\left(\frac{x}{C_j}\right)^{w_j}\right]\right\}^{n_j} \tag{2.3}$$

where j is the hydrological year ($j = 1,2,\ldots,M$), $C_j > 0$ is the Weibull scale parameter, $w_j > 0$ is the Weibull shape parameter, and n_j is the number of wet events observed in hydrological year j (Marani and Ignaccolo, 2015).

OBSERVED RETURN PERIODS

The MSWEP dataset analyzed here has 38 complete years of data. Therefore, the empirical return period associated with the maximum value on record computed according to the Weibull empirical frequency estimate is $T_{\text{observed}} = 39$ years. However, only 91 % of all cells had 38 complete years of data, so the maximum observed return period is sometimes lower: for 7 % of the cells only 37 complete years were available, and for 2 % of the cells 36 years or less were available. However, for simplicity we still refer to the corresponding maximum return level as T39 in the results.

STUDY AREAS

In order to compare the three extreme value distributions, we selected fourteen case study areas. They collectively cover a wide range of climates and domain sizes, the locations of which can be found in Fig. 2.3a. Within a single case study area, we expect the precipitation estimates to be statistically homogeneous because of their precipitation generating mechanisms (Cavanaugh and Gershunov, 2015; Cavanaugh et al., 2015), elevation (Ragulina and Reitan, 2017), or average annual rainfall.

TAIL BEHAVIOR

Both the GEV and MEV distributions are flexible and can describe different tail behaviors. The interpretation of the tail parameter of the two distributions differs, as illustrated in Supporting Information Section 2.4 Fig. S2.5 for different combinations of scale and shape parameters. The shape parameter ξ of the GEV distribution, obtained either through the annual maxima or POT approach, encodes the nature of the tail of the

distribution. Based on the value of ξ, the GEV can take one of three forms: a positive GEV shape parameter ($\xi > 0$, *"Fréchet"*) corresponds to a power-law tail, i.e., to a slowly-decaying probability of large events. This heavy-tail behavior contrasts with the case of an exponential tail ($\xi = 0$, *"Gumbel"*), and with the case of a distribution with an upper end point, which corresponds to negative values of the shape parameter ($\xi < 0$, *"inverse Weibull"*).

The MEV distribution assumes that precipitation events are Weibull-distributed. The tail decay of this distribution is controlled by its shape parameter: for $w < 1$ its tail behavior is "sub-exponential", i.e., heavier than that of an exponential (recovered for $w = 1$), albeit with a characteristic scale (Wilson and Toumi, 2005; Laherrere and Sornette, 1998). For $w > 1$ the Weibull tail is super-exponential, with a fast decaying tail, while still retaining an infinite upper end point. Hence, the shape parameter of the Weibull distribution encodes the propensity of a site to be subjected to large extreme events (Wilson and Toumi, 2005; Zorzetto et al., 2016). However, the tail decay of the MEV distribution is not only dependent on that of ordinary values (through w) but is also affected by the yearly number of events (Marra et al., 2018) and by the inter-annual variations of C_j, w_j and n_j.

Whereas the tail behavior of GEV and POT can easily be inferred from the shape parameter of their distributions, for MEV it depends on multiple parameters, making direct comparison between MEV and GEV/POT based on their parameters alone cumbersome. In an effort to nonetheless compare these methods, we have come up with a measure of heaviness that is based on the return levels themselves (Fig. 2.1). It quantifies how much distributions differ from an exponential one. For an exponential distribution, the 100-year return level (E100) is as follows: E100 = T1 + b + b. Where b (blue arrows Fig. 2.1) is the difference between the 10-year (T10) and 1-year (T1) return level, i.e.: b = T10 − T1. For any distribution that differs from a purely exponential one, the difference between the 100-year return level (T100) and the 1-year return level (T1) can be described as:

$$\mathrm{T100} = \mathrm{T1} + b + b + a \tag{2.4}$$

In this equation a (red arrow in Fig. 2.1) is the additional increase caused by the heaviness of the tail, a = T100−T1−2b (Fig. 2.1). For any given extreme value distribution (red dashed line in Fig. 2.1), a positive a is indicative of heavy tails, and a negative a of thin tails. For pure exponential tails (blue dotted line in Fig. 2.1) it holds that $a = 0$. The value for a is highly dependent on the local precipitation systems, so we defined the heaviness amplification factor $h_{\mathrm{T1-T10-T100}}$ to be a normalization of a:

$$h_{T1-T10-T100} = \frac{a}{b} = \frac{\mathrm{T100} - \mathrm{T1} - 2 \times (\mathrm{T10} - \mathrm{T1})}{\mathrm{T10} - \mathrm{T1}} = \frac{\mathrm{T100} - 2 \times \mathrm{T10} + \mathrm{T1}}{\mathrm{T10} - \mathrm{T1}} = \frac{\mathrm{T100} - \mathrm{T10}}{\mathrm{T10} - \mathrm{T1}} - 1 \tag{2.5}$$

In words, the meaning of $h_{\mathrm{T1-T10-T100}}$ is the fractional additional increase between T100 and T10 that is more than the increase that could be expected from a pure exponentially tailed distribution. A distribution has a heavy tail for $h > 0$ and a thin tail for $h < 0$. Here, we chose a range for the heaviness metric over return periods from 1 to 100 years, since these return levels are known to be mostly influenced by the underlying data

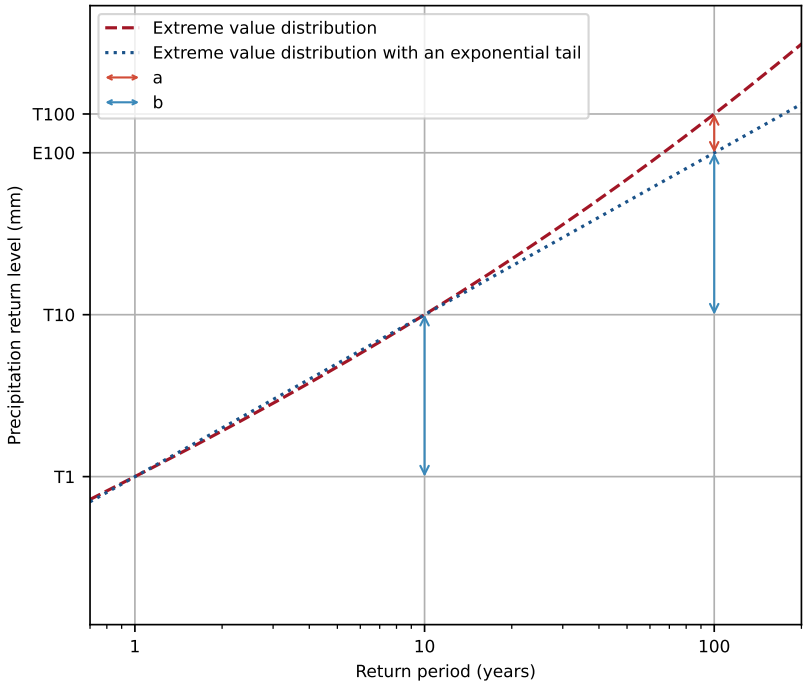

Figure 2.1: Illustration of our method to measure the tail heaviness for any distribution based on return levels only. E100 is the 100-year return level if the extreme value distribution has an exponential tail. T100 is the 100-year return level for any extreme value distribution that differs from an exponential one.

(Rajulapati et al., 2020). Yet, it should be noted that this metric may easily be adjusted to other return periods and other factors between the return periods. For GEV and POT the heaviness metric is independent of the return period range as long as the return periods are a factor 10 apart, because it is solely determined by the shape parameter. Although for MEV this heaviness metric is only valid for the return period range over which it is computed, using other ranges (T2-T20-T200, T5-T50-T500, and T10-T100-T1000) did not yield significant differences (Supporting Information Section 2.5+2.6, Fig. S2.7+2.8).

2.3 RESULTS AND DISCUSSION

2.3.1 HYDROLOGICAL YEAR

Fig. 2.2 shows the frequency distribution of 1000-year return levels estimated using calendar and hydrological years for GEV and MEV. The spatial distribution of the T1000 differences is presented in Supporting Information Fig. S2.2b for GEV and Fig. S2.2c for MEV, and Fig. S2.3 presents the frequency distributions of all analyzed return levels. The difference between the return levels estimated using calendar or hydrological years is greatest when the hydrological year starts around April-September, as in the Mediterranean, Middle-East, Southern Africa, Brazil, Indonesia and Western US (see Support-

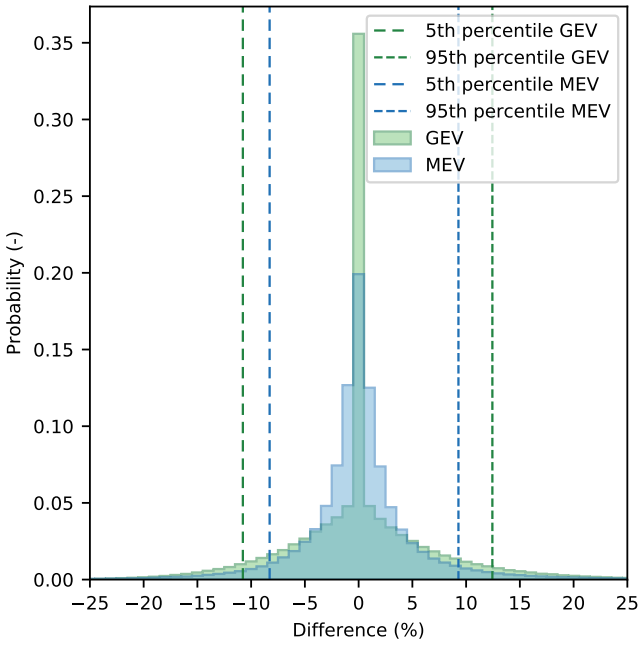

Figure 2.2: Weighted histogram showing the percentage difference in the values of T1000 quantiles calculated using calendar years and hydrological years. Included in the figure are all cells where the start of the hydrological year is different than the calendar year (i.e., the hydrological year does not start in January, see Supporting Information Fig. 2.2a). A negative difference indicates that the T1000 estimate is larger using hydrological years, whereas a positive difference indicates that the T1000 estimate is larger using calendar years.

ing Information Fig. S2.2). This is the case because there are many different events included in hydrological compared to calendar years, resulting in different events and annual maxima and therefore differences in the estimated extremes. For MEV the overall sensitivity in T1000 estimates remains lower than that of GEV, suggesting that regional sensitivity to the definition of block maxima can be quite significant for the GEV approach.

On the other hand, we found that in the case of GEV quantiles the fraction of sites characterized by differences within ±0.5 % is larger than for MEV. When the hydrological year starts around November-February, it is only shifted by a few months so the annual maxima mostly stay the same between the calendar and hydrological years. For GEV this means that for many cells there is almost no difference in the T1000 estimates, whereas for MEV the difference is small.

2.3.2 EXTREME PRECIPITATION ESTIMATES

Fig. 2.3 shows the 100-year precipitation return levels for a 24-hour duration. Extreme value estimates for other durations and return periods are featured in the Global Precipitation EXtremes (GPEX) dataset (Gründemann et al., 2020). The spatial patterns of

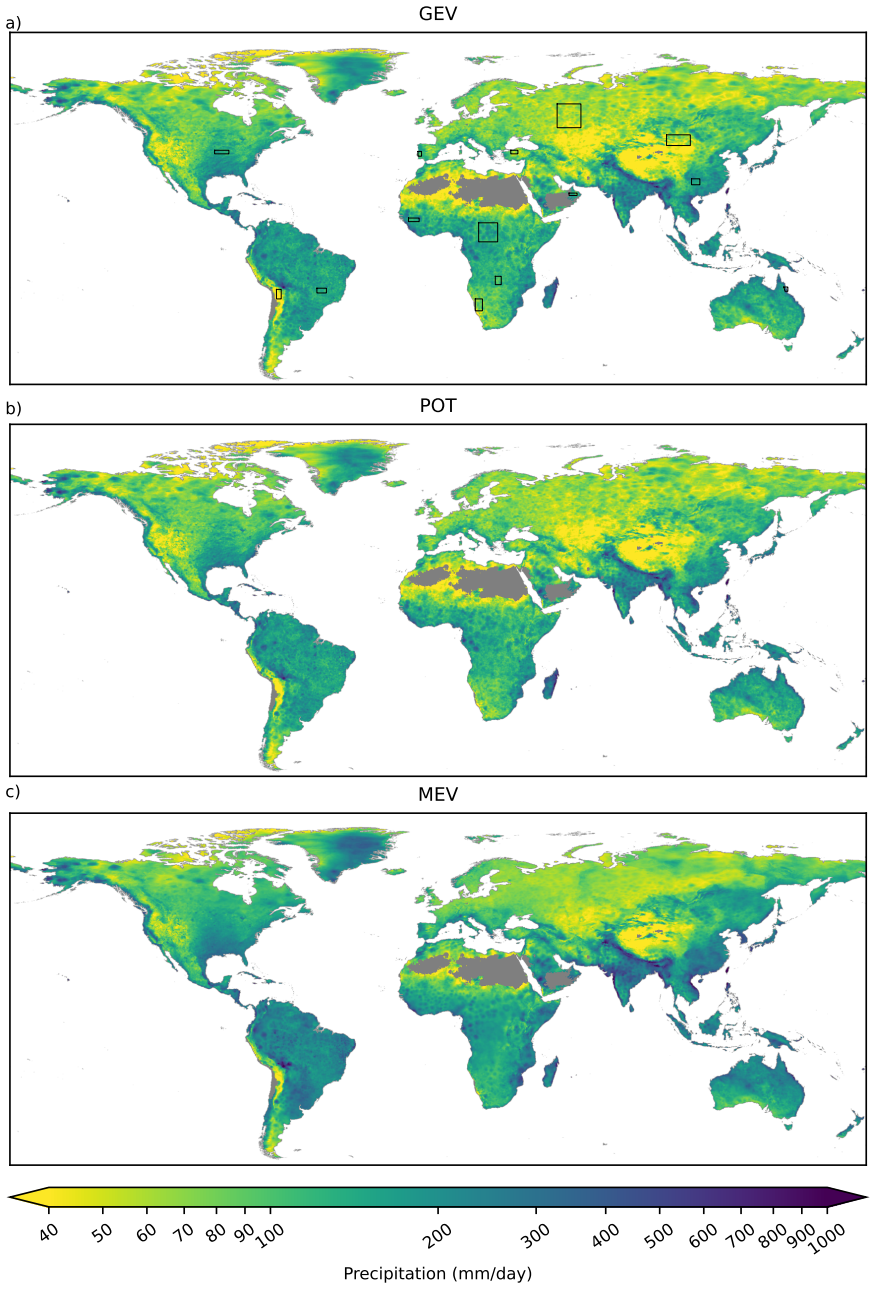

Figure 2.3: Precipitation return levels with a duration of 24-hours for a 100-year return period for different extreme value distributions: (a) the Generalized Extreme Value (GEV) distribution, (b) the Peak Over Threshold (POT) method, and (c) the Metastatistical Extreme Value (MEV) distribution. The colorbar has a logarithmic scale, where yellow and purple colors respectively indicate low and very high 100-year precipitation return levels. The black rectangles in panel a are the case studies corresponding to the areas in Fig. 2.4. Dry areas and cells with too many discarded values are masked in gray following the method in section 2.1.1.

the extremes estimated by GEV and MEV are similar to Zorzetto and Marani (2020, their Figure 9), while the spatial pattern of the underlying GEV parameters are consistent with Courty et al. (2019, their Figure 1). The global spatial pattern of return levels for the three EV methods is similar, although large regional differences can be observed. The GEV and POT results are similar in magnitude and show similar differences when compared to MEV. The estimated precipitation extremes are generally lower for both GEV and POT compared to MEV quantiles. MEV estimates exhibit smooth spatial patterns, whereas the spatial patterns using GEV and POT are more irregular, consistent with the results of Zorzetto and Marani (2020) for the conterminous US. Furthermore, Fig. 2.3 reveals the presence of a large number of circular areas with heavier extremes, corresponding to the location of gauges used for correcting precipitation estimates in the MSWEP algorithm (Beck et al., 2019b). The effect of these local corrections is much larger for traditional EV models (POT and GEV) than for MEV. The reduced spatial coherence in patterns of extremes for GEV and POT is particularly evident in the Great Plains of North America, and in Northern Russia, Southeast Asia, and Central Africa.

In order to study the ability of the three distributions to capture the spatial coherence of precipitation extremes, we calculated the coefficient of variation (CV) for fourteen study areas, see Fig. 2.4. The CV is the ratio of the standard deviation to the mean and is used to compare the relative variation between the study areas. The higher the CV, the higher the relative spread of the precipitation estimates within a spatial domain. This figure shows quite similar behavior for GEV and POT, though POT has a slightly lower spread. The CV for MEV is generally lower, which points to more spatially coherent T100 precipitation estimates based on single point time series (with 38 years of training data). The CV for all EVDs is higher for areas that are more arid (e.g. Bolivia, Mongolia, Namibia and Oman).

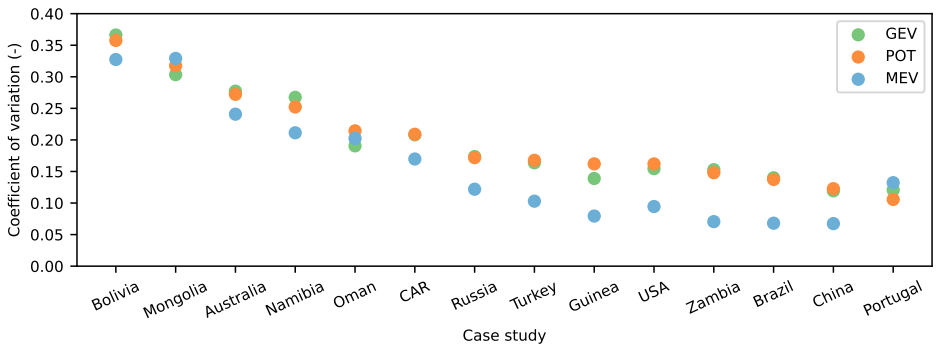

Figure 2.4: Coefficient of variation for the difference in estimated T100 quantiles for the three extreme value methods for 24-hour precipitation at selected case study areas. The locations of the case study areas are displayed in Fig 2.3a.

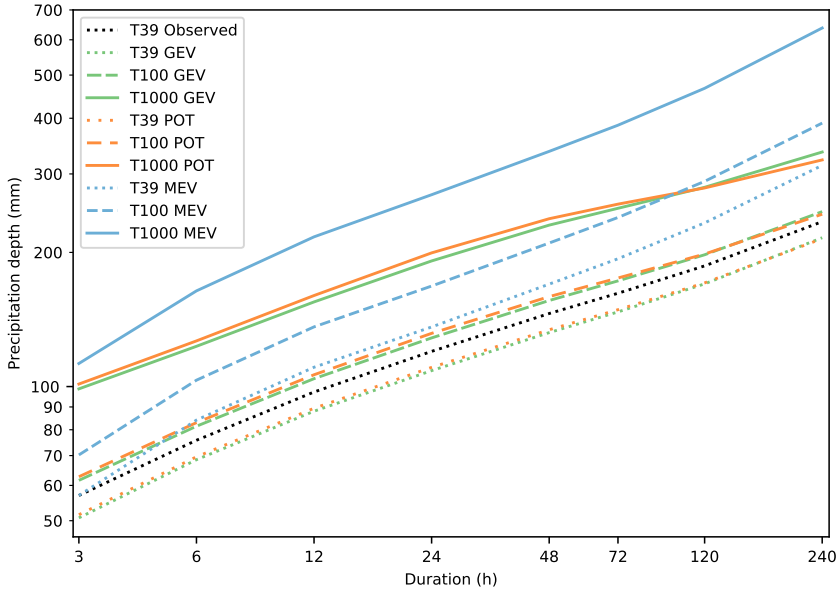

Figure 2.5: Area-weighted average depth-duration-frequency curves for the global land surface (log-log scale). T39 Observed is the mean spatially weighted maximum precipitation observed in the MSWEP-V2.2 dataset.

To further investigate the global differences in magnitude between the three methods, we examine the extremes for each distribution using a spatially weighted mean over the global land surface. This is displayed for multiple return periods and durations as depth-duration-frequency curves (Fig. 2.5). We first compare the maximum precipitation observed (T39 observed, the black dotted line in Fig. 2.5) in the dataset to the precipitation predicted from each distribution. While locally the empirical T39 estimate could be very different from the true return level, we expect the global average of this value to be representative of the true T39. For GEV and POT, we expected the estimated T39 to be close to the observed value since only the largest values are used to fit these distributions. For MEV, we did not necessarily expect a good agreement for T39, but its performance should be better for return levels greater than the length of the observation time series (Marra et al., 2018, 2019b; Schellander et al., 2019; Zorzetto et al., 2016). The results in Fig. 2.5 show that for the short duration events, the observed T39 is close to the T39 for all three distributions. For increasing durations, the deviation between empirically observed and EV modeled T39 quantiles increases, particularly for MEV. This could be because a smaller number of events per year is used for the fit of MEV-Weibull, whereas the number of events used for the fit of GEV and POT remains constant for all durations. Both GEV and POT show an underestimation and MEV an overestimation. This figure also shows again that the differences between GEV and POT are small. The global average estimated extremes for GEV and POT are notably lower than for MEV, as was already visible from Fig. 2.3. This difference is more pronounced for larger return periods and longer durations.

One reason the quantiles estimated using MEV are higher than using GEV and POT is related to the increase in estimation uncertainty of Weibull parameters and higher inter-annual variability when the number of events per hydrological year is low (Miniussi and Marani, 2020). This is especially relevant in arid regions and for long durations (Fig. 2.3 and Fig. 2.5). For instance, for 5 and 10-day durations the average annual number of events is 37 and 22 events respectively. It is therefore possible that this leads to an over-estimation by MEV. To overcome this, windows of two or more years could result in a better parameter estimation (Miniussi and Marani, 2020).

2.3.3 TAIL BEHAVIOR

To better understand the differences between extremes estimated using the three methods, we analyze their tail behavior using the heaviness amplification factor $h_{\mathrm{T1-T10-T100}}$ (Eq. 2.5). Fig. 2.6 presents $h_{\mathrm{T1-T10-T100}}$ for a 24-hour duration worldwide for each of the three distributions. We refer to Figs, S2.9-S2.15 in Section 2.7 in the Supporting Information for maps of $h_{\mathrm{T1-T10-T100}}$ for the other durations. Note that as expected the heaviness metric gives a near-identical pattern for both GEV and POT as compared to using their shape parameter directly, but this is less similar for MEV and its yearly mean shape parameter (compare Fig. 2.6 to Fig. S2.6).

Both GEV (Fig. 2.6a) and POT (Fig. 2.6b) exhibit a large spatial variability in addition to a low spatial coherence. This makes it difficult to discern clear spatial patterns with the exception of a few notable regions. For instance, in the Amazon, $h_{\mathrm{T1-T10-T100}}$ is mostly negative, suggesting a tail with an upper limit, while in Eastern and Southern Australia $h_{\mathrm{T1-T10-T100}}$ it is strongly positive, denoting strong heavy tail behavior. This map roughly corresponds to the spatial patterns of the GEV shape parameter for daily precipitation shown by Papalexiou and Koutsoyiannis (2013, their Figure 13) and Ragulina and Reitan (2017, their Figure 4) as well as a metric based on the mean excess function Nerantzaki and Papalexiou (2019, their Figure 7a). Given the more similar results between these studies, who used for a large part the same data, we think that the differences with our maps are likely caused by using different underlying data rather than the particular heaviness metric. We also find that for the GEV and POT methods, grid cells associated with heavy tails can be adjacent to cells with thin tails. Furthermore, in 28 % of the cells for daily precipitation GEV and POT show a different type of tail, heavy/thin, in the same grid cells. This highlights the large uncertainty associated with estimating reliable tail parameters from short time series and the sensitivity of the GEV and POT methods to sampling effects.

The heaviness of the MEV distribution (Fig. 2.6c) shows a more coherent spatial pattern. At virtually all grid cells the heaviness amplification factor $h_{\mathrm{T1-T10-T100}}$ (Eq. 2.5) indicates heavy tail behavior and there is a high consistency within geographic regions and for all durations (Figures S8-S14). Based on previous studies (Cavanaugh et al., 2015; Nerantzaki and Papalexiou, 2019; Papalexiou and Koutsoyiannis, 2013; Papalexiou et al., 2013; Ragulina and Reitan, 2017), this predominantly heavy-tail behavior of daily precipitation was expected and is well captured by MEV. There are also topographical patterns visible in the heaviness amplification factor (Fig. 2.6c), though they are not as clearly distinguishable as for the shape parameter itself (Fig. S2.6). The heaviness tends to be higher in arid areas, and lower in mountainous areas. Examples of arid areas with high

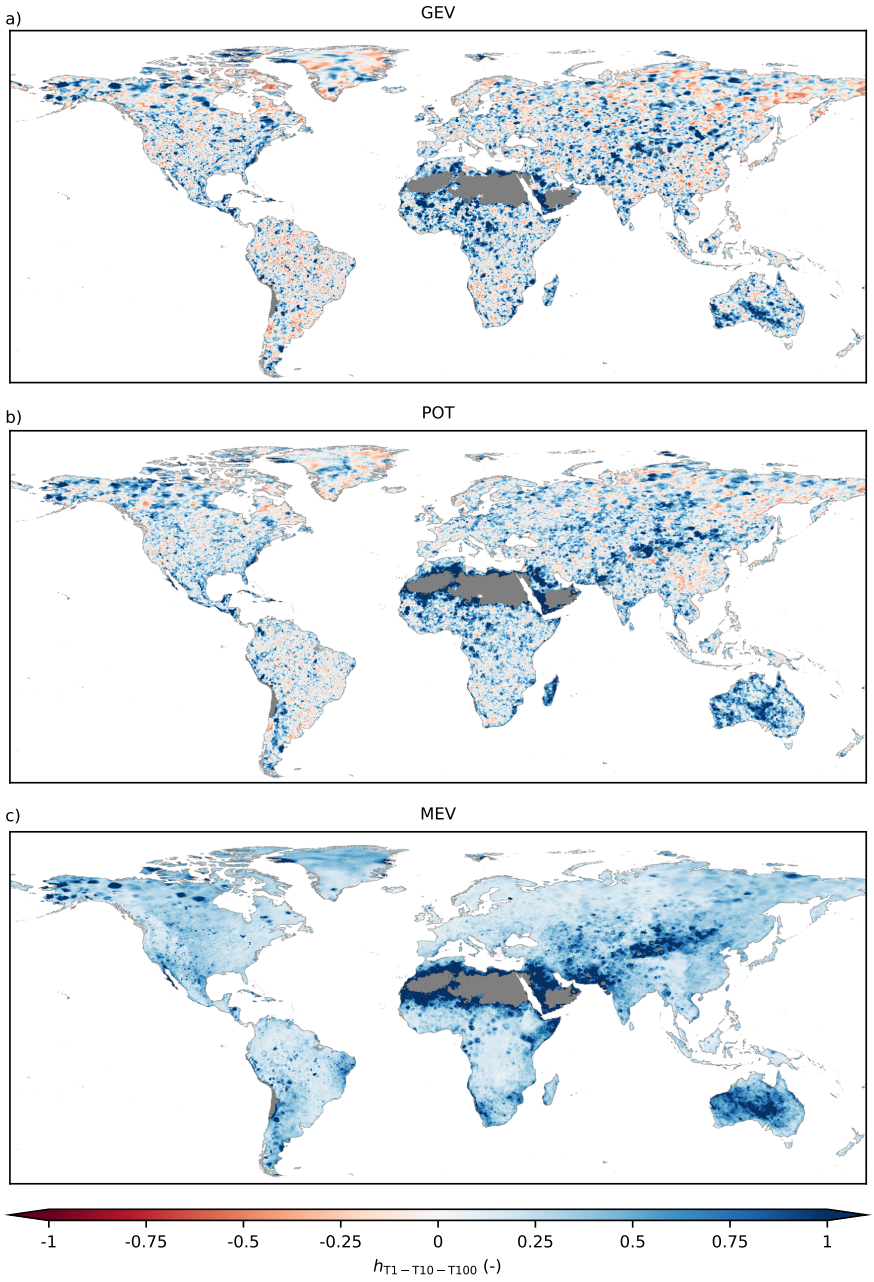

Figure 2.6: The heaviness amplification factor $h_{T1-T10-T100}$ (Eq. 2.5) for daily precipitation calculated for different extreme value methods: (a) GEV, (b) POT, (c) MEV. Red indicates a thin tail, white an exponential tail, and blue a heavy tail. See section 2.2.2 for more information on the heaviness metric, and Figures S8-S14 for maps of $h_{T1-T10-T100}$ for the other durations. Dry areas and cells with too many discarded values are masked in gray following the method in section 2.2.1.

heaviness include the Sahara, the Namib and Kalahari in Africa, the Gobi, Thar and Taklamakan in Asia, the Atacama Desert in South America, large areas of Southwestern Australia, and the Arabian desert and other areas in the Middle East. This same pattern is to a lesser extent also visible for the heaviness of GEV (Fig. 2.6a) and POT (Fig. 2.6b).

At high elevations a small $h_{T1-T10-T100}$ is usually found for MEV (Fig. 2.6c). Examples include the Rocky Mountains and the Sierra Madres in North America, the northern Andes and large areas of the Brazilian Highlands in South America, the Ethiopian Highlands, the Scandinavian Mountains, and the Tibetan Plateau. These spatial patterns are in contrast with what Papalexiou et al. (2018, their Figure 6) found for hourly Weibull tails in the USA, where the heaviest tails are in the mountainous areas, and the thin tails are in the south-east. However, our results correspond well to Ragulina and Reitan (2017, their Figure 4), who showed that heaviness decreases with elevation.

A comparison of the heaviness for different distributions and durations is presented as a boxplot in Fig. 2.7. For spatial maps of the heaviness for the different durations we refer to Figures S8-S14. For GEV and POT, predominantly heavy tails are observed for short durations and thinner tails for long durations. Furthermore, GEV and POT both show a decreasing variability in the heaviness for longer durations, indicated by both shorter whiskers and boxes. The decrease of the heaviness of the tails for increasing durations is in line with the findings of Cavanaugh and Gershunov (2015), who found that longer duration extremes exhibit thinner tails. For GEV and POT the longer durations largely indicate tails with a finite upper end point, in half of the cases for a duration

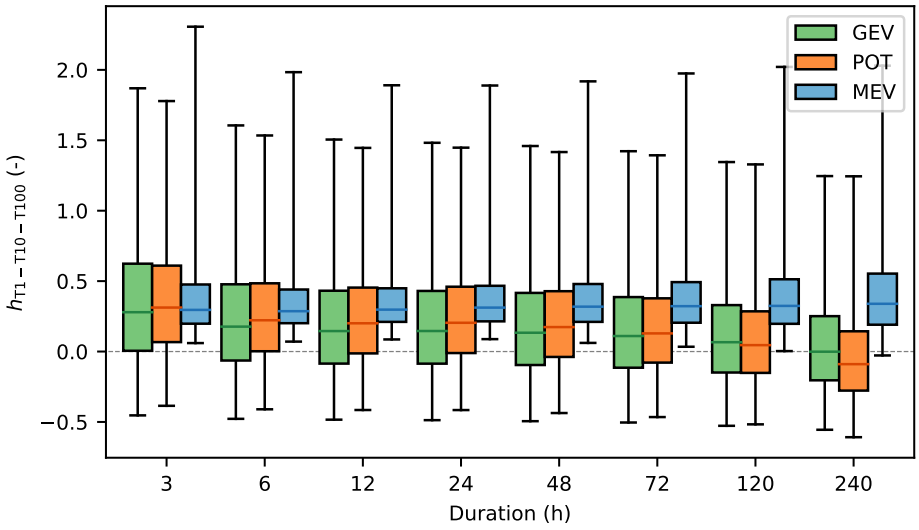

Figure 2.7: Boxplot showing the distribution of the heaviness amplification factor $h_{T1-T10-T100}$ (-) for different durations and extreme value methods: GEV, POT and MEV. The whiskers denote the 1st and 99th percentiles. The top and bottom of the boxes represent the 75th and 25th percentiles, respectively. The dashed gray horizontal lines indicate exponential tails. See section 2.2.2 for more information on the heaviness metric.

of 10 days for GEV, and more than half for POT. One implication of this finding is that, when computing return levels for a single location (see Figures S4 and S15), it is possible for the largest return periods that shorter duration quantiles estimate a higher precipitation depth than the longer duration quantiles. This is physically impossible (see Fig. S2.16a,b,f and g), and we should thus be extremely careful when interpreting such results.

MEV, on the other hand, shows different heaviness patterns than GEV and POT (Fig. 2.7 and Figures S8-S14). MEV shows almost entirely heavy-tail behavior, which remains consistent across the range of durations examined. Furthermore, also the variability for MEV is constant across durations, though with a slight increase for longer durations. This is in line with Fig. 2.5, where the difference between the T39 observed and estimated with MEV increases for the longest durations. It could be that MEV is overestimating these return levels of these largest durations. A possible way to improve the estimations would be to group multiple years together, as per Miniussi and Marani (2020).

The MEV distribution produces a spatially and temporally coherent heavy tail behavior based on a 38 years calibration sample and a single grid-cell analysis. This is a promising result, as MEV, in contrast to the traditional methods analyzed, provides a more spatially coherent picture of precipitation extremes without any prior hypothesis on its spatial structure, for example through a spatial clustering scheme (Demirdjian et al., 2018). In fact, the spatial structure of the tail heaviness obtained through the MEV analysis could be used as a measure of statistical homogeneity for regionalization studies.

2.4 CONCLUSIONS

The aim of this research was to quantitatively characterize the spatiotemporal variation of global precipitation extremes and their associated extreme value distribution tails. We have fitted three different extreme value methods (GEV, POT, and MEV) to a global precipitation dataset, MSWEP V2.2, to estimate extreme precipitation return levels for eight durations. In order to compare the tails of the three distributions, we introduced a novel heaviness amplification factor $h_{\mathrm{T1-T10-T100}}$ (Eq. 2.5). Instead of using calendar years to delineate between different years, we used hydrological years, the start of which we defined as the driest month. We demonstrated that there is a substantial difference in the extremes depending on the definition of yearly blocks used in the extreme value analysis (Fig. 2.2). Although there is no systematic bias, we still recommend to apply the extreme value analyses for estimating extreme precipitation based on hydrological years in future studies. Our analysis indicates that this can be particularly relevant in the Southern hemisphere and in regions characterized by marked seasonal cycles.

It is well known that the traditional GEV and POT methods require very long data series for accurate estimation of the tail behavior, and our study confirms that there is a low spatial coherence for the tail properties of both distributions (Fig. 2.6a and b) using just 38 years of training data. The tail properties of the MEV distribution are spatially more coherent (Fig. 2.6c) and hence the estimated return levels are more spatially coherent as well (Fig. 2.3c). This spatially coherent behavior, consistent with previous results obtained over the conterminous US (Zorzetto and Marani, 2020), shows that the MEV

distribution is able to capture spatially consistent tail behavior from short time series and by a single grid-cell analysis, without any prior information on the spatial precipitation structures. The analysis of the MEV tail behavior reveals distinct spatial patterns, as the heaviness appears to be controlled by climate zones and orography. Heavier tails are observed in arid areas, and thinner tails in mountainous regions. More in-depth analyses are necessary to draw definite conclusions on what exactly controls the heaviness of extreme value distribution tails. The performance of MEV is promising for regions without long local precipitation records. Furthermore, our study shows that the tail behavior captured by MEV is coherent and heavy both spatially and temporally (Figures 2.6, 2.7 and S8-S14). For GEV and POT, on the other hand, the tail behavior decreases with increasing event duration, resulting in a thin tail with a finite endpoint for about half of the cells for a duration of 10 days. The 'correct' relationship between heaviness and precipitation duration warrants further investigation.

We also conclude that both GEV and POT generally underestimate the observed extremes, whereas MEV overestimates them (Fig. 2.5). This occurs particularly for long-duration extremes and large return periods. For MEV an explanation could be that there are fewer events per year used for the yearly distribution fits, resulting in larger interannual variability and thus overestimation of extremes. We do consider it likely, however, that the results could be improved, for instance by changing the event threshold or by fitting the Weibull distribution over two or more years for dry areas (Miniussi and Marani, 2020), so as to reduce inter-annual variability of the parameters due to samples of limited length. Our results suggest that this issue is particularly relevant at the longest durations examined. For GEV and POT the spatial consistency of the results could also be improved by adopting spatial extreme models (Davison et al., 2012; Huser and Wadsworth, 2020).

The data generated for this study are openly available as the GPEX dataset (Gründemann et al., 2020). These data include extreme precipitation return levels and extreme value distribution parameters for durations between 3 hours and 10 days at a global gridded 0.1° resolution. They could be used by engineers as a reference of precipitation extremes for data-scarce regions in particular. For scientific purposes, all underlying parameters are also available and can be used to answer several outstanding questions, such as: what are the controls on the tail behavior of extremes, and what is driving the different changes in tail heaviness with duration for GEV, POT, and MEV?

3

SEASONALITY OF HISTORICAL PRECIPITATION EXTREMES

This chapter is based on: Gründemann, G. J., Zorzetto, E., van de Giesen, N. C., van der Ent, R. J. *Historical shifts in seasonality and timing of extreme precipitation,* accepted for publication in Geophysical Research Letters.

SUMMARY
Global warming impacts the hydrological cycle, affecting the seasonality and timing of extreme precipitation. Understanding historical changes in extreme precipitation occurrence is crucial for assessing their impacts. This study uses relative entropy to analyze historical changes in seasonality and timing of extreme daily precipitation occurrences on the global domain for 63 years of ERA5 reanalysis data. Our analysis reveals distinct regional patterns of change. During the second half of the 20th century, Africa and Asia experienced high clustering of precipitation extremes. Over the past 60 years, clustering increased in Africa while becoming more spread out in Asia. North America and Australia had initially lower clustering and showed slight increases over time. Extreme events in extra-tropical land regions mainly occurred in summer, with modest shifts in timing. These findings have implications for risk assessments of natural hazard like flash floods and landslides, emphasizing the necessity for region-specific adaptation strategies.

3.1 INTRODUCTION

Global warming is known to intensify the water cycle, leading to an increase in climate extremes (Allen and Ingram, 2002; Easterling et al., 2016; Murray and Ebi, 2012). Historical data reveals increases in observed precipitation extremes (Alexander, 2016; Asadieh and Krakauer, 2015; Papalexiou and Montanari, 2019), and projections indicate further intensification in the future (e.g., Donat et al., 2016b; Fowler et al., 2021; Gründemann et al., 2022; Meredith et al., 2019; Moustakis et al., 2021; Pfahl et al., 2017; Pendergrass and Knutti, 2018; Tandon et al., 2018; Westra et al., 2014). Yet, these patterns and shifts are not uniform across the world. Factors such as topography, oceanic cycles and atmospheric patterns influence the spatiotemporal distribution and seasonality of extreme precipitation events (Dey et al., 2021; Fernandes and Rodrigues, 2018; Gründemann et al., 2023; Haylock et al., 2006). In tropical regions for instance, extreme precipitation predominantly occurs during monsoon seasons, with monsoon-affected areas witnessing an expansion, intensification of rains, and a prolonged monsoon season (Chen and Sun, 2013; Kitoh et al., 2013). In contrast, mid-latitudes often experience precipitation extremes during the transitional seasons, with many Mediterranean basins observing a shift to earlier in the year (Tramblay et al., 2023). Polar regions, meanwhile, are witnessing an increase in precipitation extremes during summer, with a transition from snow to more rain (Landrum and Holland, 2020; Loeb et al., 2022; Wang et al., 2021).

Changes in seasonality of extreme precipitation can have negative impacts on hydrological systems, agriculture, and overall water resource management (Kundzewicz et al., 2018). Additionally, shifts in precipitation seasonality affects flood patterns (Berghuijs et al., 2019; Blöschl et al., 2017; Wasko et al., 2020b,a) and the occurrence of natural hazards, such as flash floods, landslides (Marc et al., 2018; Steger et al., 2023), and debris flow (Nikolopoulos et al., 2015). Moreover, these changes interact with other climate feedback mechanisms, such as snowmelt runoff, atmospheric rivers, and tropical cyclones, amplifying or mitigating the impacts of climate change on various parts of the hydrological cycle (Gershunov et al., 2017; Miniussi et al., 2020b; Tarasova et al., 2023).

In recent decades, relative entropy has emerged as a valuable tool to study the seasonality of precipitation and its extremes. Rooted in statistical physics and information theory (Cover and Thomas, 2005; Greven et al., 2003), this method quantifies the statistical distance between the actual distribution of extreme precipitation occurrences and a uniform distribution (Kullback and Leibler, 1951). Feng et al. (2013) introduced this tool to the field of precipitation research to study the seasonality of monthly rainfall in tropical regions. Since, several studies have used relative entropy to study rainfall seasonality across different time scales and geographical regions (Bal et al., 2019; Limsakul, 2020; Moustakis et al., 2021; Pascale et al., 2015, 2016; Sahany et al., 2018). Hitherto, however, a comprehensive global scale assessment of historically observed changes in timing and seasonality of extreme precipitation is missing.

This study aims to bridge this gap by evaluating the seasonality and timing of extreme daily precipitation. Using the relative entropy measure, we assess the degree of seasonality in extreme precipitation and to evaluate historical trends. By defining extreme precipitation above a relative threshold, we investigate the spatial patterns of these changes across different regions. We use the fifth generation of the European Reanalysis (ERA5)

reanalysis dataset, which provides high-quality and relatively homogeneous precipitation data, allowing for a comprehensive analysis of the observed changes in extreme precipitation seasonality.

3.2 MATERIALS AND METHODS

3.2.1 DATA

Precipitation data were obtained from the ERA5 reanalysis dataset (Hersbach et al., 2018, 2020). This dataset was chosen for its continuous coverage and relatively long temporal span at high spatial and temporal resolutions. While reanalysis datasets provide a comprehensive estimate of the global atmosphere-land-ocean system, it has known issues in accurately simulating convective processes, data assimilation inconsistencies, and limited observations over areas like oceans. The performance of ERA5 in capturing precipitation extremes varies depending on the intensity and location (Lei et al., 2022). ERA5 performs well over the extra-tropics, but exhibits larger errors over the tropics (Lavers et al., 2022). Notably, while ERA5 tends to underestimate the heaviest precipitation events, it reliably captures their general patterns, locations, and magnitude of less intense events (Bandhauer et al., 2022; Hénin et al., 2018; Lavers et al., 2022; Shen et al., 2022).

Hourly precipitation data from 01-01-1959 to 31-12-2021 at a resolution of 0.25° latitude × 0.25° longitude (approximately 30 by 30 km at the equator). These data were aggregated into daily estimates covering 63 years. The analysis involved moving 30-year windows through the dataset, starting with the first 30 years (01-01-1959 to 31-12-1988) and shifting forward by one calendar year for each new 30-year segment. This resulted in 33 such 30-year windows.

3.2.2 PRECIPITATION EXTREMES

We defined precipitation extremes as the highest 3 events per year on average, corresponding to the highest 90 events per 30-year window (or the 99.18th percentile of all day precipitation, or a return period of 0.335 years). Different thresholds were explored to quantify rainfall extremes across various regions, with little impact on the observed trends. Inclusion of more events reduced seasonality (see Fig. S3.1), likely because that incorporates precipitation from various precipitation-generating mechanisms which may be characterized by different magnitudes and seasonal occurrence. This results in more evenly distributed occurrences throughout the year.

3.2.3 RELATIVE ENTROPY AS A MEASURE FOR SEASONALITY

To assess the seasonality of extreme precipitation occurrences, we use Relative Entropy, also known as Kullback-Leiber distance (D_{KL}; Kullback and Leibler, 1951). Relative entropy is a measure of the statistical distance between two probability distributions: (1) the actual monthly distribution of extreme precipitation occurrences and (2) the uniform distribution (Cover and Thomas, 2005). The calculation of relative entropy (D_{KL}) is represented by the following equation:

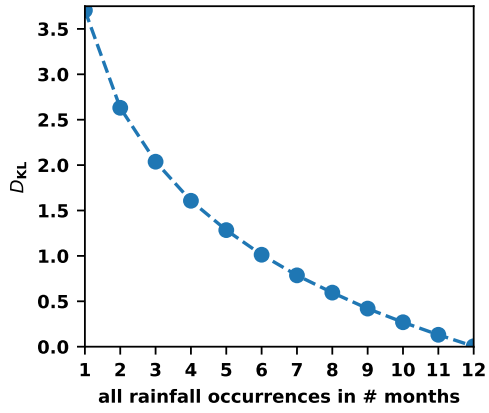

Figure 3.1: The value of the relative entropy D_{KL} (Eq. (3.1) when all extreme rainfall occurrences are evenly distributed over 1 to 12 months.

$$D_{\mathrm{KL}} = \sum_{m=1}^{12} p_m \log_2 \left(\frac{p_m}{q_m} \right) \tag{3.1}$$

In this equation, p_m represents the actual probability distribution of monthly extreme precipitation occurrences, while q_m denotes the uniform distribution of monthly occurrences. p_m is calculated by dividing the number of monthly extreme precipitation occurrences (n_m) by the total number of occurrences ($N = 90$). Therefore, $p_m = n_m / N$. The uniform distribution (q_m) is approximately 0.083 for each month, taking into account the actual number of days in each month. The resulting value of D_{KL} is measured in bits, as the base of the logarithm is 2 (Cover and Thomas, 2005), with a range between 0.005 and 3.7. Higher values indicate a clustering of extreme precipitation occurrences, while lower values suggest a more evenly spread distribution throughout the year. Fig. 3.1 serves as a reference to aid in the interpretation of D_{KL}. A single D_{KL} value is calculated for each 30-year window, resulting in 33 values per grid cell. We note that if two areas have a similar D_{KL} value, that does not mean that the rainfall events in both areas have similar magnitude, precipitation-generating mechanism, or timing.

3.2.4 TIMING

To evaluate the timing and duration of precipitation extremes, the centroid (C) and the spread (Z) of the seasonal distribution were computed as the first and second moments of n_m, respectively. The formulas for calculating C and Z are as follows:

$$C = \frac{1}{N} \sum_{m=1}^{12} m \times n_m \tag{3.2}$$

$$Z = \sqrt{\frac{1}{N} \sum_{m=1}^{12} |m - C|^2 \times n_m} \tag{3.3}$$

C represents the timing, while Z indicates clustering of the extremes around the centroid. Even though C can be estimated for each grid cell, it is not useful for locations with low D_{KL} values, as there is no clear clustering of extremes. These metrics were only estimated for gridcells where the mean $D_{\mathrm{KL}} > 0.27$, indicating clustering of extremes in less than 10 months. To address potential errors related to events around November to February, a six-month shift was applied and C and Z were recalculated and then shifted six months back, yielding C_{shift} and Z_{shift}. The choice between the original and shifted values depended on which produced a lower mean spread for each grid cell. The mean of the original C and C_{shift} as well as Z and Z_{shift} are included in Fig. S3.2. Another approach to do this is using the circular mean as in Dey et al. (2021), but it yields similar results.

3.2.5 REGIONAL ANALYSIS

The regional analysis was conducted for IPCC WGI reference regions (WGI-v4; Iturbide et al., 2020), focusing on land regions. We pooled all events within a region, weighed them by cell size, and calculated the regional D_{KL}, C and Z (Eq. 1-3). To ensure a focus on regions with significant precipitation patterns, areas with very low rainfall, such as the Sahara, were excluded from this study. These dry areas were identified as cells where the mean value of the 90th highest rainfall event in the 30-year windows was below 5 mm day^{-1} (gray cells in Fig. 3.2a). In the regional analysis, we only included regions containing at least 50% of the cells meeting this criterion, excluding the Sahara, Arabian Peninsula, and Eastern Antarctica.

3.2.6 STATISTICAL SIGNIFICANCE

Spearman rank correlation was performed to assess positive and negative monotonic relationships between D_{KL} and C over time in grid cells and regions. The correlation coefficient (ρ) ranges from -1 to 1, indicating the strength of the relationship. Significance was determined for $p < 0.05$. We also have repeated this analysis testing for field significance, following the false discovery rate approach described in (Wilks, 2016, Eq. 3), with minimal impact detected (see Fig. S3.3).

3.3 RESULTS

Fig. 3.2a displays the relative entropy (D_{KL}) of daily extreme precipitation occurrences as the mean value over all 30-year windows per grid cell. D_{KL} follows geographical features like mountain ranges and coastlines. Notably, mountain peaks exhibit low D_{KL} values, while slopes have higher values. Examples are found in the Andes, Patagonia, Scandinavia, Ural Mountains, and Himalayas. Coastlines also display distinctive D_{KL} patterns, with land areas often exhibiting higher values compared to adjacent oceans, seen around western Europe and Morocco, the Red Sea, the coast of eastern Africa, eastern Madagascar, western India, Myanmar, eastern Malaysia, and western Australia. In ERA5, D_{KL} is generally higher on land than over oceans, with the exceptions of the South Pacific ocean, subtropical Atlantic and Arabian Sea. Panel b shows the D_{KL} for each WGI-v4 reference region over land, with regions like Madagascar, Western Africa, and parts of Asia displaying the highest regional D_{KL} values. Conversely, Eastern and West-

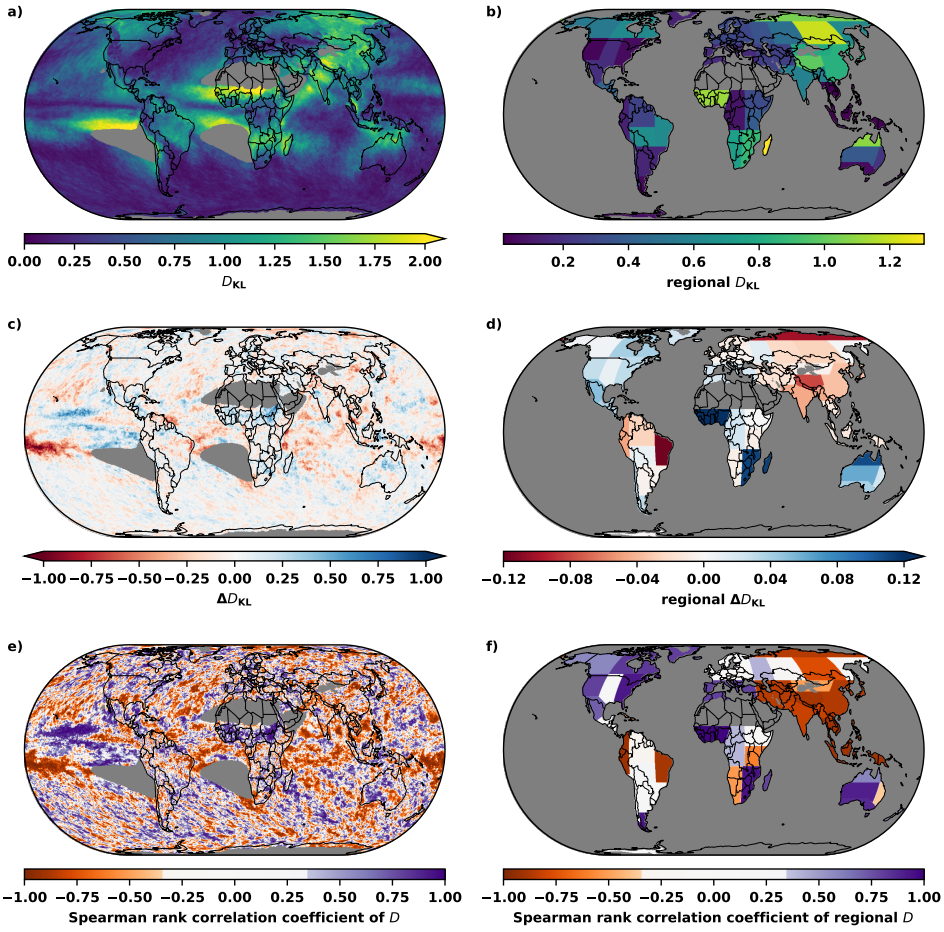

Figure 3.2: Relative entropy of extreme daily precipitation occurrences (D_{KL}, Eq. 3.1). Presented as a) the mean of all 30-year windows analyzed per grid cell, where a low value signifies an even distribution of extreme rainfall throughout the year, and a high value suggest clustering in a specific period. Panel b) shows D_{KL} calculated per WGI-v4 reference region over land. Panel c) shows the difference in D_{KL} between the first land last windows for each grid cell ($\Delta D = D_{1992-2021} - D_{1959-1988}$), with a negative ΔD indicating a more even distribution of rainfall extremes and a positive ΔD indicating more clustering. Panel d) shows the same difference calculated per WGI-v4 reference region over land. Panel e) shows the Spearman rank correlation coefficient of D_{KL} over time, the non-white values indicate statistical significance ($p < 0.05$). Panel f) shows the correlation coefficients calculated per WGI-v4 reference region over land. Dry areas, defined as cells with a mean value of the 90th highest rainfall event in all 30-year windows below 5 mm day^{-1}, are masked in gray. Regions in panels b), d) and f) only include those containing at least 50% of the cells.

ern United States, Southern South America, Southeast Asia and Southern Australia and New Zealand exhibit the lowest D_{KL} values on land.

When comparing the relative entropy of extreme precipitation occurrences in ERA5 (Fig. 3.2a) to that of extreme precipitation of gauge data and a regional climate model in the US (Moustakis et al., 2021, their Fig. 7a and b), the results look largely similar. The main difference is that our threshold of extreme events exhibits a stronger seasonality along the entire west coast and lower seasonality in Arizona and Utah than (Moustakis et al., 2021, their Fig. 7a and b). Furthermore, a comparison of our results to that of monthly precipitation in GPCC (Pascale et al., 2015, 2016, their Figs. 1c), CMAP (Pascale et al., 2015, their Fig. 1d), and CMIP5 historical simulations (Pascale et al., 2016, their Fig. 1d), similar patterns emerge again. However, the relative entropy of extreme occurrences is higher, indicating a greater clustering of extreme events compared to monthly precipitation. Regions such as northern North America, northern Europe, and various parts of Asia show a particularly pronounced clustering of extremes. Additionally, the geographical features of mountain ranges and coastlines are more prominent in the relative entropy of extreme occurrences compared to monthly precipitation.

Figs. 3.2c and d demonstrate the changes in relative entropy between the first and last window for each grid cell and for WGI-v4 reference regions, respectively. The observed changes display a mixed pattern of increases and decreases in precipitation seasonality. Notably, Sub-Saharan Africa, Australia, and North America exhibit increasing trends, suggesting a greater clustering of extreme events. Western Africa and North-Eastern Africa shows the highest increase in D_{KL}, indicating a further intensification of extreme event clustering. Conversely, Asia, the Caribbean and North-East South America display decreasing trends, implying a transition towards a more even distribution of extreme events.

Figs. 3.2e and f present the Spearman rank correlation coefficient of D_{KL} over time. The correlation patterns align closely with those seen in $\Delta\ D_{\mathrm{KL}}$, albeit with stronger signals. The correlation coefficient is statistically significant ($p < 0.05$) in 73.0% of all cells and 73.4% of land cells (see Table 3.1). Out of the significant cells, approximately half of the land cells have become more and less clustered. When correcting for field significance, the results obtained in Fig. 3.2e do not change appreciably (see Fig. S3.3a).

Figs. 3.3a and e showcase the zonal means of D_{KL} for each latitude on respectively the global domain and over land only. Lower D_{KL} values are evident in the southern hemisphere, with greater variability observed over land. The subtropics and most northern latitudes exhibit high D_{KL} values. Drier areas display the highest inter-annual spread,

Table 3.1: Statistical significance ($p < 0.05$) of D_{KL} trends with time, using the Spearman rank correlation coefficient. Dry areas, namely the cells in which the mean value of the 90th highest rainfall event in the 30-year windows is below 5 mm day^{-1}, are not included.

	global	global land
Correlation coefficient significant	73.0%	73.4%
- of which positively	47.9%	50.1%
- of which negatively	52.1%	49.9%

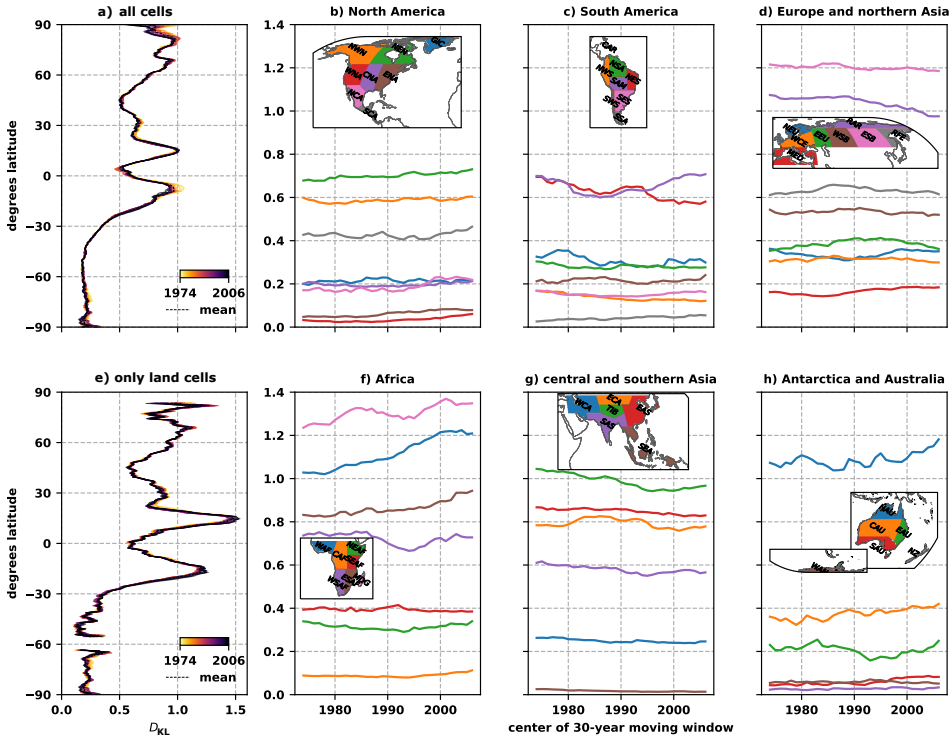

Figure 3.3: The relative entropy D_{KL} indicating seasonality of extreme daily precipitation occurrences (Eq. 3.1) presented as: a) mean value for each latitude across grid cells and e) across land cells. The colorbar in the legend of these panels indicate the middle of a 30-year window. The mean value across all 30-year windows is presented by the dashed black line. Panels b-d and f-h) show D_{KL} calculated for each WGI-V4 land region. Each line corresponds to a region with the same color as shown on the map in that panel. The x-axis presents the middle of a 30-year window. Dry areas, defined as cells with a mean value of the 90th highest rainfall event below 5 mm day^{-1} in all 30-year windows, are removed from this analysis.

encompassing the southernmost and northernmost latitudes, as well as the range between approximately -15 and -5° latitude.

The multidecadal variability in D_{KL} for each WGI-v4 land region are depicted in Figs. 3.3b-d and f-h. Regions such as the Caribbean, South American Monsoon and Northern Australia display substantial variability, whereas regions such as Western Africa or eastern South Africa show long-term increasing trends. Conversely, regions such as East North America, Southern South America, the Mediterranean, and New Zealand exhibit consistent relative entropy patterns over the years analyzed. Moreover, the highest values of D_{KL}, so the highest clustering of precipitation extremes, are observed in geographically diverse regions, specifically Western Africa, Madagascar, Tibetan Plateau, Eastern Siberia, Russian Arctic, and Northern Australia.

The mean seasonal centroid C, which represents the timing of extreme precipitation occurrences, is presented in Fig. 3.4. Panel a displays the mean of all 30-year windows

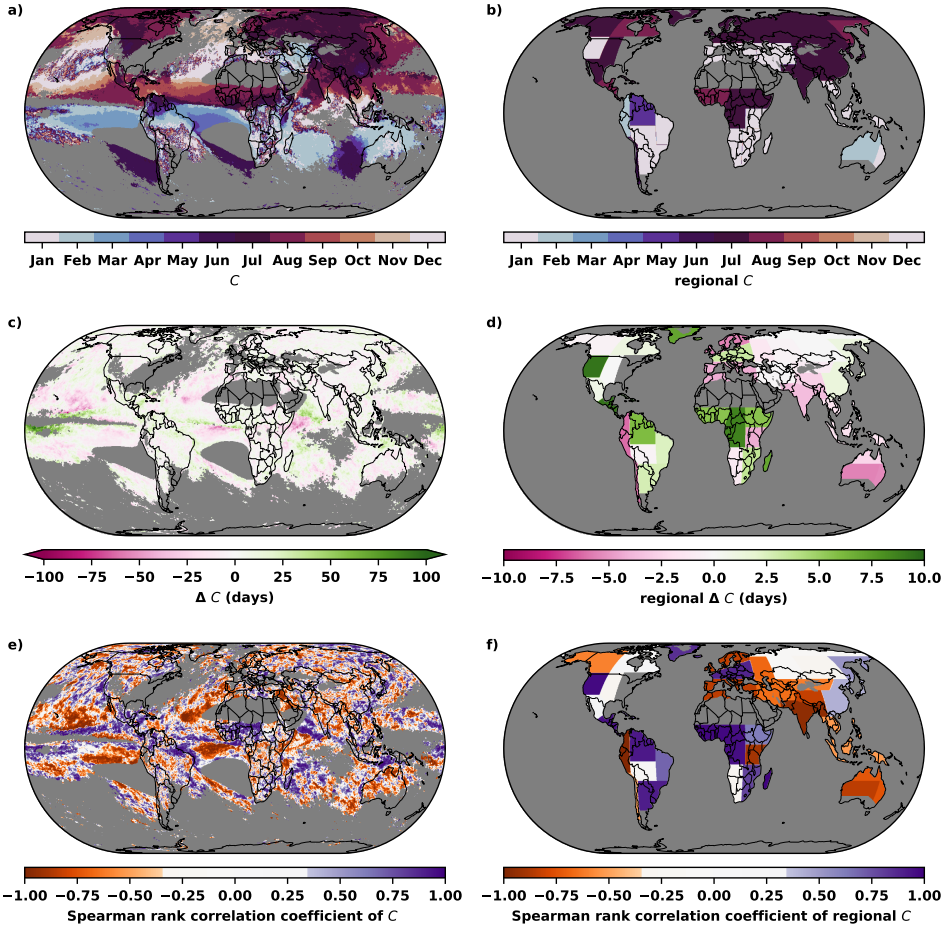

Figure 3.4: Mean seasonal centroid of the seasonality of extreme daily precipitation occurrences (C, Eq. 3.2). Presented as a) the mean of all 30-year windows analyzed per grid cell, and b) calculated per WGI-v4 reference region over land. Panel c) shows the difference in C between the first and last window for each grid cell in number of days ($\Delta C = C_{1992-2021} - C_{1959-1988}$), with a negative ΔC indicating that the central date of extreme rainfall occurrences are taking place earlier in the year and a positive ΔC indicating later in the year. Panel d) shows the same difference calculated per WGI-v4 reference region over land. Panel e) shows the Spearman rank correlation coefficient of C for each grid cell, the non-white values indicate statistical significance ($p < 0.05$). Panel f) shoes the correlation coefficients calculated per WGI-v4 reference region over land. Cells with $D_{\mathrm{KL}} < 0.27$ (rainfall occurrences occurring in more than 10 months) are excluded. Also dry areas, defined as cells with a mean value of the 90th highest rainfall event in all 30-year windows below 5 mm day^{-1}, are masked in gray. Regions in panels b), d) and f) only include those containing at least 50% of the cells based on the two criteria above.

for each grid cell, while panel b shows C per WGI-v4 reference region over land. The centroid of extreme precipitation occurrences over extra-tropical land regions predominantly falls in the summer months, with December-February in the Southern Hemisphere and June-August in the Northern hemisphere. The exception is the Mediterranean and west central Asia, where C occurs in winter (January - February). These patterns are comparable to those observed in the GPCC dataset over land (Pascale et al., 2015, 2016, respectivly their Figs. 15a and 1g), and CMIP5 historical simulations (Pascale et al., 2016, their Fig. 1h), indicating a similarity between the centroid of extreme precipitation occurrences and all precipitation. Furthermore, our results closely align to those of (Dey et al., 2021, their Fig. 2a and d), who estimated the timing of extreme precipitation over Australia, defined as the maximum consecutive 5-day precipitation, using the circular mean instead of C.

Fig. 3.4c and d present the difference in the number of days between the centroids of the first and last window. In most WGI-V4 regions, there is a difference of only a few days between the first and last window, indicating minimal changes in the timing of extreme precipitation occurrences. In some specific regions, such as Australia, western South America, northeastern Europe, the Mediterranean and South Asia, the centroid falls a few days earlier in the year. Conversely in Western North America, South Central America, the Caribbean, eastern South America, and most regions in Sub-Sahran Africa, the centroid occurs a few days later in the year in the last window compared to the first. The pattern for West Africa is in agreement with findings by Van de Giesen et al. (2010), who noted that the onset of the rainy season has shifted to 10 days later in the year.

Figs. 3.4e and f present the Spearman rank correlation coefficient of C over time. Like with Figs. 3.2e-f, the correlation patterns are similar with those seen in ΔC. Fig. S3.3b shows Fig. 3.4e correcting for field significance, displaying very similar patterns. The regional Spearman rank correlation coefficient is significant in 30 of the 38 included regions, half of them have a positive and negative correlation coefficient.

When comparing the significant trends of the relative entropy (D_{KL}, Fig. 3.2f) and seasonal centroid (C, Fig. 3.4f) interesting global patterns emerge. In Australia, the Mediterranean and northwest North America, the value of D_{KL} increases while C decreases. This means a higher degree of clustering combined with extremes that occur earlier. In southern Asia, northwest South America and southeastern Africa, the value of D_{KL} decreases while C decreases too, so more evenly spread out extremes and earlier in the year. In western Africa, central Africa, eastern Southern Africa and Madagascar, both D_{KL} and C are increasing. The same is observed over western North America and Greenland.

3.4 CONCLUSIONS

In this study, we examined the seasonality of extreme daily precipitation occurrences using a metric based on relative entropy (D_{KL}) as an indicator of intra-annual clustering. By analyzing more than 60 years of precipitation data from ERA5 (1959-2021), our findings highlight significant historical shifts in the seasonality of extreme precipitation occurrences across different regions. In Africa, characterized by large seasonality at the beginning of the analyzed time period, we observed a further increase in the concentration of extreme precipitation events during specific times of the year. In Asia, although initial

D_{KL} values were also high, a decrease in clustering was observed over time. Australia and North America, characterized by initially low D_{KL} values, experienced an increase in the clustering of extreme precipitation events. In parts of South America D_{KL} has decreased, whereas in Europe D_{KL} has remained relatively constant. Future work may seek to extend this analysis and that of Pascale et al. (2015, 2016) by evaluating whether historical climate model simulations capture the trends in extreme rainfall seasonality we observed in ERA5 reanalysis. Such an approach could then be used for improved projections of future changes in extreme precipitation seasonality.

Examining the timing of extreme precipitation occurrences, we found that the peak of extreme events over extra-tropical land regions typically falls within summer. The observed patterns align with those of monthly precipitation, suggesting a similarity in the seasonality between extreme event occurrence and total precipitation amounts. The observed shift in timing of the centroid usually just spans a few days, suggesting a modest change in the timing of the extreme precipitation events. Changes in the timing of precipitation extremes have implications for flood risk (Blöschl et al., 2017; Wasko et al., 2020a,b), for instance when earlier extreme precipitation occurrences are combined with earlier snowmelt due to increasing global temperatures (Tarasova et al., 2023). Conversely, when extreme events occur outside of the main rainy season, the probabilities of soil erosion and landslides are higher (Steger et al., 2023). As such our work highlights the importance of taking changes in timing of extremes into account in climate adaptation scenarios.

4

FUTURE PRECIPITATION EXTREMES

This chapter is based on:

Gründemann, G. J., van de Giesen, N. C., Brunner, L., van der Ent, R. J., *Rarest rainfall events will see the greatest relative increase in magnitude under future climate change,* Communications Earth & Environment, **3**, 235, 2022.

SUMMARY
Future rainfall extremes are projected to increase with global warming according to theory and climate models, but common (annual) and rare (decennial or centennial) extremes could be affected differently. Here, using 25 models from the Coupled Model Intercomparison Project Phase 6 driven by a range of plausible scenarios of future greenhouse gas emissions, we show that the rarer the event, the more likely it is to increase in a future climate. By the end of this century, daily land rainfall extremes could increase in magnitude between 10.5% and 28.2% for annual events, and between 13.5% and 38.3% for centennial events, for low and high emission scenarios respectively. The results are consistent across models though with regional variation, but the underlying mechanisms remain to be determined.

4.1 INTRODUCTION

Global warming will result in an intensification of the water cycle (Allen and Ingram, 2002). An increase in rainfall extremes is already observed in many regions in the world (e.g., Alexander, 2016; Asadieh and Krakauer, 2015; Donat et al., 2016a; Papalexiou and Montanari, 2019; Westra et al., 2013), and research shows that extremes will increase in the future depending on the emission scenario (Donat et al., 2016b; Kharin et al., 2013; Moustakis et al., 2021; Myhre et al., 2019; Sillmann et al., 2013). Global climate models (GCMs) are the only available tools to study future daily rainfall extremes on the global domain, but come with limitations. A large limitation is that GCMs do not resolve convective processes, which are important drivers of extreme precipitation (Loriaux et al., 2013; Westra et al., 2014). Recent research demonstrates that GCMs included in the Coupled Model Intercomparison Project Phase 6 (CMIP6; Eyring et al., 2016) have decent skill in modeling extreme rainfall in comparison to observations (Li et al., 2021). Yet, when interested in absolute magnitudes or specific locations, a careful selection of models based on observations or advanced bias correction approaches are necessary (Johnson and Sharma, 2012; Mehrotra and Sharma, 2021; Photiadou et al., 2016), but these are less relevant when studying relative changes over time.

Studies investigating the simulation of rainfall extremes in global climate models typically focus on one of two types of extremes: (1) common and (2) rare. Climate indices focusing on “common" extremes typically have probabilistic return times of a year or less. Examples of such indices include annual maxima (Asadieh and Krakauer, 2015; Borodina et al., 2017), a percentile-based threshold, e.g. the 90th, 95th, 99th, or 99.9th percentile (Fischer and Knutti, 2016; Pendergrass and Knutti, 2018; Scoccimarro and Gualdi, 2020), or indices like R20mm (the number of days per year in which precipitation depth exceeds 20 mm) as defined by “the expert team on climate change detection and indices" (Alexander and Arblaster, 2017; Bador et al., 2018; Myhre et al., 2019). These indices are well-studied on global and regional domains, and many regions expect a substantial increase in such common extremes (Bador et al., 2018; Borodina et al., 2017; Donat et al., 2016b; Dong et al., 2021; Fischer and Knutti, 2016; Scoccimarro and Gualdi, 2020). The second type of extremes are the “rare" ones with multi-year or multi-decade return time periods, which are important for infrastructure design (Kharin et al., 2013). In hydrology these are typically estimated based on extreme value theory (using a historical time series of the same location), but model-based (e.g., Aalbers et al., 2018; Maher et al., 2021) or spatial pooling based approaches (e.g., Olsson et al., 2019; Overeem et al., 2008) also exist to increase the time series length. There are fewer studies on the effect of global warming on such rare extremes (Chan et al., 2018; DeGaetano and Castellano, 2017; Hodnebrog et al., 2019), or on the differences in future changes between “common" to “rare" extremes (Aalbers et al., 2018; Li et al., 2021). The latter studies point to a possible larger relative increase of the rare extremes.

The scientific debate regarding the effect of global warming on rainfall extremes has not yet fully addressed this difference in the expected change for the common and rare extremes, and if that differs for different climatic regions across the world. Here, we investigate the spatiotemporal patterns of a range of common to rare extremes using a large ensemble of precipitation estimates from the GCMs included in CMIP6 (Eyring et al., 2016).

4.2 METHODS

4.2.1 CMIP6 MODEL DATA

Daily precipitation simulations from the Coupled Model Intercomparison Project Phase 6 (CMIP6) archive are analyzed for the historical and future scenarios. The future late twenty-first century scenarios are Shared Socioeconomic Pathways (SSPs) coupled with the previous Representative Concentration Pathways (RCPs) (O'Neill et al., 2016). We included in our analyses SSP1-2.6, SSP2-4.5, SSP3-7.0 and SSP5-8.5, ranging from the least to the most emissions. The two time periods that are compared are (1) the simulated historical late twentieth century period 1971-2000, and (2) the late twenty-first century period 2071-2100 (or 2070-2099 or 2069-2098, depending on the available climate-model output and ensuring that the latest 30 years leading up to 2100 are used). We use all 25 GCMs that provide complete simulations for the two time periods and all analyzed scenarios (ESGF). For the main analysis we used only one realization per GCM, but we also analyzed all the different realizations with complete simulations for all five scenarios (one historical and four SSP scenarios, see Supporting Information Figs. S4.12-S4.22 in Gründemann, 2023). We arbitrarily selected the first available realization of each GCM, however, the similarity between different realizations (Supporting Information Figs. S4.12-S4.22) led us to believe that this did not affect our main findings. An overview of the models is displayed in Table 4.1. As there are large differences in the resolution of the different GCMs, the analyses are performed on each model's native grid. The results are then remapped to a $0.25° \times 0.25°$ grid using the nearest neighbor interpolation method for the ensemble means. The results remain mostly unaffected by the remapping, as the $0.25° \times 0.25°$ grid is a higher resolution than the native grid of each of the models. Specifically, the remapped grid-cells are 4 to 63 times smaller depending on the model resolution, and as we used nearest neighbor interpolation no spatial averaging is taking place. Moreover, as the main results of this study are relative values instead of absolute values, the different resolutions of the models do not influence these results.

4.2.2 MODEL WEIGHTING

To account for GCM performance as well as model inter-dependencies in the used multi-model ensemble, we apply the Climate model Weighting by Independence and Performance (ClimWIP) method (Brunner et al., 2020; Knutti et al., 2017; Lorenz et al., 2018; Merrifield et al., 2020). ClimWIP assigns a weight w_i to each model to account for the models' performance in simulating historical climate (D_i) and independence from the other models ($j = 1...M$) in the ensemble (S_{ij}):

$$w_i = \frac{e^{-\left(\frac{D_i}{\sigma_D}\right)^2}}{1 + \sum_{j \neq i}^{M} e^{-\left(\frac{S_{ij}}{\sigma_S}\right)^2}}, \tag{4.1}$$

with the shape parameters σ_D and σ_S determining the strength of the performance and independence weighting, respectively (see Brunner et al. (2020) for more details). We use an implementation of ClimWIP within the Earth System Model Evaluation Tool (ESMValTool) (Eyring et al., 2020) version 2.3 (Andela et al., 2021).

Table 4.1: Overview of the CMIP6 GCMs and the weights for each GCM included in this study.

Model	No. of cells (Lat × Lon)	No. of realizations	Institution, country	Weight
ACCESS-CM2	144 × 192	3	CSIRO-ARCCSS, Australia	0.0711098
BCC-CSM2-MR	160 × 320	1	BCC, China	0.0375146
CAMS-CSM1-0	160 × 320	1	CAMS, China	0.0205778
CanESM5	64 × 128	50	CCCMA-ECCC, Canada	0.0161621
CESM2	192 × 288	2	NCAR, USA	0.0736632
CESM2-WACCM	192 × 288	1	NCAR, USA	0.0346487
CMCC-CM2-SR5	192 × 288	1	CMCC, Italy	0.0414861
CNRM-CM6-1	128 × 256	1	CNRM-CERFACS, France	0.0350501
CNRM-ESM2-1	128 × 256	1	CNRM-CERFACS, France	0.0547842
EC-Earth3	256 × 512	7	EC-Earth consortium	0.0016417
EC-Earth3-Veg	256 × 512	4	EC-Earth consortium	0.0834485
FGOALS-g3	80 × 180	3	LASG-IAP-CAS, China	0.0091949
GFDL-ESM4	180 × 288	1	GFDL-NOAA, USA	0.1476730
IITM-ESM	94 × 192	1	CCCR-IITM, India	0.0372205
INM-CM4-8	120 × 180	1	INM-RAS, Russia	0.0141569
INM-CM5-0	120 × 180	1	INM-RAS, Russia	0.0323639
IPSL-CM6A-LR	143 × 144	6	IPSL, France	0.0362602
KACE-1-0-G	144 × 192	3	NIMS/KMA, Republic of Korea	0.0497750
MIROC6	128 × 256	3	CCSR-UT-JAMSTEC-NIES, Japan	0.0668575
MIROC-ES2L	64 × 128	1	CCSR-UT-JAMSTEC-NIES, Japan	0.0093852
MPI-ESM1-2-HR	192 × 384	1	MPI, Germany	0.0504672
MRI-ESM2-0	160 × 320	2	MRI, Japan	0.0302788
NorESM2-LM	96 × 144	1	NCC, Norway	0.0199261
NorESM2-MM	192 × 288	1	NCC, Norway	0.0201326
UKESM1-0-LL	144 × 192	5	MO-NERC, UK	0.0062219

The independence weighting is based on model-model distances in 1979-2014 climatologies of temperature and sea level pressure in the same setup as used by Brunner et al. (2020) but updated for the 25 GCMs used in this study. These metrics have been shown to cluster models by known development families and account for dependencies (Brunner et al., 2020; Merrifield et al., 2020).

For model performance we adapted the metrics used in ref. (Brunner et al., 2020) to the target of global precipitation change. In contrast to other important climate variables, most prominently future warming (Brunner et al., 2020; Nijsse et al., 2020; Tokarska et al., 2020; Zelinka et al., 2020), emergent constraints (Hall et al., 2019) for global precipitation changes have only recently been suggested (Shiogama et al., 2022; Thackeray et al., 2022). Here, our main aim was to reduce the influence of models which simulate variables considered important for the representation of precipitation very different from observations rather than applying a constraint that necessarily reduces model spread. Performance weights were, therefore, based on five metrics: (1) the temperature trend, which has been found to be an important constraint for temperature and precipitation changes alike (Shiogama et al., 2022; Tokarska et al., 2020), (2) the temperature climatology, (3) the variability of temperature, (4) the precipitation climatology and (5) the variability of precipitation, all in the period 1979-2014. Models which perform poorly in one or more of these metrics received less weight in the calculation of multi-model statistics as we trust their projections of future precipitation less. The strength of the weighting was established using a leave-one-out model-as-truth test (Brunner et al., 2019, 2020; Knutti et al., 2017) on the target of global mean precipitation change. The resulting weights for each model are included in Table 4.1 and have a range comparable to recent studies, such as Brunner et al. (2020) (their Table S4.2 in the supplement). The weights of the models were used to create the multi-model weighted ensemble means for Figs. 1, 2, 4, and Supporting Information Figs. S4.4, S4.7-S4.9, and S4.23-S4.25. The multi-model ensemble means shown in this manuscript are weighted using the described method, but we note that using unweighted estimates does not considerably affect the results and conclusions drawn in this study (see Supporting Information Figs. S4.1-S4.3).

4.2.3 EXTREME PRECIPITATION ESTIMATES

In this study, we estimated the common and rare extreme precipitation at each model grid-cell using three different methods: (1) the Metastatistical Extreme Value (MEV) distribution, (2) the Generalized Extreme Value (GEV) distribution, and (3) quantiles directly obtained from the precipitation simulations of all models. By using different methods for the calculation of precipitation extremes, we show the robustness of our results and allow for comparison with other studies. We found the results to be largely independent of the statistical method, but here we mainly show the results obtained by using the MEV distribution (Marani and Ignaccolo, 2015; Zorzetto et al., 2016) as it produces the smoothest spatial patterns (Gründemann et al., 2023; Zorzetto and Marani, 2020) and reduces uncertainty for the rarest extremes (Zorzetto et al., 2016).

The rare precipitation extremes (with return levels of 10 and 100 years) we present in this paper are calculated using the first method: the MEV distribution (Marani and Ignaccolo, 2015). As opposed to traditional extreme value distributions, MEV uses all available data, and is, therefore, able to estimate return periods higher than the period

of record with reduced uncertainty if the tail of the true distribution matches (Marra et al., 2018, 2019b; Schellander et al., 2019; Zorzetto et al., 2016), and shows more consistent geographical patterns than traditional methods as GEV (Gründemann et al., 2023; Marra et al., 2019a; Zorzetto and Marani, 2020). Following the approach of Zorzetto et al. (2016), for each individual year the Weibull distribution is fitted to all days with a precipitation depth exceeding 1 mm. Years are grouped together if the number of events per year is lower than twenty, to allow for more accurate parameter estimation (Miniussi and Marani, 2020). The Weibull parameters are fitted using probability weighted moments (Greenwood et al., 1979). The cumulative distribution function of MEV-Weibull is as follows:

$$\zeta_m(x) = \frac{1}{M}\sum_{j=1}^{M}\left\{1-\exp\left[-\left(\frac{x}{C_j}\right)^{w_j}\right]\right\}^{n_j} \tag{4.2}$$

where j is the year ($j = 1,2,\ldots,M$), $C_j > 0$ is the Weibull scale parameter, $w_j > 0$ is the Weibull shape parameter, and n_j is the number of wet events in hydrological year j (Marani and Ignaccolo, 2015).

The second method to calculate the rare extremes is using the traditional GEV distribution. Annual maxima are used to estimate the GEV parameters with the L-moments approach (Hosking, 1990). The cumulative distribution function of GEV is:

$$G(z) = \begin{cases} \exp\left\{-\left[1+\xi\left(\frac{z-\mu}{\sigma}\right)\right]^{-\frac{1}{\xi}}\right\}, \xi \neq 0 \\ \exp\left\{-\exp\left[-\left(\frac{z-\mu}{\sigma}\right)\right]\right\}, \xi = 0 \end{cases} \tag{4.3}$$

with location parameter $\mu \in (-\infty,\infty)$, scale parameter $\sigma > 0$, and shape parameter $\xi \in (-\infty,\infty)$. The results for GEV are included in Supporting Information Fig. S4.10.

The third method is to obtain the precipitation extremes directly from the precipitation estimation of each model, using all-day percentiles. The common extremes we present in this paper, the ones with a return level of 1 year (99.7262th percentile), are directly estimated from the precipitation time series for each grid-cell. This is because extreme value distributions are designed for return levels greater than the length of the time series. We also estimated the precipitation depths for all-day percentiles corresponding to the 0.3-year (approximately once every 109 days), 3-year, and 30-year (highest value in the 30-year time-series) return levels: the 99.0874th, 99.9087th, and 99.9909th percentile respectively. For the 30-year return level it is particularly uncertain whether the maximum observed precipitation event actually represents an event with a 30-year return period, which is why we did not use this as a primary method. Yet, averaged over large regions or globally this approach can still be considered valid. The results for this method are included in the Supporting Information Fig. S4.11.

4.2.4 CHANGES IN PRECIPITATION ESTIMATES

This study is focused on relative changes in precipitation extremes in order to overcome the issues of systematic bias and different climate model resolutions. Moreover, relative changes allow for comparison between geographical regions with highly different precipitation amounts. As a reference for absolute values, we show the weighted mean precipitation depth for a precipitation event that would occur on average once every 100

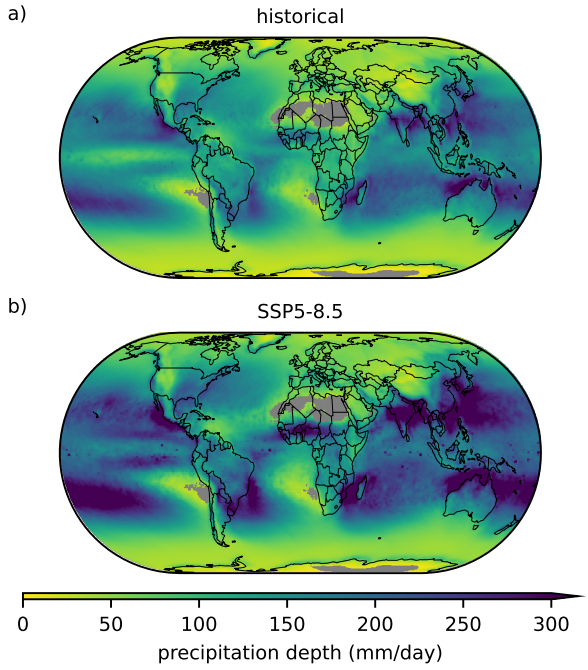

Figure 4.1: The 100-year return level of daily precipitation. The 100-year return level of daily precipitation weighted mean across 25 CMIP6 models for **a** historical (1971-2000) and **b** SSP5-8.5 future (2071-2100) periods. The individual model results are shown in Supporting Information Figs. S4.4 and S4.5. Dry areas (weighted mean of less than 3 events per year) are masked in gray.

years in Fig. 4.1 (see Supporting Information Figs. S4.4 and S4.5 for the individual models). The highest model-agreement is shown over the higher latitudes and arid regions, the lowest over the tropics, which most models have issues simulating correctly (Bador et al., 2018; O'Gorman, 2015; Kharin et al., 2013) (see Supporting Information Fig. S4.6).

To study if the relative change in common extremes is different from the relative change in rare extremes, we use the following two equations:

$$C_{\mathrm{rel,t,x}} = \frac{\mathrm{Tt_{SSPx}} - \mathrm{Tt_{historical}}}{\mathrm{Tt_{historical}}} \tag{4.4}$$

$$D_{100-1,\mathrm{x}} = C_{\mathrm{rel,100,x}} - C_{\mathrm{rel,1,x}} = \frac{\mathrm{T100_{SSPx}} - \mathrm{T100_{historical}}}{\mathrm{T100_{historical}}} - \frac{\mathrm{T1_{SSPx}} - \mathrm{T1_{historical}}}{\mathrm{T1_{historical}}} \tag{4.5}$$

With eq. 4.4 we estimate ($C_{\mathrm{rel,t,x}}$), which is the relative change between historical and future precipitation for each of the return levels (Tt) and for any SSP scenario (SSPx). We use eq. 4.4 as input for eq. 4.5, where $D_{100\text{-}1,\mathrm{x}}$ stands for the difference in change of rare and common extremes, T100 stands for the 100-year return level and T1 for the 1-year return level. For the all-day percentile method the same formula applies, but T100 and T1 were substituted by T30 and T0.3.

4.2.5 STATISTICAL ANALYSIS

To determine whether the results found that rarest extremes will increase more than the common ones ($D_{100-1,x} > 0$, eq. 4.5) are statistically significant, we followed Livezey and Chen (1983). To account for spatial correlation, we first calculated the number of spherical harmonics that explain 95 % of the observed variation in change in T1 ($C_{rel,1,x}$, eq. 4.4) and change in T100 ($C_{rel,100,x}$, eq. 4.4) for each of the 25 GCMs and SSP scenarios. The degrees of freedom in these data were set to be equal to this number of harmonics. Note that the lower the percentage used, the more conservative the test will be, with 95 % being conservative. We then drew a number, equal to the degrees of freedom, of random samples from the change in T1 and T100 estimates for each GCM and SSP scenario, and calculated the median of these samples. The drawing excluded masked pixels (weighted mean of less than 3 events per year, see Section Mask dry areas) and was weighted according to the area of the pixels. This analysis was done as a monte carlo (mc) simulation and repeated 10,000 times to determine the Cumulative Distribution Function of the median of samples of size degrees of freedom of randomly chosen pixels. Finally, the values that exceeded 5 %, 2 %, and 1 % of the medians of the samples, were taken as the 95 %, 98 %, and 99 % confidence levels with which the null-hypothesis that there was no increase could be rejected.

We also applied the Spearman's rank correlation to analyze if the median change in the monte carlo 100-year return level (mc-$C_{rel,100,x}$, eq. 4.4) is significantly larger than the median change in the monte carlo 1-year return level (mc-$C_{rel,1,x}$). We assumed that each GCM is an independent experiment resulting in an estimate for mc-$C_{rel,100,x}$ and mc-$C_{rel,1,x}$. The null-hypothesis is that there is no statistical relationship between the change and being a member of either the mc-$C_{rel,100,x}$ or the mc-$C_{rel,1,x}$ family (i.e., mc-$C_{rel,100,x}$ = mc-$C_{rel,1,x}$). We tested whether the changes in 100-year return levels are significantly larger than the changes in 1-year return levels at 99 %, 99.9 %, and 99.99 % significance levels.

4.2.6 MASK DRY AREAS

Estimating the difference between common and rare extremes for highly arid places, such as the Sahara, makes little sense as precipitation occurs so seldom. Therefore, we created a mask to remove very dry areas from our study, based on the mean number of dry events per year combined with the performance-based weights for each model. We calculated the mean number of events per year for each of the 25 models, each individual pixel, and for the one historical and four future scenarios. We used this information to create a mask per model and scenario, with a 1 if the number of events is equal to or exceeds three events per year, and a 0 if there are less than three events per year. These individual masks are then remapped to a $0.25° \times 0.25°$ grid using the nearest neighbor interpolation method. The masks for the individual models and scenarios, consisting of 0 and 1 values, are multiplied by the performance-based weights for each model. After which, the sum of the 25 weighted masks for each pixel and each individual scenario is taken. If the sum of the 25 weighted masks es equal to or greater than 0.75 at the pixel level, that pixel will get the value of 1. If the sum of the weighted masks are smaller than 0.75, that pixel will get the value of 0. This results in five masks with values of 0 and 1: one for the historical scenario and four for the SSP scenarios. The final mask is created

by multiplying all five masks, to ensure that there are on average 3 events per year for all individual scenarios. The areas where there are not enough events per year are marked as gray on the maps, and these pixels are not considered for any analyses.

4.2.7 REGIONAL ANALYSIS

We conducted the regional analysis based on the Intergovernmental Panel on Climate Change Working Group I (IPCC WGI) reference regions, version 4 (Iturbide et al., 2020). Supporting Information Fig. S4.26 shows an overview of the geographical locations of these reference regions, whereas the region name corresponding to the abbreviations are included in Table 4.2. The IPCC WGI reference regions were chosen in order to allow for consistency with other scientific research. These IPCC WGI regions were used to calculate the weighted multi-model ensemble regional means, for Table 1, and Supporting Information Tables S4.3 and S4.4. Furthermore, weights were applied to reflect the cell sizes, so that cells with larger land masses (around the equator) get higher weights than the cells with small land masses (higher latitudes around the poles).

4.3 RESULTS

Future precipitation extremes for the climate scenarios are expected to increase in magnitude over land compared to historical extremes (Fig. 4.2 and Supporting Information Figs. S4.7-4.9). This increase has high model agreement, irrespective of the climate scenario or how rare the extremes are. Regions with the largest magnitude increase in future extremes are mainly located in areas around and just north of the equator, stretching from the Equatorial Pacific Ocean, via northwest South America, through the Sahara and Western, Central and Eastern Africa, the Arabian-Peninsula and Arabian Sea to South Asia and the Tibetan Plateau. There are some locations over the subtropical Atlantic and South Pacific oceans where extreme precipitation is expected to decrease in the future, though more so for the common return levels. This is in agreement with findings by Pfahl et al. (2017), who demonstrated that the dynamic contribution of daily precipitation over subtropical oceans causes robust regional decreases in extreme precipitation. These regional patterns of increasing and decreasing precipitation extremes are similar to those of Li et al. (2021), their Fig. 5. Furthermore, the areas with the highest increases and lowest decreases overlap with the areas with the most positive and negative scaling with dew point temperature (Ali et al., 2021, their Fig. 4).

The rarest precipitation extremes (i.e. the blue squares in Fig. 4.3) will increase more relative to the more common ones (i.e. the green triangles in Fig. 4.3). As expected, all individual models predict a global median magnitude increase in extreme precipitation for each of the four SSPs. However, the finding that this increase is relatively larger for rarer extremes is to the best of our knowledge the novel part of the results. Technically, this implies that the tails of extreme value distributions (Gründemann et al., 2023) become heavier in a future climate. This behavior is consistent at the global domain across all 25 CMIP6 models analyzed (Fig. 4.3) and statistically significant for all SSP scenarios (Supporting Information Table S4.1), as well as for other statistical methods (Supporting Information Figs. S4.10 and S4.11) and other GCM realizations (Supporting Information Figs. S4.12-S4.22). Furthermore, these findings are statistically significant for most indi-

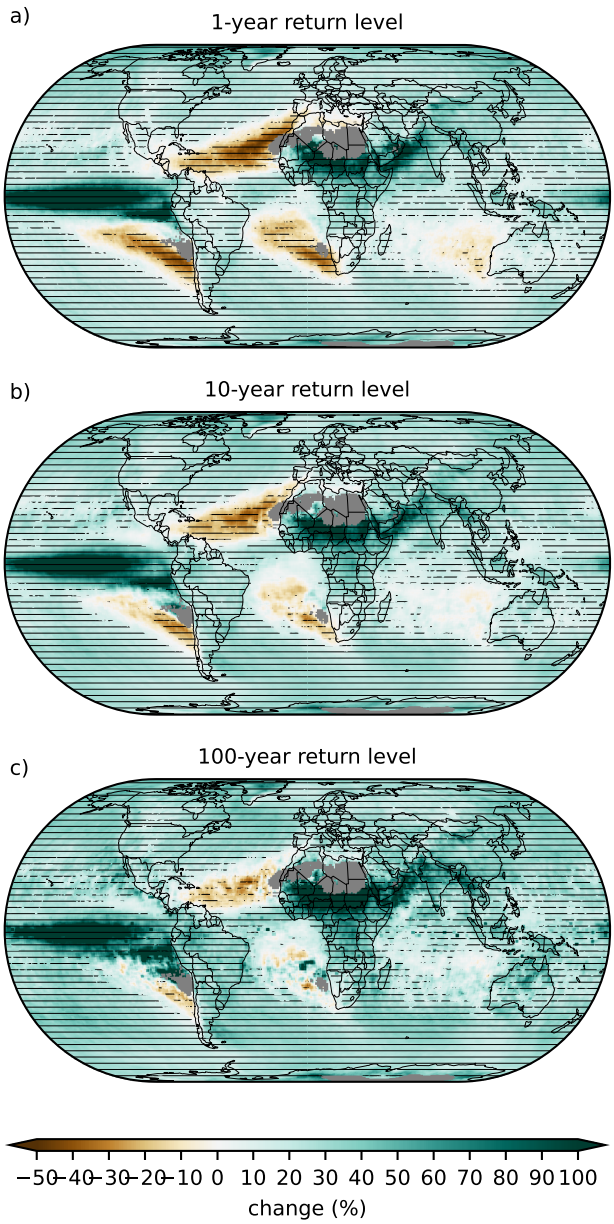

Figure 4.2: Relative change of future vs historical precipitation return levels. Relative change of the **a** 1, **b** 10 and **c** 100-year return levels of daily precipitation expressed as weighted mean across 25 CMIP6 models for the SSP5-8.5 future period (2071-2100) with respect to the historical period (1971-2000) (eq. 4.4). Hatching is in the locations where >75 % of the weighted models agree on the sign of the change. Dry areas (weighted mean of less than 3 events per year) are masked in gray.

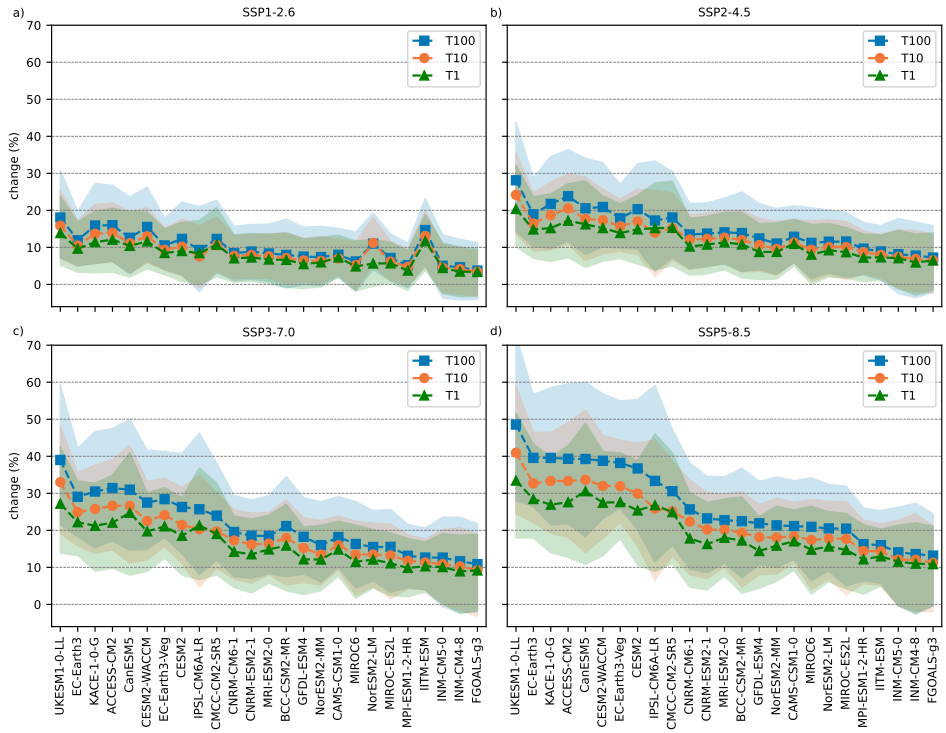

Figure 4.3: Global relative change of precipitation extremes for each individual climate model. Relative change of daily precipitation extremes simulated using 25 CMIP6 GCMs for the future period (2071-2100) SSP scenario **a** 1-2.6, **b** 2-4.5, **c** 3-7.0 and **d** 5-8.5, with respect to the historical period (1971-2000), eq 2. Triangle, circle and square markers respectively represent the global area-weighted median values of the 1, 10 and 100-year return levels. The shaded areas are the area-weighted 25th to 75th percentile intervals. The dashed lines between markers are added for visibility.

vidual GCMs, particularly for the high emission scenarios (21 out of 25 GCMs for SSP3-7.0 and SSP5-8.5, Supporting Information Table S4.2) and more so for the GCMs with the highest resolutions (Table 4.1).

Our main result that the magnitude of rarer extremes are expected to increase relatively more is also backed by earlier observation based studies over Australia (Guerreiro et al., 2018) and over Europe and the USA (Fischer and Knutti, 2016). As well as based on a single model initial-condition large ensemble study over Western Europe (Aalbers et al., 2018), and on CMIP6 global climate models (Li et al., 2021). The relative magnitude increase is also stronger with higher emission scenarios (see also Table 4.2), underlining the importance of emission reduction for extreme precipitation hazards.

Fig. 4.4 and Table 4.2 show where the magnitude of most rare extremes increases relatively more than the common ones, as the difference in relative changes in the 100-year and 1-year return level estimates (see eq. 4.5 in Section 4.2.4). Land regions with the largest relative magnitude increase of rare extremes with respect to the common ones

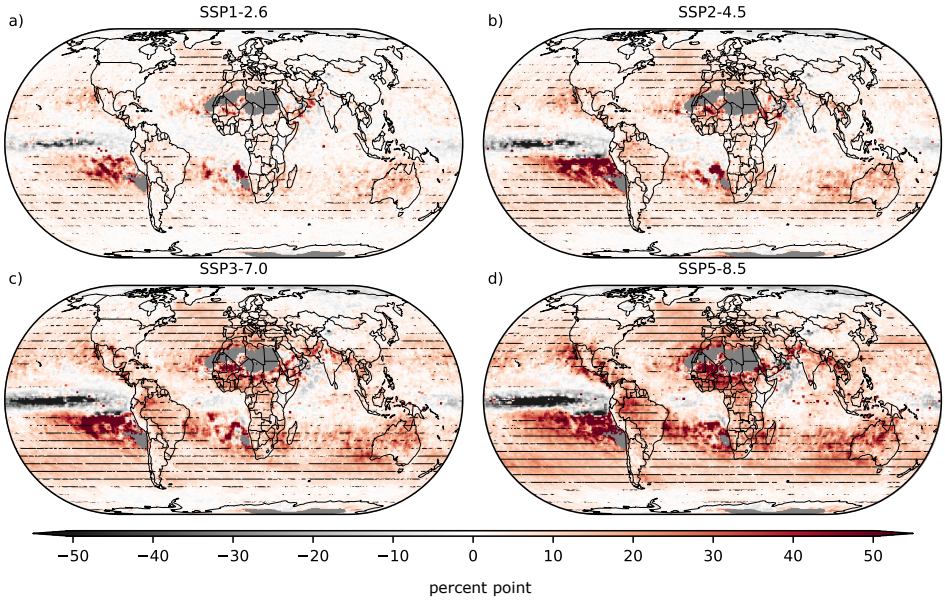

Figure 4.4: Difference in future changes between rare and common extremes. Difference in weighted mean change for the 100- and 1-year return levels between the historical and future SSP scenarios **a** 1-2.6, **b** 2-4.5, **c**, 3-7.0 and **d** 5-8.5. Panel **d** is the difference of Fig.4.2c and a. A positive change indicates that the 100-year return levels will increase relatively more than the 1-year return level (eq. 4.5) The hatching represents areas where more than 75 % of the models agree on the sign of change. Dry areas (weighted mean of less than 3 events per year) are masked in gray.

are around the subtropics (Sahara and surroundings, Amazon and Central America, and Central and Northern Australia), and oceanic regions include the South Pacific, South Atlantic, South Indic, and to a lesser extent their Northern counterparts. A few regions are exceptions where the common extremes instead are expected to increase relatively more than the rare ones, which are around the Equatorial Pacific Ocean and the poles. For future low-emission SSP scenarios, the models show large spatial discrepancies, contrary to high model agreement for the highest emission scenarios, predominantly over the subtropics. At the high latitudes and tropics, however, the models show more disagreement, which can be explained by more model uncertainty of extreme precipitation over the tropics in general due to the GCM differences (Bador et al., 2018).

4.4 DISCUSSION

We showed that in the future rare daily precipitation extremes are expected to increase more than common extremes. The CMIP6 GCMs exhibit high model agreement for this finding in general, particularly for the highest emission scenario (Fig. 4.4), but some spatial differences exist. The higher the emission scenario, the higher the relative difference found between rare (100-year return level) and common extremes (1-year return level), and with higher statistical significance (Table S4.1). Particularly we found for low

Table 4.2: Regional difference in weighted mean change for the 100- (Supporting Information Table S4.4) and 1-year return levels (Supporting Information Table S4.3) between the historical (1971-2000) and four future SSP scenarios (2071-2100). The regions in the table are the IPCC WGI reference regions (version 4, Iturbide et al., 2020), as well as global land cells and all global cells (italic). Values are ordered in descending order for SSP5-8.5. A positive change indicates that the 100-year return levels will increase relatively more than the 1-year return level.

Abbreviation	Region	SSP1-2.6	SSP2-4.5	SSP3-7.0	SSP5-8.5
SAH	Sahara	10.69	18.81	24.93	34.45
WAF	Western-Africa	3.62	8.29	19.30	25.71
CAU	C.Australia	12.27	11.94	18.54	23.56
SCA	S.Central-America	4.28	7.17	12.92	22.29
CAF	Central-Africa	3.51	6.69	15.35	21.44
NSA	N.South-America	4.60	9.75	15.78	21.09
NAU	N.Australia	8.69	12.20	15.43	19.65
SPO	S.Pacific-Ocean	7.72	12.85	16.14	19.52
NCA	N.Central-America	7.25	10.62	16.15	19.31
MDG	Madagascar	6.39	8.21	13.72	19.06
NES	N.E.South-America	4.35	7.03	13.37	19.00
SAO	S.Atlantic-Ocean	8.04	11.00	13.55	18.58
SAM	South-American-Monsoon	4.98	9.03	14.27	18.56
WSAF	W.Southern-Africa	8.13	11.05	13.78	18.55
MED	Mediterranean	6.27	9.34	15.13	17.96
SAS	S.Asia	3.07	5.10	12.04	17.84
ESAF	E.Southern-Africa	7.23	9.16	14.23	17.70
SAU	S.Australia	4.89	8.94	13.85	17.32
SWS	S.W.South-America	6.64	10.07	12.51	16.51
SIO	S.Indic-Ocean	5.44	8.67	12.53	15.33
EAU	E.Australia	3.99	6.63	11.78	13.90
NWS	N.W.South-America	3.45	8.12	9.73	13.43
NAO	N.Atlantic-Ocean	5.33	7.74	10.52	12.69
NZ	New-Zealand	3.70	5.82	10.11	11.73
SSA	S.South-America	2.51	6.10	8.05	11.39
-	*Global (land)*	3.06	4.96	8.25	10.65
SES	S.E.South-America	3.21	5.37	7.87	10.48
SEA	S.E.Asia	1.95	3.47	7.94	10.40
WCA	W.C.Asia	2.96	5.44	8.29	9.87
NEAF	N.Eastern-Africa	4.23	7.98	10.86	9.81
CAR	Caribbean	2.24	4.84	8.64	9.74
-	*Global (all)*	3.31	5.18	7.54	9.61
EAS	E.Asia	1.14	3.10	6.36	8.62
NPO	N.Pacific-Ocean	3.10	4.63	7.01	8.56
BOB	Bay-of-Bengal	2.09	1.46	4.45	8.12
WCE	West&Central-Europe	2.55	3.86	5.78	8.06
SEAF	S.Eastern-Africa	1.97	2.60	6.34	7.50
CNA	C.North-America	1.70	3.26	4.69	6.82
ARP	Arabian-Peninsula	6.40	9.00	11.48	6.76
SOO	Southern-Ocean	1.55	2.74	4.64	6.26

Continued on the next page.

Continued from the previous page.

Abbreviation	Region	SSP1-2.6	SSP2-4.5	SSP3-7.0	SSP5-8.5
ENA	E.North-America	1.59	3.04	4.85	6.22
TIB	Tibetan-Plateau	0.95	1.17	3.64	5.99
WNA	W.North-America	2.28	2.81	4.57	5.57
EIO	Equatorial.Indic-Ocean	1.24	1.51	2.71	5.47
EEU	E.Europe	1.74	2.35	3.66	5.28
NEU	N.Europe	1.28	2.20	2.59	4.05
EAO	Equatorial.Atlantic-Ocean	0.21	0.64	3.70	3.29
RFE	Russian-Far-East	0.66	1.01	2.45	3.14
EAN	E.Antarctica	1.08	2.43	2.27	2.63
ECA	E.C.Asia	0.72	0.12	0.14	2.24
WSB	W.Siberia	0.11	-0.16	0.50	1.67
GIC	Greenland/Iceland	0.71	0.39	1.19	1.32
WAN	W.Antarctica	0.33	0.62	0.96	1.32
NWN	N.W.North-America	0.10	-0.08	0.64	1.04
ESB	E.Siberia	0.05	0.04	0.43	0.97
NEN	N.E.North-America	0.26	0.56	0.91	0.79
ARS	Arabian-Sea	2.12	-1.14	-3.46	-5.45
RAR	Russian-Arctic	-2.08	-3.45	-4.75	-6.04
ARO	Arctic-Ocean	-2.96	-4.17	-5.70	-6.74
EPO	Equatorial.Pacific-Ocean	-2.19	-4.33	-8.78	-11.11

emission scenario SSP1-2.6 and high emission scenario SSP5-8.5 global (land and ocean) daily rainfall extremes will increase by 8.6 % and 23.1 %, respectively, for 1-year events (Table S4.3) and by 11.9 % and 32.5 % for for 100-year (Table S4.4) events by the end of this century. Furthermore, regions are not affected equally, Africa and regions around and just north of the equator particularly will face a disproportionate increase in rare extreme precipitation hazards. This is notably the case for the higher emission scenarios, and much more than the regions most responsible for greenhouse gas emissions that often are expected to have a smaller increase than the global mean (Fig. 4.2). There are also areas in the subtropical Atlantic and South Pacific oceans that show decreasing precipitation extremes in the future. It should be noted that while the larger patterns of rarer extremes increasing relatively more is quite robust, there are also some regions with model disagreement. For such regions particularly, when compiling future extreme rainfall-intensity-frequency curves a more careful selection and weighting of climate models based on regional observations and advanced bias-correction techniques is advisable.

Here we did not formulate a hypothesis of why we observe this behavior of rare extremes increasing relative more than common extremes under climate change. Yet, when looking at the changes in the parameters underlying the MEV-Weibull distribution (eq. 4.2), the statistics themselves give some indication about the processes (Supporting Information Figs. S4.23-S4.25). It should be noted that the behavior could be caused by either a decrease in the number of wet days N (combined with an increase in the scale parameter C) (Schär et al., 2016) or a decrease in the shape parameter W, which may, for example, be the result of dynamical feedback processes related to latent heat-

ing (Nie et al., 2018). It appears that both the rainfall frequency (Supporting Information Fig. S4.23) and dynamical feedback processes (Supporting Information Fig. S4.25) play a role. This may serve as a starting point for future research to further disentangle the processes behind this behavior. Regardless of the underlying mechanisms, the results of this study have important implications for the design of engineering standards as they are built on the basis of our knowledge of the frequency of precipitation events. If rare extreme precipitation events become more frequent in the future as suggested here, engineering design standards, such as those used for storm water drainage and other critical water system infrastructure, will need to be updated. Yet, it should be noted that bias correction methods ought to take into account the fact that the rarest quantiles of today's climate are made up of different processes than the rarest quantiles in a future climate. Whereas the challenge of accurately predicting future changes in precipitation has been noted as one of the 'real holes in climate science' (Schiermeier, 2010), we think that the fact that the model agreement is so high should give confidence in the robustness of our climate models, and our own findings in particular, making that hole just a little bit smaller.

5

Conclusions

5.1 MAIN FINDINGS

Extreme precipitation characteristics are changing all over the world, both in recent past and projected future. The global-scale analyses of precipitation extremes revealed the strong influence of geographical features, such as orography, coastlines, and aridity. These factors play an important role in shaping the seasonality of extreme precipitation events and their tail heaviness in different regions around the world. The altered timing, shifts in seasonality, and projected increase in precipitation extremes pose immense future challenges. Many people and sectors will be impacted by this, including rain-fed agriculture, infrastructure design, and water resource management.

A key and novel finding of this research is that the rarest precipitation extremes are projected to increase relatively more than common ones by the end of the 21st century. This increase is expected to be even more pronounced under higher emission scenarios, emphasizing the urgent need for global emission reduction efforts. The research also shows vast regional differences in the historical and projected changes in extreme precipitation patterns. Notably, Africa emerges as a critical example of facing disproportionate effects of climate change. Already having experienced a significant increase in the seasonality and a shift in the timing of precipitation extremes, Africa is also projected to face the greatest relative increase in future precipitation extremes. It is evident that certain regions will bear a disproportionately greater burden of these changes and the ensuing negative impacts.

5.2 IMPLICATIONS

The findings of this dissertation directly allow for the provision of valuable information, such as extreme precipitation return levels and changes in seasonality. This can support sectors such as engineering design in areas which traditionally lack adequate input data. This research has shown it is crucial to acknowledge the influence of extreme value distribution choices on return level estimates, which can significantly impact design decisions in vulnerable sectors. By using open global-scale datasets, advanced methodology, and by openly providing our results, including code, this work fosters transparency and collaboration.

The shift in seasonality and timing of extreme precipitation occurrences, particularly in Africa, demands proactive measures to mitigate the consequences. Delayed start of the growing season, coupled with increased clustering of extreme events presents serious challenges for rain-fed agriculture. These regions may also face increased risks of floods, landslides, and other weather-related disasters due to shifts in seasonality. Incorporating these shifts into critical infrastructure design is vital to enhance resilience and preparedness for extreme events occurring at different times of the year.

A key contribution to the scientific knowledge is a greater projected relative increase in rarest precipitation extremes in the future. This study also further strengthens the consensus that precipitation extremes over land are projected to intensify by the end of the 21st century. As such, it underscores the importance of considering non-stationarity in engineering design, especially for critical infrastructure such as dikes and dams, designed to withstand highly rare events occurring once every 500 or 1000 years.

This study also indicates that precipitation extremes are projected to increase even

more for higher emission scenarios. This emphasizes the urgent need for global efforts to mitigate greenhouse gas emissions. Implementing effective climate mitigation measures, such as adopting emission reduction policies and transitioning to renewable energy sources, is crucial to limit the severity of future extreme precipitation events. Collaborative action among governments, scientific communities, international organizations, and citizens is essential to address the challenges posed by extreme precipitation events and build a more resilient and sustainable future.

5.3 OUTLOOK

The insights gained from this dissertation provide a strong foundation for future research endeavors aimed at understanding and predicting precipitation extremes. It also opens the path for follow-up scientific questions like: What other factors are important for determining the heaviness of the tail of extreme value distributions? Which physical processes cause the rarest precipitation extremes to increase relatively more under climate change? Beyond the scientific advancements, this topic offers opportunities for cross-disciplinary research and research-to-application. To further advance research outcomes, the following areas deserve priority and attention.

To enhance our understanding of extreme precipitation, efforts should be directed towards improving and expanding precipitation datasets. This can involve increasing the number and quality of gauging stations, refining remotely-sensed precipitation estimates, and enhancing the numerical models and data assimilation techniques used in reanalysis datasets. Openly sharing precipitation data for research purposes will help overcome data limitations and ensure more comprehensive coverage, especially in regions with limited historical records.

As we continue to acquire and refine climate data, it is crucial to complement these efforts with cutting-edge statistical approaches to derive meaningful information. Future research should explore innovative statistical techniques and machine learning approaches to extract even more detailed insights into precipitation extremes. By developing more sophisticated models that consider additional climate drivers and their interactions, we can further enhance our understanding and prediction of extreme precipitation events. This integrated approach will ensure a comprehensive advancement in our knowledge of these phenomena.

Climate models play a crucial role in projecting future climate conditions. However, their coarse spatiotemporal resolutions cannot capture the fine-scale variations in climate features that occur at smaller geographical areas, such as around the coast, in mountainous regions and regions with many different land uses. To make climate model output more locally applicable, downscaling techniques can be used to achieve higher spatiotemporal resolutions. This could be achieved by applying statistical or machine learning approaches or using climate model output as boundary conditions for regional climate models. These fine-scale variations and projections are vital for local climate adaptation, impact assessment, and resource management.

As climate change continues to shape the dynamics of precipitation extremes, continuous research will be fundamental to keep pace with the evolving climate. Collaboration between different scientific groups, such as those generating precipitation data,

climate modeling groups, and scientists performing impact assessments, is crucial for advancing the field. Interdisciplinary collaborations between scientists and policymakers is essential for effectively translating research findings into policy and practice. Integrating (downscaled) climate model projections into regional and local planning is needed for fostering climate resilience and ensuring sustainable development in the face of shifting precipitation patterns. By fostering a ongoing dialogue among scientists, policymakers, stakeholders, and citizens, we can collectively strive to build a climate-resilient and sustainable future for generations to come.

REFERENCES

Aalbers, E. E., Lenderink, G., van Meijgaard, E., and van den Hurk, B. J. J. M.: Local-Scale Changes in Mean and Heavy Precipitation in Western Europe, Climate Change or Internal Variability?, Climate Dynamics, 50, 4745–4766, doi:10.1007/s00382-017-3901-9, 2018.

Alexander, L. V.: Global observed long-term changes in temperature and precipitation extremes : A review of progress and limitations in IPCC assessments and beyond, Weather and Climate Extremes, 11, 4–16, doi:10.1016/j.wace.2015.10.007, 2016.

Alexander, L. V. and Arblaster, J. M.: Historical and projected trends in temperature and precipitation extremes in Australia in observations and CMIP5, Weather and Climate Extremes, 15, 34–56, doi:10.1016/j.wace.2017.02.001, 2017.

Ali, H., Peleg, N., and Fowler, H. J.: Global scaling of rainfall with dewpoint temperature reveals considerable ocean-land difference, Geophysical Research Letters, 48, e2021GL093 798, doi:10.1029/2021GL093798, 2021.

Alijanian, M., Rakhshandehroo, G. R., Mishra, A. K., and Dehghani, M.: Evaluation of satellite rainfall climatology using CMORPH, PERSIANN-CDR, PERSIANN, TRMM, MSWEP over Iran, International Journal of Climatology, 37, 4896–4914, doi:10.1002/joc.5131, 2017.

Allan, R. P. and Soden, B. J.: Atmospheric warming and the amplification of precipitation extremes, Science, 321, 1481–1484, doi:10.1126/science.1160787, 2008.

Allen, M. R. and Ingram, W. J.: Constraints on future changes in climate and the hydrologic cycle, Nature, 419, 224–232, doi:10.1038/nature01092, 2002.

Andela, B., Broetz, B., de Mora, L., Drost, N., Eyring, V., Koldunov, N., Lauer, A., Mueller, B., Predoi, V., Righi, M., Schlund, M., Vegas-Regidor, J., Zimmermann, K., Adeniyi, K., Arnone, E., Bellprat, O., Berg, P., Bock, L., Caron, L.-P., Carvalhais, N., Cionni, I., Cortesi, N., Corti, S., Crezee, B., Davin, E. L., Davini, P., Deser, C., Diblen, F., Docquier, D., Dreyer, L., Ehbrecht, C., Earnshaw, P., Gier, B., Gonzalez-Reviriego, N., Goodman, P., Hagemann, S., von Hardenberg, J., Hassler, B., Hunter, A., Kadow, C., Kindermann, S., Koirala, S., Lledó, L., Lejeune, Q., Lembo, V., Little, B., Loosveldt-Tomas, S., Lorenz, R., Lovato, T., Lucarini, V., Massonnet, F., Mohr, C. W., Amarjiit, P., Pérez-Zanón, N., Phillips, A., Russell, J., Sandstad, M., Sellar, A., Senftleben, D., Serva, F., Sillmann, J., Stacke, T., Swaminathan, R., Torralba, V., Weigel, K., and Roberts, C.: ESMValTool, doi:10.5281/zenodo.3401363, URL https://github.com/ESMValGroup/ESMValTool/, 2021.

Arguez, A. and Vose, R. S.: The definition of the standard WMO climate normal: The key to deriving alternative climate normals, Bulletin of the American Meteorological Society, 92, 699–704, doi:10.1175/2010BAMS2955.1, 2011.

Asadieh, B. and Krakauer, N. Y.: Global trends in extreme precipitation: climate models versus observations, Hydrology and Earth System Sciences, 19, 877–891, doi:10.5194/hess-19-877-2015, 2015.

Bador, M., Donat, M. G., Geoffroy, O., and Alexander, L. V.: Assessing the Robustness of Future Extreme Precipitation Intensification in the CMIP5 Ensemble, Journal of Climate, 31, 6505–6525, doi:10.1175/JCLI-D-17-0683.1, 2018.

Bai, P. and Liu, X.: Evaluation of five satellite-based precipitation products in two gauge-scarce basins on the Tibetan Plateau, Remote Sensing, 10, doi:10.3390/RS10081316, 2018.

Bal, P. K., Pathak, R., Mishra, S. K., and Sahany, S.: Effects of global warming and solar geoengineering on precipitation seasonality, Environmental Research Letters, 14, 034 011, doi:10.1088/1748-9326/aafc7d, 2019.

Ball, J., Babister, M., Nathan, R., Weeks, W., Weinmann, E., Retallick, M., and Testoni, I.: Australian Rainfall and Runoff: A guide to flood estimation, Commonwealth of Australia (Geoscience Australia), URL http://hdl.handle.net/10453/85297, 2019.

Bandhauer, M., Isotta, F., Lakatos, M., Lussana, C., Båserud, L., Izsák, B., Szentes, O., Tveito, O. E., and Frei, C.: Evaluation of Daily Precipitation Analyses in E-OBS (V19.0e) and ERA5 by Comparison to Regional High-resolution Datasets in European Regions, International Journal of Climatology, 42, 727–747, doi:10.1002/joc.7269, 2022.

Beck, H. E., Vergopolan, N., Pan, M., Levizzani, V., van Dijk, A. I. M., Weedon, G. P., Brocca, L., Pappenberger, F., Huffman, G. J., and Wood, E. F.: Global-scale evaluation of 22 precipitation datasets using gauge observations and hydrological modeling, Hydrology and Earth System Sciences, 21, 6201–6217, doi:10.5194/hess-21-6201-2017, 2017.

Beck, H. E., Pan, M., Roy, T., Weedon, G. P., Pappenberger, F., van Dijk, A. I. J. M., Huffman, G. J., Adler, R. F., and Wood, E. F.: Daily evaluation of 26 precipitation datasets using Stage-IV gauge-radar data for the CONUS, Hydrology and Earth System Sciences, 23, 207–224, doi:10.5194/hess-23-207-2019, 2019a.

Beck, H. E., Wood, E. F., Pan, M., Fisher, C. K., Miralles, D. G., van Dijk, A. I. J. M., McVicar, T. R., and Adler, R. F.: MSWEP V2 Global 3-Hourly 0.1° Precipitation: Methodology and Quantitative Assessment, Bulletin of the American Meteorological Society, 100, 473–500, doi:10.1175/BAMS-D-17-0138.1, 2019b.

Beck, H. E., Westra, S., Tan, J., Pappenberger, F., Huffman, G. J., McVicar, T. R., Gründemann, G. J., Vergopolan, N., Fowler, H. J., Lewis, E., et al.: PPDIST, global 0.1 daily and 3-hourly precipitation probability distribution climatologies for 1979–2018, Scientific data, 7, 302, doi:10.1038/s41597-020-00631-x, 2020.

Becker, A., Finger, P., Meyer-Christoffer, A., Rudolf, B., Schamm, K., Schneider, U., and Ziese, M.: A description of the global land-surface precipitation data products of the Global Precipitation Climatology Centre with sample applications including centennial (trend) analysis from 1901-present, Earth System Science Data, 5, 71, doi:10.5194/essd-5-71-2013, 2013.

Beersma, J., Versteeg, R., and Hakvoort, H.: Neerslagstatistieken voor korte duren actualisatie 2018, Tech. rep., STOWA, Amersfoort, 2018.

Berghuijs, W. R., Harrigan, S., Molnar, P., Slater, L. J., and Kirchner, J. W.: The Relative Importance of Different Flood-Generating Mechanisms Across Europe, Water Resources Research, p. 2019WR024841, doi:10.1029/2019WR024841, 2019.

Biondini, R.: Cloud Motion and Rainfall Statistics, Journal of Applied Meteorology and Climatology, 15, 205 – 224, doi:10.1175/1520-0450(1976)015<0205:CMARS>2.0.CO;2, 1976.

Blöschl, G., Hall, J., Parajka, J., Perdigão, R. A. P., Merz, B., Arheimer, B., Aronica, G. T., Bilibashi, A., Bonacci, O., Borga, M., Ivan, Č., Castellarin, A., and Chirico, G. B.: Changing climate shifts timing of European floods, Science, 357, 588–590, doi:10.1126/science.aan2506, 2017.

Borodina, A., Fischer, E. M., and Knutti, R.: Models are likely to underestimate increase in heavy rainfall in the extratropical regions with high rainfall intensity, Geophysical Research Letters, 44, 7401–7409, doi:10.1002/2017GL074530, 2017.

Bosilovich, M. G., Chen, J., Robertson, F. R., and Adler, R. F.: Evaluation of Global Precipitation in Reanalyses, Journal of Applied Meteorology and Climatology, 47, 2279 – 2299, doi:10.1175/2008JAMC1921.1, 2008.

Brunner, L., Lorenz, R., Zumwald, M., and Knutti, R.: Quantifying uncertainty in European climate projections using combined performance-independence weighting, Environmental Research Letters, 14, 124 010, doi:10.1088/1748-9326/ab492f, 2019.

Brunner, L., Pendergrass, A. G., Lehner, F., Merrifield, A. L., Lorenz, R., and Knutti, R.: Reduced global warming from CMIP6 projections when weighting models by performance and independence, Earth System Dynamics, 11, 995–1012, doi:10.5194/esd-11-995-2020, 2020.

Buishand, T.: Some remarks on the use of daily rainfall models, Journal of Hydrology, 36, 295–308, doi:10.1016/0022-1694(78)90150-6, 1978.

Camuffo, D., della Valle, A., Becherini, F., and Zanini, V.: Three centuries of daily precipitation in Padua, Italy, 1713–2018: history, relocations, gaps, homogeneity and raw data, Climatic Change, 162, 923–942, doi:10.1007/s10584-020-02717-2, 2020.

Cao, Q., Painter, T. H., Currier, W. R., Lundquist, J. D., and Lettenmaier, D. P.: Estimation of Precipitation over the OLYMPEX Domain during Winter 2015/16, Journal of Hydrometeorology, 19, 143 – 160, doi:10.1175/JHM-D-17-0076.1, 2018.

Casson, D. R., Werner, M., Weerts, A., and Solomatine, D.: Global re-analysis datasets to improve hydrological assessment and snow water equivalent estimation in a sub-Arctic watershed, Hydrology and Earth System Sciences, 22, 4685–4697, doi:10.5194/hess-22-4685-2018, 2018.

Cavanaugh, N. R. and Gershunov, A.: Probabilistic tail dependence of intense precipitation on spatiotemporal scale in observations, reanalyses, and GCMs, Climate Dynamics, 45, 2965–2975, doi:10.1007/s00382-015-2517-1, 2015.

Cavanaugh, N. R., Gershunov, A., Panorska, A. K., and Kozubowski, T. J.: The probability distribution of intense daily precipitation, Geophysical Research Letters, 42, 1560–1567, doi:10.1002/2015GL063238, 2015.

Chan, S. C., Kahana, R., Kendon, E. J., and Fowler, H. J.: Projected changes in extreme precipitation over Scotland and Northern England using a high-resolution regional climate model, Climate Dynamics, 51, 3559–3577, doi:10.1007/s00382-018-4096-4, 2018.

Chen, H.-P. and Sun, J.-Q.: How Large Precipitation Changes over Global Monsoon Regions by CMIP5 Models?, Atmospheric and Oceanic Science Letters, 6, 306–311, doi:10.3878/j.issn.1674-2834.13.0002, 2013.

Coles, S.: An introduction to statistical modeling of extreme values, Springer Series in Statistics; Springer: London, UK, 2001.

Contractor, S., Donat, M., Alexandre, L. V., Ziese, M., Meyer-Christoffer, A., Schneider, U., Rustemeier, E., Becker, A., Durre, I., and Vose, R. S.: Rainfall Estimates on a Gridded Network (REGEN)–a global land-based gridded dataset of daily precipitation from 1950 to 2016, Hydrology and Earth System Sciences, 24, 919–943, doi:10.5194/hess-24-919-2020, 2020.

Courty, L. G., Wilby, R. L., Hillier, J. K., and Slater, L. J.: Intensity-duration-frequency curves at the global scale, Environmental Research Letters, 14, 084 045, doi:10.1088/1748-9326/ab370a, 2019.

Cover, T. M. and Thomas, J. A.: Entropy, Relative Entropy, and Mutual Information, chap. 2, pp. 13–55, John Wiley Sons, Ltd, doi:10.1002/047174882X.ch2, 2005.

CRED: Natural disasters 2018, Tech. rep., Institute Health and Society UClouvain, Brussels, Belgium, URL https://www.cred.be/sites/default/files/CREDNaturalDisaster2018.pdf, 2019.

Davison, A. C. and Smith, R. L.: Models for Exceedances over High Thresholds, Journal of the Royal Statistical Society. Series B (Methodological), 52, 393–442, URL https://www.jstor.org/stable/2345667, 1990.

Davison, A. C., Padoan, S. A., Ribatet, M., et al.: Statistical modeling of spatial extremes, Statistical science, 27, 161–186, doi:10.1214/11-STS376, 2012.

De Paola, F., Giugni, M., Pugliese, M., Annis, A., and Nardi, F.: GEV parameter estimation and stationary vs. non-stationary analysis of extreme rainfall in African test cities, Hydrology, 5, doi:10.3390/hydrology5020028, 2018.

Decker, M., Brunke, M. A., Wang, Z., Sakaguchi, K., Zeng, X., and Bosilovich, M. G.: Evaluation of the Reanalysis Products from GSFC, NCEP, and ECMWF Using Flux Tower Observations, Journal of Climate, 25, 1916–1944, doi:10.1175/JCLI-D-11-00004.1, 2012.

DeGaetano, A. T. and Castellano, C. M.: Future projections of extreme precipitation intensity-duration-frequency curves for climate adaptation planning in New York State, Climate Services, 5, 23–35, doi:10.1016/j.cliser.2017.03.003, 2017.

Demirdjian, L., Zhou, Y., and Huffman, G. J.: Statistical modeling of extreme precipitation with TRMM data, Journal of applied meteorology and climatology, 57, 15–30, doi:10.1175/JAMC-D-17-0023.1, 2018.

Dey, R., Bador, M., Alexander, L. V., and Lewis, S. C.: The drivers of extreme rainfall event timing in Australia, International Journal of Climatology, 41, 6654–6673, doi:10.1002/joc.7218, 2021.

Ding, J., Wallner, M., Müller, H., and Haberlandt, U.: Estimation of Instantaneous Peak Flows from Maximum Mean Daily Flows Using the HBV Hydrological Model: Estimation of Instantaneous Peak Flow from Maximum Mean Daily Flow, Hydrological Processes, 30, 1431–1448, doi:10.1002/hyp.10725, 2016.

Donat, M. G., Alexander, L. V., Herold, N., and Dittus, A. J.: Temperature and precipitation extremes in century-long gridded observations, reanalyses, and atmospheric model simulations, Journal of Geophysical Research: Atmospheres, 121, 174–189, doi:10.1002/2016JD025480, 2016a.

Donat, M. G., Lowry, A. L., Alexander, L. V., Gorman, P. A. O., and Maher, N.: More extreme precipitation in the world's dry and wet regions, Nature Climate Change, 6, 508–513, doi:10.1038/NCLIMATE2941, 2016b.

Dong, S., Sun, Y., Li, C., Zhang, X., Min, S.-K., and Kim, Y.-H.: Attribution of extreme precipitation with updated observations and CMIP6 simulations, Journal of Climate, 34, 871–881, doi:10.1175/jcli-d-19-1017.1, 2021.

Dunn, R. J., Alexander, L. V., Donat, M. G., Zhang, X., Bador, M., Herold, N., Lippmann, T., Allan, R., Aguilar, E., Barry, A. A., et al.: Development of an updated global land in situ-based data set of temperature and precipitation extremes: HadEX3, Journal of Geophysical Research: Atmospheres, 125, e2019JD032 263, doi:10.1029/2019JD032263, 2020.

Easterling, D. R., Kunkel, K. E., Wehner, M. F., and Sun, L.: Detection and attribution of climate extremes in the observed record, Weather and Climate Extremes, 11, 17–27, doi:10.1016/j.wace.2016.01.001, 2016.

ESGF: World Climate Research Programme - CMIP6 data, https://esgf-node.llnl.gov/search/cmip6/, last accessed on 01/12/2020.

Eyring, V., Bony, S., Meehl, G. A., Senior, C. A., Stevens, B., Stouffer, R. J., and Taylor, K. E.: Overview of the Coupled Model Intercomparison Project Phase 6 (CMIP6) experimental design and organization, Geoscientific Model Development, 9, 1937–1958, doi:10.5194/gmd-9-1937-2016, 2016.

Eyring, V., Bock, L., Lauer, A., Righi, M., Schlund, M., Andela, B., Arnone, E., Bellprat, O., Brötz, B., Caron, L.-p., Carvalhais, N., Cionni, I., Cortesi, N., Crezee, B., Davin, E. L., Davini, P., Debeire, K., de Mora, L., Deser, C., Docquier, D., Earnshaw, P., Ehbrecht, C., Gier, B. K., Gonzalez-Reviriego, N., Goodman, P., Hagemann, S., Hardiman, S., Hassler, B., Hunter, A., Kadow, C., Kindermann, S., Koirala, S., Koldunov, N., Lejeune, Q., Lembo, V., Lovato, T., Lucarini, V., Massonnet, F., Müller, B., Pandde, A., Pérez-Zanón, N., Phillips, A., Predoi, V., Russell, J., Sellar, A., Serva, F., Stacke, T., Swaminathan, R., Torralba, V., Vegas-Regidor, J., von Hardenberg, J., Weigel, K., and Zimmermann, K.: Earth System Model Evaluation Tool (ESMValTool) v2.0 – an extended set of large-scale diagnostics for quasi-operational and comprehensive evaluation of Earth system models in CMIP, Geoscientific Model Development, 13, 3383–3438, doi:10.5194/gmd-13-3383-2020, URL https://gmd.copernicus.org/articles/13/3383/2020/, 2020.

Feng, X., Porporato, A., and Rodriguez-Iturbe, I.: Changes in rainfall seasonality in the tropics, Nature Climate Change, 3, 811–815, doi:10.1038/NCLIMATE1907, 2013.

Fernandes, L. G. and Rodrigues, R. R.: Changes in the patterns of extreme rainfall events in southern Brazil, International Journal of Climatology, 38, 1337–1352, doi:10.1002/joc.5248, 2018.

Fischer, E. M. and Knutti, R.: Observed heavy precipitation increase confirms theory and early models, Nature Climate Change, 6, 986–991, doi:10.1038/nclimate3110, 2016.

Fowler, H. J., Lenderink, G., Prein, A. F., Westra, S., Allan, R. P., Ban, N., Barbero, R., Berg, P., Blenkinsop, S., Do, H. X., Guerreiro, S., Haerter, J. O., Kendon, E. J., Lewis, E., Schaer, C., Sharma, A., Villarini, G., Wasko, C., and Zhang, X.: Anthropogenic Intensification of Short-Duration Rainfall Extremes, Nature Reviews Earth & Environment, 2, 107–122, doi:10.1038/s43017-020-00128-6, 2021.

Fréchet, M.: Sur la loi de probabilité de l'écart maximum, Ann. Soc. Math. Polon., 6, 93–116, URL https://cir.nii.ac.jp/crid/1571135649485618816, 1927.

Fukutome, S., Liniger, M., and Süveges, M.: Automatic threshold and run parameter selection: a climatology for extreme hourly precipitation in Switzerland, Theoretical and Applied Climatology, 120, 403–416, doi:10.1007/s00704-014-1180-5, 2015.

Gelaro, R., McCarty, W., Suárez, M. J., Todling, R., Molod, A., Takacs, L., Randles, C. A., Darmenov, A., Bosilovich, M. G., Reichle, R., Wargan, K., Coy, L., Cullather, R., Draper, C., Akella, S., Buchard, V., Conaty, A., Da Silva, A. M., Wei, G., Kim, G.-K., Koster, R., Lucchesi, R., Merkova, D., Nielsen, J. E., Partyka, G., Pawson, S., Putman, W., Rienecker, M., Schubert, S. D., Sienkiewicz, M., and Zhao, B.: The modern-era retrospective analysis for research and applications, version 2 (MERRA-2), Journal of Climate, 30, 5419–5454, doi:10.1175/JCLI-D-16-0758.1, 2017.

Gershunov, A., Shulgina, T., Ralph, F. M., Lavers, D. A., and Rutz, J. J.: Assessing the Climate-scale Variability of Atmospheric Rivers Affecting Western North America, Geophysical Research Letters, 44, 7900–7908, doi:10.1002/2017GL074175, 2017.

Greenwood, J. A., Landwehr, J., Matalas, N., and Wallis, J.: Probability weighted moments: definition and relation to parameters of several distributions expressable in inverse form, Water Resources Research, 15, 1049–1054, doi:10.1029/WR015i005p01049, 1979.

Greven, A., Keller, G., and Warnecke, G.: Entropy, Princeton University Press, New Jersey, US, 2003.

Gründemann, G. J.: Supporting information for: Precipitation extremes around the world, Unraveling historical extremes and future changes, URL https://surfdrive.surf.nl/files/index.php/s/CIrlkvgdH7QnLyA, 2023.

Gründemann, G. J., Werner, M., and Veldkamp, T. I. E.: The potential of global reanalysis datasets in identifying flood events in Southern Africa, Hydrology and Earth System Sciences, 22, 4667–4683, doi:10.5194/hess-22-4667-2018, 2018.

Gründemann, G. J., Beck, H. E., Schleiss, M., van de Giesen, N., Marani, M., and van der Ent, R.: Global Precipitation EXtremes dataset, doi:10.4121/uuid:12b5c941-cd54-45db-8d7b-fefaacecaa69, 2020.

Gründemann, G. J., van de Giesen, N., Brunner, L., and van der Ent, R.: Rarest rainfall events will see the greatest relative increase in magnitude under future climate change, Communications Earth & Environment, 3, doi:10.1038/s43247-022-00558-8, 2022.

Gründemann, G. J., Zorzetto, E., Beck, H. E., Schleiss, M., van de Giesen, N., Marani, M., and van der Ent, R. J.: Extreme precipitation return levels for multiple durations on a global scale, Journal of Hydrology, 621, 129 558, doi:10.1016/j.jhydrol.2023.129558, 2023.

Guerreiro, S. B., Fowler, H. J., Barbero, R., Westra, S., Lenderink, G., Blenkinsop, S., Lewis, E., and Li, X.-F.: Detection of Continental-Scale Intensification of Hourly Rainfall Extremes, Nature Climate Change, 8, 803–807, doi:10.1038/s41558-018-0245-3, 2018.

Gumbel, E. J.: The return period of flood flows, The annals of mathematical statistics, 12, 163–190, URL https://www.jstor.org/stable/2235766, 1941.

Gumbel, E. J.: Statistics of extremes, Columbia university press, New York, USA, doi:10.7312/gumb92958, 1958.

Hall, A., Cox, P., Huntingford, C., and Klein, S.: Progressing emergent constraints on future climate change, Nature Climate Change, 9, 269–278, doi:10.1038/s41558-019-0436-6, 2019.

Haylock, M. R., Peterson, T. C., Alves, L. M., Ambrizzi, T., Anunciação, Y. M. T., Baez, J., Barros, V. R., Berlato, M. A., Bidegain, M., Coronel, G., Corradi, V., Garcia, V. J., Grimm, A. M., Karoly, D., Marengo, J. A., Marino, M. B., Moncunill, D. F., Nechet, D., Quintana, J., Rebello, E., Rusticucci, M., Santos, J. L., Trebejo, I., and Vincent, L. A.: Trends in Total and Extreme South American Rainfall in 1960–2000 and Links with Sea Surface Temperature, Journal of Climate, 19, 1490 – 1512, doi:https://doi.org/10.1175/JCLI3695.1, 2006.

Hersbach, H., Bell, B., Berrisford, P., Biavati, G., Horányi, A., Muñoz Sabater, J., Nicolas, J., Peubey, C., Radu, R., Rozum, I., Schepers, D., Simmons, A., Soci, C., Dee, D., and Thépaut, J.-N.: ERA5 hourly data on single levels from 1959 to present. Copernicus Climate Change Service (C3S) Climate Data Store (CDS) (last accessed on 20 January 2023), doi:10.24381/cds.adbb2d47, 2018.

Hersbach, H., Bell, B., Berrisford, P., Hirahara, S., Horányi, A., Muñoz-Sabater, J., Nicolas, J., Peubey, C., Radu, R., Schepers, D., Simmons, A., Soci, C., Abdalla, S., Abellan, X., Balsamo, G., Bechtold, P., Biavati, G., Bidlot, J., Bonavita, M., De Chiara, G., Dahlgren, P., Dee, D., Diamantakis, M., Dragani, R., Flemming, J., Forbes, R., Fuentes, M., Geer, A., Haimberger, L., Healy, S., Hogan, R. J., Hólm, E., Janisková, M., Keeley, S., Laloyaux, P., Lopez, P., Lupu, C., Radnoti, G., de Rosnay, P., Rozum, I., Vamborg, F., Villaume, S., and Thépaut, J.-N.: The ERA5 global reanalysis, Quarterly Journal of the Royal Meteorological Society, 146, 1999–2049, doi:10.1002/qj.3803, 2020.

Hodnebrog, Ø., Marelle, L., Alterskjær, K., Wood, R. R., Ludwig, R., Fischer, E. M., Richardson, T. B., Forster, P. M., Sillmann, J., and Myhre, G.: Intensification of Summer Precipitation with Shorter Time-Scales in Europe, Environmental Research Letters, 14, 124 050, doi:10.1088/1748-9326/ab549c, 2019.

Hong, Y., Hsu, K.-L., Sorooshian, S., and Gao, X.: Precipitation Estimation from Remotely Sensed Imagery using an Artificial Neural Network Cloud Classification System, Journal of Applied Meteorology, 43, 1834–1853, doi:10.1175/JAM2173.1, 2004.

Hosking, J. and Wallis, J.: Some statistics useful in regional frequency analysis, Water resources research, 29, 271–281, doi:10.1029/92WR01980, 1993.

Hosking, J. R.: Algorithm AS215: Maximum-likelihood estimation of the parameters of the Generalized Extreme-Value distribution, Applied Statistics, 34, 301–310, doi:/10.2307/2347483, 1985.

Hosking, J. R. M.: L-Moments: Analysis and estimation of distributions using linear combinations of order statistics, Journal of the Royal Statistical Society. Series B (Methodological), 52, 105–124, URL http://www.jstor.org/stable/2345653, 1990.

Hosking, J. R. M. and Wallis, J. R.: Parameter and Quantile Estimation for the Generalized Pareto Distribution Parameter and Quantile Estimation Generalized Pareto Distribution, Technometrics, 23, 339–349, doi:10.1080/00401706.1987.10488243, 1987.

Hosking, J. R. M., Wallis, J. R., and Wood, E. F.: Estimation of the Generalized Extreme Value Distribution by the Method of Probability-Weighted-Moments, Technometrics, 27, 251–261, doi:10.1080/00401706.1985.10488049, 1985.

Hosseini, S. R., Scaioni, M., and Marani, M.: Extreme Atlantic hurricane probability of occurrence through the Metastatistical Extreme Value Distribution, Geophysical Research Letters, 47, doi:10.1029/2019GL086138, 2020.

Hsu, K.-l., Gao, X., Sorooshian, S., and Gupta, H. V.: Precipitation Estimation from Remotely Sensed Information Using Artificial Neural Networks, Journal of Applied Meteorology, 36, 1176 – 1190, doi:10.1175/1520-0450(1997)036<1176:PEFRSI>2.0.CO;2, 1997.

Hu, L., Nikolopoulos, E. I., Marra, F., Morin, E., and Marani, M.: Evaluation of MEVD-based precipitation frequency analyses from quasi- global precipitation datasets against dense rain gauge networks, Journal of Hydrology, 590, 125 564, doi:10.1016/j.jhydrol.2020.125564, 2020.

Huffman, G. J., Bolvin, D. T., Nelkin, E. J., Wolff, D. B., Adler, R. F., Gu, G., Hong, Y., Bowman, K. P., and Stocker, E. F.: The TRMM Multisatellite Precipitation Analysis (TMPA): Quasi-Global, Multiyear, Combined-Sensor Precipitation Estimates at Fine Scales, Journal of Hydrometeorology, 8, 38 – 55, doi:10.1175/JHM560.1, 2007.

Huffman, G. J., Bolvin, D. T., Braithwaite, D., Hsu, K., Joyce, R., Kidd, C., Nelkin, E. J., and Xie, P.: NASA Global Precipitation Measurement (GPM) Integrated Multi-satellitE Retrievals for GPM (IMERG): Algorithm Theoretical Basis Document (ATBD) Version 4.5, Tech. rep., NASA/GSFC, Greenbelt, MD 20771, USA, 2015.

Huser, R. and Wadsworth, J. L.: Advances in statistical modeling of spatial extremes, Wiley Interdisciplinary Reviews: Computational Statistics, p. e1537, doi:10.1002/wics.1537, 2020.

Hénin, R., Liberato, M. L. R., Ramos, A. M., and Gouveia, C. M.: Assessing the Use of Satellite-Based Estimates and High-Resolution Precipitation Datasets for the Study of Extreme Precipitation Events over the Iberian Peninsula, Water, 10, doi:10.3390/w10111688, URL https://www.mdpi.com/2073-4441/10/11/1688, 2018.

Iturbide, M., Gutiérrez, J. M., Alves, L. M., Bedia, J., Cerezo-Mota, R., Cimadevilla, E., Cofiño, A. S., Di Luca, A., Faria, S. H., Gorodetskaya, I. V., Hauser, M., Herrera, S., Hennessy, K., Hewitt, H. T., Jones, R. G., Krakovska, S., Manzanas, R., Martínez-Castro, D., Narisma, G. T., Nurhati, I. S., Pinto, I., Seneviratne, S. I., van den Hurk, B., and Vera, C. S.: An Update of IPCC Climate Reference Regions for Subcontinental Analysis of Climate Model Data: Definition and Aggregated Datasets, Earth System Science Data, 12, 2959–2970, doi:10.5194/essd-12-2959-2020, 2020.

Johnson, F. and Sharma, A.: A nesting model for bias correction of variability at multiple time scales in general circulation model precipitation simulations, Water Resources Research, 48, W01 504, doi:10.1029/2011WR010464, 2012.

Joyce, R. J., Janowiak, J. E., Arkin, P. A., and Xie, P.: CMORPH: A method that produces global precipitation estimates from passive microwave and infrared data at

high spatial and temporal resolution, Journal of Hydrometeorology, 5, 487–503, doi:10.1175/1525-7541(2004)005<0487:CAMTPG>2.0.CO;2, 2004.

Kang, S. and Ahn, J.-B.: Global energy and water balances in the latest reanalyses, Asia-Pacific Journal of Atmospheric Sciences, 51, 293–302, doi:10.1007/s13143-015-0079-0, 2015.

Kendon, E. J., Blenkinsop, S., and Fowler, H. J.: When will we detect changes in short-duration precipitation extremes?, Journal of Climate, 31, 2945–2964, doi:10.1175/JCLI-D-17-0435.1, 2018.

Kharin, V. V., Zwiers, F. W., Zhang, X., and Wehner, M.: Changes in temperature and precipitation extremes in the CMIP5 ensemble, Climatic Change, 119, 345–357, doi:10.1007/s10584-013-0705-8, 2013.

Kidd, C., Becker, A., Huffman, G. J., Muller, C. L., Joe, P., Skofronick-Jackson, G., and Kirschbaum, D. B.: So, how much of the Earth's surface is covered by rain gauges?, Bulletin of the American Meteorological Society, 98, 69–78, doi:10.1175/BAMS-D-14-00283.1, 2017.

Kitoh, A., Endo, H., Krishna Kumar, K., Cavalcanti, I. F. A., Goswami, P., and Zhou, T.: Monsoons in a changing world: A regional perspective in a global context, Journal of Geophysical Research: Atmospheres, 118, 3053–3065, doi:10.1002/jgrd.50258, 2013.

Knutti, R., Sedláček, J., Sanderson, B. M., Lorenz, R., Fischer, E. M., and Eyring, V.: A Climate Model Projection Weighting Scheme Accounting for Performance and Interdependence: Model Projection Weighting Scheme, Geophysical Research Letters, 44, 1909–1918, doi:10.1002/2016GL072012, 2017.

Kobayashi, S., Ota, Y., Harada, Y., Ebita, A., Moriya, M., Onoda, H., Onogi, K., Kamahori, H., Kobayashi, C., Endo, H., et al.: The JRA-55 reanalysis: General specifications and basic characteristics, Journal of the Meteorological Society of Japan, 93, 5–48, doi:10.2151/jmsj.2015-001, 2015.

Koutsoyiannis, D.: Statistics of extremes and estimation of extreme rainfall: I. Theoretical investigation, Hydrological Sciences Journal, 49, 575–590, doi:10.1623/hysj.49.4.575.54430, 2004a.

Koutsoyiannis, D.: Statistics of extremes and estimation of extreme rainfall: II. Empirical investigation of long rainfall records, Hydrological Sciences Journal, 49, 591–610, doi:10.1623/hysj.49.4.591.54424, 2004b.

Kullback, S. and Leibler, R. A.: On information and sufficiency, The annals of mathematical statistics, 22, 79–86, 1951.

Kundzewicz, Z. W., Pińskwar, I., and Brakenridge, G. R.: Changes in river flood hazard in Europe: a review, Hydrology research, 49, 294–302, doi:10.1080/02626667.2016.1241398, 2018.

Laherrere, J. and Sornette, D.: Stretched exponential distributions in nature and economy:"fat tails" with characteristic scales, The European Physical Journal B-Condensed Matter and Complex Systems, 2, 525–539, doi:10.1007/s100510050276, 1998.

Landrum, L. and Holland, M. M.: Extremes become routine in an emerging new Arctic, Nature Climate Change, 10, 1108–1115, doi:10.1038/s41558-020-0892-z, 2020.

Langousis, A., Mamalakis, A., Puliga, M., and Deidda, R.: Threshold Detection for the Generalized Pareto Distribution: Review of Representative Methods and Application to the NOAA NCDC Daily Rainfall Database, Water Resources Research, 52, 2659–2681, doi:10.1002/2015WR018502, 2016.

Lavers, D. A., Simmons, A., Vamborg, F., and Rodwell, M. J.: An evaluation of ERA5 precipitation for climate monitoring, Quarterly Journal of the Royal Meteorological Society, 148, 3152–3165, doi:10.1002/qj.4351, 2022.

Lei, X., Xu, W., Chen, S., Yu, T., Hu, Z., Zhang, M., Jiang, L., Bao, R., Guan, X., Ma, M., Wei, J., Feng, A., and Gao, L.: How Well Does the ERA5 Reanalysis Capture the Extreme Climate Events Over China? Part I: Extreme Precipitation, Frontiers in Environmental Science, 10, doi:10.3389/fenvs.2022.921658, 2022.

Levizzani, V., Laviola, S., and Cattani, E.: Detection and Measurement of Snowfall from Space, Remote Sensing, 3, 145–166, doi:10.3390/rs3010145, 2011.

Li, C., Zwiers, F., Zhang, X., Li, G., Sun, Y., and Wehner, M.: Changes in Annual Extremes of Daily Temperature and Precipitation in CMIP6 Models, Journal of Climate, 34, 3441–3460, doi:10.1175/JCLI-D-19-1013.1, 2021.

Limsakul, A.: Change in rainfall seasonality in Thailand during 1955-2018, Agriculture and Natural Resources, 54, 369–376, doi:10.34044/j.anres.2020.54.4.05, 2020.

Liu, Z., Liu, Y., Wang, S., Yang, X., Wang, L., Baig, M. H. A., Chi, W., and Wang, Z.: Evaluation of Spatial and Temporal Performances of ERA-Interim Precipitation and Temperature in Mainland China, Journal of Climate, 31, 4347–4365, doi:10.1175/JCLI-D-17-0212.1, 2018.

Livezey, R. E. and Chen, W. Y.: Statistical Field Significance and its Determination by Monte Carlo Techniques, Monthly Weather Review, 11, 46–59, doi:10.1007/s00382-017-3901-9, 1983.

Loeb, N. A., Crawford, A., Stroeve, J. C., and Hanesiak, J.: Extreme Precipitation in the Eastern Canadian Arctic and Greenland: An Evaluation of Atmospheric Reanalyses, Frontiers in Environmental Science, 10, doi:10.3389/fenvs.2022.866929, 2022.

Lorenz, R., Herger, N., Sedláček, J., Eyring, V., Fischer, E. M., and Knutti, R.: Prospects and Caveats of Weighting Climate Models for Summer Maximum Temperature Projections Over North America, Journal of Geophysical Research: Atmospheres, 123, 4509–4526, doi:10.1029/2017JD027992, 2018.

Loriaux, J. M., Lenderink, G., De Roode, S. R., and Siebesma, A. P.: Understanding convective extreme precipitation scaling using observations and an entraining plume model, Journal of the Atmospheric Sciences, 70, 3641–3655, doi:10.1175/JAS-D-12-0317.1, 2013.

Maher, N., Milinski, S., and Ludwig, R.: Large ensemble climate model simulations: introduction, overview, and future prospects for utilising multiple types of large ensemble, Earth System Dynamics, 12, 401–418, doi:10.5194/esd-12-401-2021, 2021.

Mailhot, A. and Duchesne, S.: Design criteria of urban drainage infrastructures under climate change, Journal of Water Resources Planning and Management, 136, 201–208, doi:10.1061/(asce)wr.1943-5452.0000023, 2009.

Marani, M. and Ignaccolo, M.: A metastatistical approach to rainfall extremes, Advances in Water Resources, 79, 121–126, doi:10.1016/j.advwatres.2015.03.001, 2015.

Marani, M. and Zanetti, S.: Long-term oscillations in rainfall extremes in a 268 year daily time series, Water Resources Research, 51, 639–647, doi:10.1002/2014WR015885, 2015.

Marc, O., Stumpf, A., Malet, J.-P., Gosset, M., Uchida, T., and Chiang, S.-H.: Initial insights from a global database of rainfall-induced landslide inventories: the weak influence of slope and strong influence of total storm rainfall, Earth Surface Dynamics, 6, 903–922, doi:10.5194/esurf-6-903-2018, 2018.

Marra, F., Nikolopoulos, E. I., Anagnostou, E. N., and Morin, E.: Metastatistical Extreme Value analysis of hourly rainfall from short records: Estimation of high quantiles and impact of measurement errors, Advances in Water Resources, 117, 27–39, doi:10.1016/j.advwatres.2018.05.001, 2018.

Marra, F., Nikolopoulos, E. I., Anagnostou, E. N., Bárdossy, A., and Morin, E.: Precipitation frequency analysis from remotely sensed datasets: A focused review, Journal of Hydrology, 574, 699–705, doi:10.1016/j.jhydrol.2019.04.081, 2019a.

Marra, F., Zoccatelli, D., Armon, M., and Morin, E.: A simplified MEV formulation to model extremes emerging from multiple nonstationary underlying processes, Advances in Water Resources, 127, 280–290, doi:10.1016/j.advwatres.2019.04.002, 2019b.

Mascaro, G.: On the distributions of annual and seasonal daily rainfall extremes in central Arizona and their spatial variability, Journal of Hydrology, 559, 266–281, doi:10.1016/j.jhydrol.2018.02.011, 2018.

McGraw, D., Nikolopoulos, E. I., Marra, F., and Anagnostou, E. N.: Precipitation frequency analyses based on radar estimates: An evaluation over the contiguous United States, Journal of Hydrology, 573, 299–310, doi:10.1016/j.jhydrol.2019.03.032, 2019.

Mehrotra, R. and Sharma, A.: A Robust Alternative for Correcting Systematic Biases in Multi-Variable Climate Model Simulations, Environmental Modelling & Software, 139, 105 019, doi:10.1016/j.envsoft.2021.105019, 2021.

Ménégoz, M., Gallée, H., and Jacobi, H. W.: Precipitation and snow cover in the Himalaya: from reanalysis to regional climate simulations, Hydrology and Earth System Sciences, 17, 3921–3936, doi:10.5194/hess-17-3921-2013, 2013.

Meredith, E. P., Ulbrich, U., and Rust, H. W.: The Diurnal Nature of Future Extreme Precipitation Intensification, Geophysical Research Letters, 46, 7680–7689, doi:10.1029/2019GL082385, 2019.

Merrifield, A. L., Brunner, L., Lorenz, R., Medhaug, I., and Knutti, R.: An investigation of weighting schemes suitable for incorporating large ensembles into multi-model ensembles, Earth System Dynamics, 11, 807–834, doi:10.5194/esd-11-807-2020, 2020.

Miniussi, A. and Marani, M.: Estimation of Daily Rainfall Extremes Through the Metastatistical Extreme Value Distribution: Uncertainty Minimization and Implications for Trend Detection, Water Resources Research, 56, e2019WR026 535, doi:10.1029/2019WR026535, 2020.

Miniussi, A., Marani, M., and Villarini, G.: Metastatistical Extreme Value Distribution applied to floods across the continental United States, Advances in Water Resources, 136, 103 498, doi:10.1016/j.advwatres.2019.103498, 2020a.

Miniussi, A., Villarini, G., and Marani, M.: Analyses Through the Metastatistical Extreme Value Distribution Identify Contributions of Tropical Cyclones to Rainfall Extremes in the Eastern United States, Geophysical Research Letters, 47, e2020GL087 238, doi:10.1029/2020GL087238, 2020b.

Mishra, A. K. and Coulibaly, P.: Developments in hydrometric network design: A review, Reviews of Geophysics, 47, doi:10.1029/2007RG000243, 2009.

Mishra, A. K., Özger, M., and Singh, V. P.: An entropy-based investigation into the variability of precipitation, Journal of Hydrology, 370, 139–154, doi:10.1016/j.jhydrol.2009.03.006, 2009.

Morrison, J. E. and Smith, J. A.: Stochastic Modeling of Flood Peaks Using the Generalized Extreme Value Distribution: flood peak modeling using GEV, Water Resources Research, 38, doi:10.1029/2001WR000502, 2002.

Moustakis, Y., Papalexiou, S. M., Onof, C. J., and Paschalis, A.: Seasonality, Intensity, and Duration of Rainfall Extremes Change in a Warmer Climate, Earth's Future, 9, e2020EF001 824, doi:10.1029/2020EF001824, 2021.

Murray, V. and Ebi, K. L.: IPCC Special Report on Managing the Risks of Extreme Events and Disasters to Advance Climate Change Adaptation (SREX). , Tech. rep., Cambridge University Press, Cambridge, UK, and New York, NY, USA, 582 pp, doi:10.1136/jech-2012-201045, 2012.

Myhre, G., Alterskjær, K., Stjern, C. W., Hodnebrog, Marelle, L., Samset, B. H., Sillmann, J., Schaller, N., Fischer, E., Schulz, M., and Stohl, A.: Frequency of extreme precipitation increases extensively with event rareness under global warming, Nature Scientific Reports, 9, 1–10, doi:10.1038/s41598-019-52277-4, 2019.

Nerantzaki, S. D. and Papalexiou, S. M.: Tails of extremes: Advancing a graphical method and harnessing big data to assess precipitation extremes, Advances in Water Resources, 134, 103 448, doi:10.1016/j.advwatres.2019.103448, 2019.

Nie, J., Sobel, A. H., Shaevitz, D. A., and Wang, S.: Dynamic amplification of extreme precipitation sensitivity, Proceedings of the National Academy of Sciences, 115, 9467–9472, doi:10.1073/pnas.1800357115, 2018.

Nijsse, F. J. M. M., Cox, P. M., and Williamson, M. S.: Emergent constraints on transient climate response (TCR) and equilibrium climate sensitivity (ECS) from historical warming in CMIP5 and CMIP6 models, Earth Syst. Dyn., 11, 737–750, doi:10.5194/esd-11-737-2020, 2020.

Nikolopoulos, E. I., Borga, M., Marra, F., Crema, S., and Marchi, L.: Debris flows in the eastern Italian Alps: seasonality and atmospheric circulation patterns, Natural Hazards and Earth System Sciences, 15, 647–656, doi:10.5194/nhess-15-647-2015, 2015.

Nissen, K. M. and Ulbrich, U.: Increasing frequencies and changing characteristics of heavy precipitation events threatening infrastructure in Europe under climate change, Natural Hazards and Earth System Sciences, 17, 1177–1190, doi:10.5194/nhess-17-1177-2017, 2017.

O'Gorman, P. A.: Precipitation Extremes Under Climate Change, Current Climate Change Reports, 1, 49–59, doi:10.1007/s40641-015-0009-3, 2015.

Olsson, J., Södling, J., Berg, P., Wern, L., and Eronn, A.: Short-duration rainfall extremes in Sweden: A regional analysis, Hydrology Research, 50, 945–960, doi:10.2166/nh.2019.073, 2019.

O'Neill, B. C., Tebaldi, C., Van Vuuren, D. P., Eyring, V., Friedlingstein, P., Hurtt, G., Knutti, R., Kriegler, E., Lamarque, J. F., Lowe, J., Meehl, G. A., Moss, R., Riahi, K., and Sanderson, B. M.: The Scenario Model Intercomparison Project (ScenarioMIP) for CMIP6, Geoscientific Model Development, 9, 3461–3482, doi:10.5194/gmd-9-3461-2016, 2016.

Overeem, A., Buishand, A., and Holleman, I.: Rainfall depth-duration-frequency curves and their uncertainties, Journal of Hydrology, 348, 124–134, doi:10.1016/j.jhydrol.2007.09.044, 2008.

Papalexiou, S. M. and Koutsoyiannis, D.: Battle of extreme value distributions: A global survey on extreme daily rainfall, Water Resources Research, 49, 187–201, doi:10.1029/2012WR012557, 2013.

Papalexiou, S. M. and Koutsoyiannis, D.: A global survey on the seasonal variation of the marginal distribution of daily precipitation, Advances in Water Resources, 94, 131–145, doi:10.1016/j.advwatres.2016.05.005, 2016.

Papalexiou, S. M. and Montanari, A.: Global and Regional Increase of Precipitation Extremes Under Global Warming, Water Resources Research, 55, 4901–4914, doi:10.1029/2018WR024067, 2019.

Papalexiou, S. M., Koutsoyiannis, D., and Makropoulos, C.: How extreme is extreme? An assessment of daily rainfall distribution tails, Hydrology and Earth System Sciences, 17, 851–862, doi:10.5194/hess-17-851-2013, 2013.

Papalexiou, S. M., Aghakouchak, A., and Foufoula-Georgiou, E.: A diagnostic framework for understanding climatology of tails of hourly precipitation extremes in the United States, Water Resources Research, 54, 6725–6738, doi:10.1029/2018WR022732, 2018.

Pascale, S., Lucarini, V., Feng, X., Porporato, A., and Hasson, S.: Analysis of rainfall seasonality from observations and climate models, Climate Dynamics, 44, 3281–3301, doi:10.1007/s00382-014-2278-2, 2015.

Pascale, S., Lucarini, V., Feng, X., Porporato, A., and Hasson, S.: Projected changes of rainfall seasonality and dry spells in a high greenhouse gas emissions scenario, Climate Dynamics, 46, 1331–1350, doi:10.1007/s00382-015-2648-4, 2016.

Pendergrass, A. G. and Knutti, R.: The Uneven Nature of Daily Precipitation and Its Change, Geophysical Research Letters, 45, 980–988, doi:10.1029/2018GL080298, 2018.

Perica, S., Pavlovic, S., St. Laurent, M., Trypaluk, C., Unruh, D., Martin, D., and Wilhite, O.: NOAA Atlas 14 Volume 10, Precipitation-Frequency Atlas of the United States, Northeastern States., Tech. rep., NOAA, National Weather Service, 2015.

Perica, S., Pavlovic, S., St. Laurent, M., Trypaluk, C., Unruh, D., and Wilhite, O.: NOAA Atlas 14: Precipitation-frequency atlas of the United States, Texas, Tech. rep., NOAA, National Weather Service, 2018.

Pfahl, S., Gorman, P. A. O., and Fischer, E. M.: Understanding the regional pattern of projected future changes in extreme precipitation, Nature Climate Change, 7, 423–428, doi:10.1038/NCLIMATE3287, 2017.

Photiadou, C., van den Hurk, B., van Delden, A., and Weerts, A.: Incorporating circulation statistics in bias correction of GCM ensembles: hydrological application for the Rhine basin, Climate Dynamics, 46, 187–203, doi:10.1007/s00382-015-2578-1, 2016.

Prakash, S., Mitra, A. K., AghaKouchak, A., Liu, Z., Norouzi, H., and Pai, D.: A preliminary assessment of GPM-based multi-satellite precipitation estimates over a monsoon dominated region, Journal of Hydrology, 556, 865–876, doi:j.jhydrol.2016.01.029, 2018.

Ragulina, G. and Reitan, T.: Generalized extreme value shape parameter and its nature for extreme precipitation using long time series and the Bayesian approach precipitation, Hydrological Sciences Journal, 62, 863–879, doi:10.1080/02626667.2016.1260134, 2017.

Rajulapati, C. R., Papalexiou, S. M., Clark, M. P., Razavi, S., Tang, G., and Pomeroy, J. W.: Assessment of extremes in global precipitation products: How reliable are they?, Journal of Hydrometeorology, 21, 2855–2873, doi:10.1175/JHM-D-20-0040.1, 2020.

Rasmusson, E. M. and Arkin, P. A.: A global view of large-scale precipitation variability, Journal of Climate, 6, 1495–1522, doi:10.1175/1520-0442(1993)006<1495:AGVOLS>2.0.CO;2, 1993.

Sahany, S., Mishra, S. K., Pathak, R., and Rajagopalan, B.: Spatiotemporal Variability of Seasonality of Rainfall Over India, Geophysical Research Letters, 45, 7140–7147, doi:10.1029/2018GL077932, 2018.

Sahlu, D., Moges, S. A., Nikolopoulos, E. I., Anagnostou, E. N., and Hailu, D.: Evaluation of high-resolution multisatellite and reanalysis rainfall products over East Africa, Advances in Meteorology, 2017, doi:10.1155/2017/4957960, 2017.

Satgé, F., Ruelland, D., Bonnet, M.-P., Molina, J., and Pillco, R.: Consistency of satellite-based precipitation products in space and over time compared with gauge observations and snow-hydrological modelling in the Lake Titicaca region, Hydrology and Earth System Sciences, 23, 595–619, doi:10.5194/hess-23-595-2019, 2019.

Schär, C., Ban, N., Fischer, E. M., Rajczak, J., Schmidli, J., Frei, C., Giorgi, F., Karl, T. R., Kendon, E. J., Tank, A. M., O'Gorman, P. A., Sillmann, J., Zhang, X., and Zwiers, F. W.: Percentile indices for assessing changes in heavy precipitation events, Climatic Change, 137, 201–216, doi:10.1007/s10584-016-1669-2, 2016.

Schellander, H., Lieb, A., and Hell, T.: Error Structure of Metastatistical and Generalized Extreme Value Distributions for Modeling Extreme Rainfall in Austria, Earth and Space Science, 6, 1616–1632, doi:10.1029/2019EA000557, 2019.

Schiermeier, Q.: The Real Holes in Climate Science, Nature, 463, 284–287, doi:10.1038/463284a, 2010.

Schleiss, M.: How intermittency affects the rate at which rainfall extremes respond to changes in temperature, Earth System Dynamics, 9, 955–968, doi:10.5194/esd-9-955-2018, 2018.

Schneider, U., Becker, A., Finger, P., Meyer-Christoffer, A., Rudolf, B., and Ziese, M.: GPCC Full Data Reanalysis Version 6.0 at 0.5°: Monthly Land-Surface Precipitation from Rain-Gauges built on GTS-based and Historic Data, doi:10.5676/DWD_GPCC/FD_M_V6_050, 2011.

Schneider, U., Becker, A., Finger, P., Meyer-Christoffer, A., Ziese, M., and Rudolf, B.: GPCC's new land surface precipitation climatology based on quality-controlled in situ data and its role in quantifying the global water cycle, Theoretical and Applied Climatology, 115, 15–40, doi:10.1007/s00704-013-0860-x, 2014.

Scoccimarro, E. and Gualdi, S.: Heavy daily precipitation events in the CMIP6 worst-case scenario: Projected twenty-first-century changes, Journal of Climate, 33, 7631–7642, doi:10.1175/JCLI-D-19-0940.1, 2020.

Serinaldi, F. and Kilsby, C. G.: Rainfall extremes: Toward reconciliation after the battle of distributions, Water Resources Research, 50, 336–352, doi:10.1002/2013WR014211, 2014.

Shen, L., Wen, J., Zhang, Y., Ullah, S., Meng, X., and Chen, G.: Performance Evaluation of ERA5 Extreme Precipitation in the Yangtze River Delta, China, Atmosphere, 13, doi:10.3390/atmos13091416, 2022.

Shiogama, H., Watanabe, M., Kim, H., and Hirota, N.: Emergent Constraints on Future Precipitation Changes, Nature, 602, 612–616, doi:10.1038/s41586-021-04310-8, 2022.

Sillmann, J., Kharin, V. V., Zwiers, F. W., Zhang, X., and Bronaugh, D.: Climate extremes indices in the CMIP5 multimodel ensemble: Part 2. Future climate projections, Journal of Geophysical Research Atmospheres, 118, 2473–2493, doi:10.1002/jgrd.50188, 2013.

Stacy, E. W.: A Generalization of the Gamma Distribution, The Annals of Mathematical Statistics, 33, 1187–1192, URL http://www.jstor.org/stable/2237889, 1962.

Steger, S., Moreno, M., Crespi, A., Zellner, P. J., Gariano, S. L., Brunetti, M. T., Melillo, M., Peruccacci, S., Marra, F., Kohrs, R., Goetz, J., Mair, V., and Pittore, M.: Deciphering Seasonal Effects of Triggering and Preparatory Precipitation for Improved Shallow Landslide Prediction Using Generalized Additive Mixed Models, Natural Hazards and Earth System Sciences, 23, 1483–1506, doi:10.5194/nhess-23-1483-2023, 2023.

Sun, Q., Miao, C., Duan, Q., Ashouri, H., Sorooshian, S., and Hsu, K.: A review of global precipitation data sets: Data sources, estimation, and intercomparisons, Review of Geophysics, 56, 79–107, doi:10.1002/2017RG000574, 2018.

Swift, L. W. and Schreuder, H. T.: Fitting Daily Precipitation Amounts Using the SB Distribution, Monthly Weather Review, 109, 2535 – 2540, doi:10.1175/1520-0493(1981)109<2535:FDPAUT>2.0.CO;2, 1981.

Tandon, N. F., Zhang, X., and Sobel, A. H.: Understanding the Dynamics of Future Changes in Extreme Precipitation Intensity, Geophysical Research Letters, 45, 2870–2878, doi:10.1002/2017GL076361, 2018.

Tarasova, L., Lun, D., Merz, R., Blöschl, G., Basso, S., Bertola, M., Miniussi, A., Rakovec, O., Samaniego, L., Thober, S., and Kumar, R.: Shifts in Flood Generation Processes Exacerbate Regional Flood Anomalies in Europe, Communications Earth & Environment, 4, 49, doi:10.1038/s43247-023-00714-8, 2023.

Thackeray, C. W., Hall, A., Norris, J., and Chen, D.: Constraining the increased frequency of global precipitation extremes under warming, Nature Climate Change, 12, 441–448, doi:10.1038/s41558-022-01329-1, 2022.

Tokarska, K. B., Stolpe, M. B., Sippel, S., Fischer, E. M., Smith, C. J., Lehner, F., and Knutti, R.: Past warming trend constrains future warming in CMIP6 models, Sci. Adv., 6, eaaz9549, doi:10.1126/sciadv.aaz9549, 2020.

Tramblay, Y., Villarini, G., El Khalki, E. M., Gründemann, G., and Hughes, D.: Evaluation of the drivers responsible for flooding in Africa, Water Resources Research, p. e2021WR029595, doi:10.1029/2021WR029595, 2021.

Tramblay, Y., Arnaud, P., Artigue, G., Lang, M., Paquet, E., Neppel, L., and Sauquet, E.: Changes in Mediterranean flood processes and seasonality, Hydrology and Earth System Sciences, 27, 2973–2987, doi:10.5194/hess-27-2973-2023, 2023.

UNSIDR: Sendai Framework for Disaster Risk Reduction 2015 - 2030, Tech. rep., URL www.unisdr.org/we/inform/publications/43291, 2015.

Ushio, T., Sasashige, K., Kubota, T., Shige, S., Okamoto, K., Aonashi, K., Inoue, T., Takahashi, N., Iguchi, T., Kachi, M., Oki, R., Morimoto, T., and Kawasaki, Z. I.: A kalman filter approach to the Global Satellite Mapping of Precipitation (GSMaP) from combined passive microwave and infrared radiometric data, Journal of the Meteorological Society of Japan, 87 A, 137–151, doi:10.2151/jmsj.87A.137, 2009.

Van de Giesen, N., Liebe, J., and Jung, G.: Adapting to climate change in the Volta Basin, West Africa, Current science, 98, 1033–1037, 2010.

van de Giesen, N., Hut, R., and Selker, J.: The Trans-African Observatory (TAHMO), WIREs Water, 1, 341–348, doi:10.1002/wat2.1034, 2014.

Villarini, G., Smith, J. A., Lynn, M., Vitolo, R., Stephenson, D. B., and Krajewski, W. F.: On the frequency of heavy rainfall for the Midwest of the United States, Journal of Hydrology, 400, 103–120, doi:10.1016/j.jhydrol.2011.01.027, 2011.

Wang, P., Huang, Q., Tang, Q., Chen, X., Yu, J., Pozdniakov, S. P., and Wang, T.: Increasing annual and extreme precipitation in permafrost-dominated Siberia during 1959–2018, Journal of Hydrology, 603, 126 865, doi:https://doi.org/10.1016/j.jhydrol.2021.126865, 2021.

Ward, P. J., Kummu, M., and Lall, U.: Flood frequencies and durations and their response to El Niño Southern Oscillation: Global analysis, Journal of Hydrology, 539, 358–378, doi:10.1016/j.jhydrol.2016.05.045, 2016.

Wasko, C., Sharma, A., and Johnson, F.: Does storm duration modulate the extreme precipitation-temperature scaling relationship?, Geophysical Research Letters, 42, 8783–8790, doi:10.1002/2015GL066274, 2015.

Wasko, C., Nathan, R., and Peel, M. C.: Trends in Global Flood and Streamflow Timing Based on Local Water Year, Water Resources Research, 56, e2020WR027 233, doi:10.1029/2020WR027233, 2020a.

Wasko, C., Nathan, R., and Peel, M. C.: Changes in Antecedent Soil Moisture Modulate Flood Seasonality in a Changing Climate, Water Resources Research, 56, e2019WR026 300, doi:10.1029/2019WR026300, 2020b.

Westra, S., Alexander, L. V., and Zwiers, F. W.: Global increasing trends in annual maximum daily precipitation, Journal of Climate, 26, 3904–3918, doi:10.1175/JCLI-D-12-00502.1, 2013.

Westra, S., Fowler, H. J., Evans, J. P., Alexander, L. V., Berg, P., Johnson, F., Kendon, E. J., Lenderink, G., and Roberts, N. M.: Future changes to the intensity and frequency of short-duration extreme rainfall, Reviews of Geophysics, 52, 522–555, doi:10.1002/2014RG000465, 2014.

Wilks, D. S.: "The Stippling Shows Statistically Significant Grid Points": How Research Results are Routinely Overstated and Overinterpreted, and What to Do about It, Bulletin of the American Meteorological Society, 97, 2263 – 2273, doi:10.1175/BAMS-D-15-00267.1, 2016.

Wilson, P. S. and Toumi, R.: A fundamental probability distribution for heavy rainfall, Geophysical Research Letters, 32, doi:10.1029/2005GL022465, 2005.

Zelinka, M. D., Myers, T. A., McCoy, D. T., Po-Chedley, S., Caldwell, P. M., Ceppi, P., Klein, S. A., and Taylor, K. E.: Causes of Higher Climate Sensitivity in CMIP6 Models, Geophysical Research Letters, 47, e2019GL085 782, doi:10.1029/2019GL085782, 2020.

Zhang, D., Liu, X., Bai, P., and Li, X.-H.: Suitability of satellite-based precipitation products for water balance simulations using multiple observations in a humid catchment, Remote Sensing, 11, doi:10.3390/rs11020151, 2019.

Zorzetto, E. and Marani, M.: Downscaling of rainfall extremes from satellite observations, Water Resources Research, 55, 156–174, doi:10.1029/2018WR022950, 2019.

Zorzetto, E. and Marani, M.: Extreme value metastatistical analysis of remotely sensed rainfall in ungauged areas: Spatial downscaling and error modelling, Advances in Water Resources, 135, 103 483, doi:10.1016/j.advwatres.2019.103483, 2020.

Zorzetto, E., Botter, G., and Marani, M.: On the emergence of rainfall extremes from ordinary events, Geophysical Research Letters, 43, 8076–8082, doi:10.1002/2016GL069445, 2016.

SUPPORTING INFORMATION OVERVIEW

The supporting information of chapter 2, 3 and 4 can be accessed on the TU Delft repository.

SUPPORTING CONTENTS

LIST OF SUPPORTING FIGURES

LIST OF SUPPORTING TABLES

SUMMARY

Improved understanding of historical precipitation extremes is important to better explain their behavior, predict future occurrences, and inform planning and engineering design. The intensity, seasonality, and timing of these extremes have far-reaching consequences, and require a comprehensive analysis of both historical trends and projected future changes. By integrating historical observations, statistical methods, and climate model projections, this research provides valuable insights into precipitation extremes on the global domain.

Chapter 2 presents spatiotemporal patterns of historical extreme precipitation return levels over the global domain. Different extreme value methods are used to estimate the extreme precipitation return levels and the tail behavior of the associated distribution. A novel heaviness amplification factor is introduced to enable a comparison of the heaviness of the tail between different extreme value distributions. This factor indicates whether the tail of the extreme value distribution is heavier or lighter than an exponential one, providing insights into the likelihood of extreme precipitation events. The analyses reveal interesting regional differences. Arid areas exhibit heavier tails, indicating a higher likelihood of rare extreme events, while mountainous regions show thinner tails, suggesting a lower likelihood. Remarkably, the Metastatistical Extreme Value (MEV) distribution demonstrates spatially coherent tail behavior, even when using short time series and single grid-cell analyses, without relying on prior information about spatial precipitation structures. The Generalized Extreme Value distribution and Peak-Over-Threshold methods, on the other hand, show erratic spatial patterns in the extremes and tail heaviness. However, they do show a consistent shift from heavy to thin tails with increasing duration. This study also highlights the impact of using hydrological years over calendar years, resulting in differences in estimating extremes particularly in the Southern hemisphere. When using calendar years it is possible for one rainy season, potentially affected by cyclic phenomena as El Niño, to be split up into two calendar years. All the results of this study are openly published online as the Global Precipitation EXtremes (GPEX) dataset. This makes global extreme precipitation return levels for different distributions and their heaviness publicly and readily available for research or applied use.

Chapter 3 focuses on changes in seasonality and timing of extreme daily precipitation occurrences and reveals interesting geographical patterns. The relative entropy, a measure of seasonality, indicates higher values, meaning more clustered extremes, on mountain slopes and land areas compared to mountain peaks and adjacent oceanic regions. Significant shifts in seasonality across different continents were observed in recent decades. Specifically, Sub-Saharan Africa experienced an intensification of its already highly seasonal occurrence of precipitation extremes in the recent past. In contrast, Europe, Australia, and North America demonstrate more evenly spread occurrences,

but with an increase in clustering. Meanwhile, Asia and South America witnessed shifts towards more spread-out extremes. Furthermore, the peak occurrence of extreme precipitation is observed in extra-tropical land regions during summer, with modest shifts in timing.

Chapter 4 evaluates future changes in precipitation extremes based on climate model projections. It is revealed that the rarest precipitation extremes are expected to experience a relatively larger increase in magnitude by the end of the 21st century. There is striking agreement among 25 climate models regarding this finding, particularly for high emission scenarios. This study also further confirms a strong scientific consensus in a future increase in precipitation extremes by showing an overall increase in projected precipitation extremes over land regions, with higher emission scenarios leading to more substantial increases. Notably, Sub-Saharan Africa and regions just north of the equator are expected to face disproportionate increases in the occurrence of the rarest rainfall extremes. In contrast, regions such as Europe or North America are projected to experience relatively smaller increases in the magnitude of future extremes. These findings highlight that the areas most affected by future changes in precipitation extremes are not necessarily the largest emitters of greenhouse gases, which are the main cause for these changes.

The findings of this dissertation directly contribute valuable information about extreme precipitation characteristics in the recent past and the projected future. By examining global-scale patterns, this research offers insights that can be particularly relevant to regions lacking long-term local rain gauge records. The implications of this research extend beyond the academic realm, as it provides a foundation for policymakers, stakeholders, and communities to implement targeted adaptation and mitigation strategies in the face of changing precipitation patterns.

Looking ahead, researchers should prioritize improving and expanding precipitation datasets and complementing efforts with cutting-edge statistical approaches to derive more comprehensive insights into future precipitation extremes. Higher spatiotemporal resolutions achieved through downscaling techniques are essential for local climate adaptation and impact assessments. The findings of this dissertation emphasize the urgency of global emission reduction efforts and highlight the importance of considering shifts in extreme precipitation for effective adaptation and societal protection.

SAMENVATTING

Het is belangrijk om een beter inzicht te krijgen in historische neerslagextremen. Dit is nodig om de huidige patronen beter te begrijpen, toekomstige neerslagextremen te voorspellen en voor het plannen en ontwerpen van infrastructuur. Veranderingen in de intensiteit, jaarlijkse gang en timing van neerslagextremen hebben verstrekkende gevolgen. Dit vereist een uitgebreide analyse van zowel historische trends als verwachte toekomstige veranderingen. Door de integratie van historische waarnemingen, statistische methoden en projecties van klimaatmodellen biedt dit onderzoek waardevolle inzichten in neerslagenextremen op mondiaal niveau.

Hoofdstuk 2 presenteert patronen in ruimte en tijd van historische terugkeerniveaus van extreme neerslag in het mondiale domein. Verschillende methoden zijn gebruikt om de extreme neerslag terugkeerniveaus en het staartgedrag van de bijbehorende extreme waarde kansverdeling te schatten. Om de dikte van de staart van de verschillende kansverdelingen te vergelijken, hebben we een "*heaviness amplification factor*" ingevoerd. Deze factor geeft aan of de staart van de extreme-waarden kansverdeling dikker of dunner is dan een exponentiële verdeling, wat inzicht geeft in de waarschijnlijkheid van extreme neerslaggebeurtenissen. De analyses brengen interessante regionale verschillen aan het licht. Aride gebieden vertonen dikkere staarten, wat duidt op een hogere waarschijnlijkheid van zeldzame extreme gebeurtenissen, terwijl bergachtige gebieden dunnere staarten vertonen, wat duidt op een lagere waarschijnlijkheid. Opmerkelijk is dat de *Metastatistical Extreme Value* (MEV) kansverdeling ruimtelijk coherent staartgedrag laat zien, zelfs bij gebruik van korte tijdreeksen en door analyses voor iedere rastercel afzonderlijk, zonder gebruik te maken van informatie over ruimtelijke neerslagstructuren. De *Generalized Extreme Value* (GEV) kansverdeling en de *Peak-Over-Threshold* (POT)-methode tonen daarentegen onsamenhangende ruimtelijke patronen in de extremen en dikte van de staart. Ze laten echter wel een consistente verschuiving zien van dikke naar dunne staarten met toenemende duur. Deze studie benadrukt ook de impact van het gebruik van hydrologische jaren ten opzichte van kalenderjaren, wat resulteert in verschillen in de geschatte extremen met name op het zuidelijk halfrond. Bij het gebruik van kalenderjaren is het mogelijk dat één regenseizoen, dat eventueel wordt beïnvloed door cyclische fenomenen als El Niño, wordt opgesplitst in twee kalenderjaren. De resultaten van dit onderzoek zijn openlijk online gepubliceerd als de *Global Precipitation EXtremes* (GPEX) dataset. Dit maakt de wereldwijde terugkeerniveaus van extreme neerslag voor verschillende kansverdelingen en de dikte van de staart van de verdelingen openbaar en gemakkelijk beschikbaar voor onderzoek of toegepast gebruik.

Hoofdstuk 3 richt zich op veranderingen in de jaarlijkse gang en timing van extreme dagelijkse neerslaggebeurtenissen en onthult interessante geografische patronen. De relatieve entropie geeft de mate van jaarlijkse gang aan. Hogere relatieve entropy waarden betekenen een hogere mate van concentratie in neerslaggebeurtenissen. De relatieve

entropie laat hogere waarden zien op berghellingen en landgebieden in vergelijking met bergtoppen en aangrenzende gebieden boven zee en oceaan. In de afgelopen decennia werden significante verschuivingen in jaarlijkse gang op verschillende continenten waargenomen. Met name in Afrika bezuiden de Sahara was er in het recente verleden sprake van een intensivering van het toch al sterk seizoensgebonden voorkomen van neerslagextremen. Europa, Australië en Noord-Amerika lieten daarentegen meer gelijkmatig verspreide neerslaggebeurtenissen zien, maar met een lichte toename in clustering. In Azië en Zuid-Amerika was er een verschuiving naar meer gespreide extremen. Verder wordt de piek van extreme neerslag in extra-tropische landgebieden tijdens de zomer waargenomen, met lichte verschuivingen in timing.

Hoofdstuk 4 evalueert toekomstige veranderingen in neerslagextremen op basis van projecties van klimaatmodellen. Hieruit blijkt dat de uitzonderlijke neerslagextremen tegen het einde van de 21e eeuw naar verwachting relatief sterker zullen toenemen. Er is opvallende overeenstemming tussen 25 klimaatmodellen over deze bevinding, met name voor klimaatscenario's met hoge broeikasgasemissies. Deze studie bevestigt ook een sterke wetenschappelijke consensus over een toekomstige toename van neerslagextremen door het aantonen van een algehele toename van de voorspelde neerslagextremen over landregio's, waarbij hogere emissiescenario's tot grotere toenames leiden. Met name Afrika en regio's net ten noorden van de evenaar zullen naar verwachting te maken krijgen met een onevenredige toename van de uitzonderlijke neerslagextremen. Daarentegen zullen regio's zoals Europa of Noord-Amerika naar verwachting een relatief kleinere toename in de omvang van toekomstige extremen ervaren. Deze bevindingen laten zien dat de gebieden die het meest worden getroffen door toekomstige veranderingen in neerslagextremen niet noodzakelijkerwijs de grootste uitstoters van broeikasgassen zijn, die de hoofdoorzaak van deze veranderingen zijn.

De bevindingen van dit proefschrift dragen direct bij aan waardevolle informatie over extreme neerslag in het recente verleden en de verwachte toekomst. Door ruimtelijke patronen op wereldschaal te onderzoeken, biedt dit onderzoek inzichten die in het bijzonder relevant kunnen zijn voor regio's die niet beschikken over lange-termijn lokale neerslagtijdsreeksen. De implicaties van dit onderzoek reiken dan ook verder dan het academische domein, aangezien de verkregen inzichten als basis kunnen dienen voor beleidsmakers, belanghebbenden en gemeenschappen om gerichte adaptatie- en mitigatiestrategieën te implementeren in het licht van veranderende neerslagpatronen.

In de toekomst zouden onderzoekers prioriteit moeten geven aan het verbeteren en uitbreiden van neerslagdatasets en dit aanvullen met geavanceerde statistische methodes, om zo meer uitgebreide inzichten te verkrijgen in toekomstige neerslagextremen. Hogere resoluties in zowel ruimtelijke als tijdsschaal kunnen worden bereikt door regionaliseringtechnieken (*downscaling techniques*), die essentieel zijn voor lokale klimaatadaptatie en effectrapportages. De bevindingen van dit proefschrift benadrukken de urgentie van wereldwijde emissiereductie-inspanningen en het belang van rekening houden met verschuivingen in extreme neerslag voor effectieve adaptatie en maatschappelijke veiligheid.

ACKNOWLEDGEMENTS

It is really happening, I finished my PhD. These past 5 years have been such a long and wild ride. I can honestly say that without the support from my supervisors, colleagues, friends and family, I would not have been able to finish. Thank you all so much for helping me!

First of all, I would like to thank my promotors Ruud van der Ent and Nick van de Giesen. Ruud, thank you for trusting me to be your very first PhD candidate, and for your advice, guidance and patience. You have shown me how to combine family life with working in academia, and have been so supportive of me to do the same. Nick, I would like to thank you for all your advice and input during our meetings. I admire your availability, especially with your faraway travels and busy schedule. You both have supported me during every step of the way, including my painfully slow concussion recovery, becoming a parent, and moving to Canada - twice.

To my coauthors, Enrico Zorzetto, Hylke Beck, Marc Schleiss, Marco Marani, and Lukas Brunner, thank you so much for your excellent input, and helping me through some seriously challenging review processes. I could not have gotten through them without you.

To my committee members, thank you for all your time spent on my dissertation and positive assessment. I am looking forward to our discussions during the upcoming defense.

At TU Delft I have had the great fortune to share room 4.96 with wonderful colleagues. Laurène Bouaziz, Jerom Aerts and Bart Schilperoort, I feel privileged to have shared this PhD journey with you three. You have been there from the start, and will all play a role during the defense. Laurène and Jerom as my paranymphs: thank you so much for all your help and making sure the defense day runs smoothly. Laurène, I have such happy memories of our coffee breaks, lunch walks, and our many rubber ducky chats. Jerom, I really enjoyed starting our PhDs just months apart, and I am so glad for our long chats and shared experiences. Bart, thanks for capturing the ceremony, for showing me the inner workings of TU Delft, and for always helping me out with python.

To the supporting staff, Betty Rothfusz, Fleur van de Water, Lydia de Hoog, Tamara Auperlé, and Petra Jorritsma, thank you for keeping our department running. I am in awe of how you always seem to know the answer to our questions, or seem to know the right person to ask.

To the water management staff, Edo Abraham, Erik Mostert, Marcus Hrachowitz, Marie-Claire ten Veldhuis, Mark Bakker, Martin Bloemendaal, Miriam Coenders, Olivier Hoes, Remko Uijlenhoet, Rolf Hut, Thom Bogaard, Wim Luxemburg, thank you for our many conversations, lunch walks, and social moments during conferences and department gatherings.

To my fellow colleagues and PhD students at TU Delft, Anna Solcerová, Bahareh Kianfar, Bas des Tombe, Bas Walraven, Boran Ekin Aydin, Chelsea Kaandorp, David Agoungbome, Fransje van Oorschot, Judith Boekee, Luuk van der Valk, Mónica Estébanez Camarena, Muhammad Ibrahim, Nyein Thandar Ko, Paul Vermunt, Ties van der Heijden, and many others, thank you for the social times we shared. It makes doing a PhD a lot less lonely, and I have learned a lot from you all.

To my colleagues and friends from the Coldwater Laboratory in Canmore, Canada. Martyn Clark, thank you for hosting me at your group and guiding me during both of our stays here. You and Claudia have brought the group here together by organizing many memorable backyard fires, when covid rules forced us to only meet outside. I am really looking forward to doing a post-doc with you. Jim and Hannah, our time in Canmore would not have been the same without you. I love our adventures together, hiking up mountains, skiing in Sunshine, paddling down rivers and lakes, camping in the backcountry, and the many driveway drinks. Louise and Julius, thank you for helping Jasper explore his musical and artistic talents, riverside hangs, and making us delicious dinners when things were hectic at home. Caroline and Tom, thank you for opening up your house and letting our little family stay with you and disturb the peace and quiet of your lovely hillside home. Wouter, it has been great having a fellow Dutchie in the Coldwater Lab. I am very excited for us to work together in Calgary. John Pomeroy, thank you for continuing to host me at the Coldwater Lab and for all your support. To the other wonderful people at the Coldwater Lab, in particular Alex Cebulski, Hannah Koslowsky, Kieran Lehan, Lindsey Langs, Maddie Harasyn, Nico Vasquez and Terava Groff, I will miss our lunches together, and learning more mountain hydrology from you. I do hope to keep seeing lots of you in our small mountain town.

Natacha, thank you so much for designing the cover for my dissertation, I cannot believe how talented you are and am so grateful for your friendship.

To those who are closest to me, but have less to do with my actual dissertation. To my friends, thank you so much for being there for me through some crazy times, listening endlessly to my PhD struggles, for all the *gezelligheid*, dinners, games, and trips together. I really value our friendship and treasure spending time with you all, especially now that we live far away.

To my family, thank you for all your love and support, it means the world to me. To my Canadian family, thank you for welcoming me with open arms and making me feel at home in this beautiful country. I feel honored to follow my uncle Rob Gründemann, cousin Olivier van der Meijden, and sister-in-law Nora Casson in their PhD-footsteps. Axel, thank you for paving the way at TU Delft, and being the best brother and uncle we could wish for. Mama en papa, thank you for your love and unconditional support, not just during my PhD but throughout my entire life. Jasper, thank you for all your love, giggles, snuggles, and attending your first international scientific conference at only three months old. Dave, thank you for your unwavering support, affection, and for brightening my days. I could not have wished for a better partner in this journey, and am so excited for all adventures that lie ahead.

CURRICULUM VITÆ

Gaby Joanne GRÜNDEMANN

27-11-1992 Born in Amsterdam, the Netherlands.

EDUCATION

2018 – 2023 PhD Water Resources
Delft University of Technology, Delft, the Netherlands
Thesis: Precipitation extremes around the world: Unraveling historical extremes and future changes
Promotor: Prof. dr. ir. N. C. van de Giesen
Copromotor: Dr. ir. R. J. van der Ent

2015 – 2017 MSc Water Science & Engineering
UNESCO-IHE, Delft, the Netherlands
Thesis: The potential of global re-analysis datasets in identifying flood events in Southern Africa.

2012 – 2015 BSc Earth Science & Economics
VU University, Amsterdam, the Netherlands
Thesis: Flood simulations and damage calculations for the harbour of Amsterdam.
Minor: National geo-information minor

EXPERIENCE

2018 – 2023	PhD Water Resources (5 years) Delft University of Technology, Delft, the Netherlands
2023	Visiting Researcher (9 months) Centre for Hydrology, University of Saskatchewan, Canmore, Canada
2020 – 2021	Visiting Researcher (1 year) Centre for Hydrology, University of Saskatchewan, Canmore, Canada
2017	Advanced Class Researcher (3 months) IHE-Delft, Delft, the Netherlands
2017	MSc Thesis Researcher (6 months) IVM Institute, VU University, Amsterdam, the Netherlands
2014	Research Intern (2 months) Deltares, Delft, the Netherlands

ACADEMIC ROLES

2021 – present	Convener Board Member EGU HS 7.7 Hydrometeorologic Stochastics
2019 – 2023	PhD Representative Boussinesq Center for Hydrology

LIST OF PUBLICATIONS

Gründemann, G. J., Zorzetto, E., van de Giesen, N. C., van der Ent, R. J., *Historical shifts in seasonality and timing of extreme precipitation*, accepted for publication in Geophysical Research Letters.

Massari, C., Pellet, V. Tramblay, Y., Crow, W. T., **Gründemann, G. J.**, Hascoet, T., Modanesi, S., Penna, D., Brocca, L., Mamici, C. Marra, F., *On the relation between antecedent basin conditions and runoff coefficient for European Floods*, Journal of Hydrology, **625**, p. 130012, 2023.

Gründemann, G. J., Zorzetto, E., Beck, H. E., Schleiss, M. A., van de Giesen, N. C., Marani, M., van der Ent, R. J. *Extreme precipitation return levels for multiple durations on a global scale*, Journal of Hydrology, **621**, p. 129558, 2023.

Gründemann, G. J., van de Giesen, N. C., Brunner, L., van der Ent, R. J., *Uitzonderlijk extreme regenbuien nemen relatief gezien het sterkst toe onder toekomstige klimaatverandering*, Stromingen, **1**, 2023 (in Dutch).

Gründemann, G. J., van de Giesen, N. C., Brunner, L., van der Ent, R. J., *Rarest rainfall events will see the greatest relative increase in magnitude under future climate change*, Communications Earth & Environment, **3**, 235, 2022.

Tramblay, Y., Villarini, G., El Khalki, E. M., **Gründemann, G. J.**, Hughes, D., *Evaluation of the drivers responsible for flooding in Africa*, Water Resources Research, e2021WR029595, 2021.

Beck, H. E., Westra, S., Tan, J., Pappenberger, F., Huffman, G. J., McVicar, T. R., **Gründemann, G. J.**, Vergopolan, N., Fowler, H. J., Lewis, E., Verbist, K., Wood, E. F., *PPDIST, global 0.1° daily and 3-hourly precipitation probability distribution climatologies for 1979–2018*, Scientific Data, **7**, 2020.

Gründemann, G. J., Werner, M., Veldkamp, T. I. E. *The potential of global reanalysis datasets in identifying flood events in Southern Africa*, Hydrology and Earth System Sciences, **22**, 4667-4683, 2018.